

The following article appeared in Crystals, 9 (12): 612 (2019) and may be found at: <https://doi.org/10.3390/cryst9120612>

This is an open access article under the Creative Commons Attribution 4.0 International (CC BY 4.0) license.

<https://creativecommons.org/licenses/by/4.0/>

Review

# Nanoengineering of Gold Nanoparticles: Green Synthesis, Characterization, and Applications

Nancy Tepale <sup>1,\*</sup>, Víctor V. A. Fernández-Escamilla <sup>2</sup>, Clara Carreon-Alvarez <sup>3</sup>,  
Valeria J. González-Coronel <sup>1</sup>, Adan Luna-Flores <sup>1</sup>, Alejandra Carreon-Alvarez <sup>4</sup> and  
Jacobo Aguilar <sup>2</sup>

<sup>1</sup> Facultad de Ingeniería Química, Benemérita Universidad Autónoma de Puebla, Av. San Claudio y 18 sur, Puebla CP 72570, Mexico; valeria.gonzalez@correo.buap.mx (V.J.G.-C.); adan.luna@correo.buap.mx (A.L.-F.)

<sup>2</sup> Departamento de Ciencias Tecnológicas, Universidad de Guadalajara, Avenida Universidad No. 1115, Ocotlan 47820, Mexico; vladkrm@hotmail.com (V.V.A.F.-E.); jax781023@hotmail.com (J.A.)

<sup>3</sup> División de Biología Molecular, Instituto Potosino de Investigación Científica y Tecnológica, Camino a la Presa San Jose 2055, San Luis Potosi 78216, Mexico; clara.carreon@ipicyt.edu.mx

<sup>4</sup> Departamento de Ciencias Naturales y Exactas, Centro Universitario de los Valles, Universidad de Guadalajara, Carretera Guadalajara—Ameca Km. 45.5, Ameca CP 46600, Mexico; ale\_carreon\_a@yahoo.com.mx

\* Correspondence: ntepale@hotmail.com; Tel.: +52-222229-5500 (ext. 7252)

Received: 23 October 2019; Accepted: 20 November 2019; Published: 22 November 2019



**Abstract:** The fundamental aspects of the manufacturing of gold nanoparticles (AuNPs) are discussed in this review. In particular, attention is devoted to the development of a simple and versatile method for the preparation of these nanoparticles. Eco-friendly synthetic routes, such as wet chemistry and biosynthesis with the aid of polymers, are of particular interest. Polymers can act as reducing and/or capping agents, or as soft templates leading to hybrid nanomaterials. This methodology allows control of the synthesis and stability of nanomaterials with novel properties. Thus, this review focus on a fundamental study of AuNPs properties and different techniques to characterize them, e.g., Transmission Electron Microscopy (TEM), Atomic Force Microscopy (AFM), UV-Visible spectroscopy, Dynamic Light Scattering (DLS), X-Ray Diffraction (XRD), X-Ray Photoelectron Spectroscopy, Small-angle X-Ray Scattering (SAXS), and rheology. Recently, AuNPs obtained by “green” synthesis have been applied in catalysis, in medicine, and as antibacterials, sensors, among others.

**Keywords:** gold nanoparticles; green synthesis; polymer; nanoengineering

## 1. Introduction

Colloidal gold (a suspension of gold particles with sub-micrometer size in different fluids such as water or an organic solvent) has been known since ancient times. However, its scientific study was started by Michael Faraday in 1850. At present, with the use of the electron microscope, it is possible to observe that the diameters of the particles in colloidal gold are found even in the nanometer range. At this scale, the size of nanoparticles (NPs) modifies the spectroscopic properties of the colloid. For example, colloids have an intense red color when particles are smaller than 100 nm. On the other hand, when particles are larger, colloids exhibit a blue/purple color. In general, the properties of AuNPs are strongly dependent on their size, composition, and shape. Thus, correct stabilization during synthesis is one of the most important points to solve in modern colloid chemistry and nanoparticle technology. This stabilization may be achieved using polymers, ligands, and biological molecules [1,2]. It is noteworthy that polymers are widely used as stabilizers or even as reducing agents and/or

nanoreactors during the synthesis of metal nanoparticles. Polymers can contribute to stability and to maintaining green chemistry guidelines while generating hybrid materials with novel properties. Today, an economic, versatile, and ecological synthesis is necessary for the development of sustainable technology. Protocols to prepare AuNPs using certain types of polymers, such as homopolymers and block copolymers, may represent a “green” approach because this type of synthesis presents some advantages, such as reactions at ambient conditions, fast completion, and the least possible reactants, resulting in an economical product that can be used immediately [3]. Since the electronic, optical, and catalytic properties of AuNPs are considered attractive for their possible applications in different technological fields, their correct characterization is of vital importance. Adequate characterization increases their potential for a specific application. Therefore, with the support of various characterization techniques (UV-Vis, DLS, TEM, AFM, XRD, SAXS, XPS, and rheology), polymer/nanoparticle assemblies (hybrid metal/polymer nanomaterials) can be explored. In this context, the manner in which hybrid AuNPs with novel properties can be applied in different scientific areas is reviewed in this work. We have considered some novel AuNPs applications during the last ten years.

Based on these considerations, this review is organized as follows: the first part is devoted to immersing the new reader in the fascinating world of AuNPs. The second part offers a brief discussion on the properties of gold and gold nanoparticles, while the third section is dedicated to the green synthesis of stabilized AuNPs. However, as characterization is a fundamental part of the science of hybrid nanoparticles, some basic aspects of the different characterization techniques are explained in section four. Finally, the fifth section summarizes the novel applications of gold/polymer hybrid nanomaterials in different areas.

## 2. Gold Nanoparticles

### 2.1. Physical and Chemical Properties of Gold

Gold is distributed inequitably on the surface of Earth, mainly due to the enrichment processes that occur near the surface. Its abundance average is very low and is estimated at ca. 0.005 ppm. [4]. Gold has entertained special interest throughout history because it has been important in many areas of human existence. It has been the motive of disputes among nations, but also it has been used to make jewelry and household items [1]. Due to its outstanding qualities, it is one of the most exceptionally valuable metals. From the earliest civilizations, gold has been associated with royalty and power. The Egyptians were the first to extract gold. There are also numerous reports of gold objects found in Pre-Columbian civilizations in America. In civilizations of the ancient world, gold was used in artifacts, with decorative purposes. It has also been employed worldwide for the basis of a currency exchange rate, e.g., the Byzantine Empire used gold coins, which were later replaced by silver coins [5].

Gold, Au (0), is characterized by its yellow color, stability, and high redox potential thanks to its electronic structure. It is located in group 11 of the Periodic Table of Elements. It has excellent resistance to corrosion, being extremely malleable, with a high density ( $19.32 \text{ g/cm}^3$  at  $20 \text{ }^\circ\text{C}$ ) [1]. It melts at  $1064 \text{ }^\circ\text{C}$  and boils at  $2850 \text{ }^\circ\text{C}$ . Gold forms diverse compounds and its oxidation state ranges from  $-1$  to  $+5$ . However, Au(I) and Au(III) govern the majority of its chemistry [1,6,7]. The absorbance of gold begins at 2.4 eV, reflecting red and yellow light while absorbing blue and violet light strongly [6].

The gold unit cell is face centered cubic (fcc), with an atomic radius of 0.144 nm; this structure is responsible for its high malleability. Gold generally does not exhibit a very crystalline aspect. It is generally presented in the form of a leaf or a sphere, where cubic, octahedral, and dodecahedral surfaces can be observed [8]. In addition, it prevents the formation of oxides and sulphides due to its inactivity with regard to the components of the atmosphere. It does not react with water, oxygen, ozone, nitrogen, hydrogen, fluorine, iodine, sulfur, and hydrogen sulfide under normal conditions. Practically no organic acid solubilizes gold, even at high concentrations and at boiling temperature. In addition, alkalis do not attack gold [1].

## 2.2. Historical Perspective: From Bulk to Gold Nanoparticles

The use of gold in ancient times was restricted because people did not know how to solubilize it. However, with the discovery of Aqua regia (a combination of hydrochloric acid and nitric acid), the obtaining of a gold precipitate called Purple of Cassius was possible. This finding was attributed to Andrea Cassius (1605–1673) [1]. However, it was not until 1857 that Michael Faraday proposed that metallic gold (finely divided) was present in the solution. He demonstrated that metals such as gold possess the ability to form dilute clear solutions, which can be studied by their ability to interact with light. Faraday recognized that the color of the solutions was related to the minuscule size of the particles [2]. In 1908, 50 years later, Gustave Mie began to study the optical properties of spherical particles much smaller than the wavelength of light [1]. In recent times, the wonderful colors and novel properties of gold nanoparticles have attracted much attention. Consequently, the nanoscience and nanotechnology of gold hold great promise [9].

## 2.3. Properties of Gold Nanoparticles

Physical and chemical phenomena at the nanoscale are notably different from those observed in bulk (macroscopic) matter. Sometimes the difference is solely the result of the much larger surface area-to-volume ratio, as particles shrink in size.

Consider a ball that has a radius of 11 cm and a C<sub>60</sub> fullerene (also known as Buckyball), a spherical molecule that has a radius of 0.5 nm ( $5 \times 10^{-8}$  cm). Given that the area and the volume of a sphere are respectively,

$$A = 4\pi r^2 \quad (1)$$

$$V = \frac{4}{3}\pi r^3 \quad (2)$$

and applying simple algebra, the surface area-to-volume ratio ( $A/V$ ) for the Buckyball is over five billion times larger than for the ball [10]. A high surface/volume ratio and the great amount of surface gold atoms increases surface chemical reactivity. In catalysis, this property is crucial and it has been widely studied [11–13].

Other notable changes in AuNPs involve the following: a decrease in melting temperature (AuNPs of 2 nm melt at ca. 226 °C, in contrast to 1063 °C for bulk gold), and a lowering of the interatomic separation from 0.288 nm to 0.245 nm [1,14].

One remarkable property of AuNPs is the collective oscillation of the free conduction electrons excited by electromagnetic radiation, resulting in plasmon resonance [15]. Two different phenomena are denominated plasmon resonances, i.e., the surface plasmon resonance (SPR), and localized surface plasmon resonance (LSPR). In the first case, plasmons propagate along a metallic surface for distances on the order of tens to hundreds of microns. In the second case, light interacts with particles much smaller than the incident wavelength. This leads to a plasmon that oscillates locally around the nanoparticle. Thus, the LSPR is sensitive to changes in the local environment of the particles and to any change in size and shape they may have. The occurrence of this phenomenon in the nanoscale is immediately perceived by our eyes by the presence of very specific colors [1,15].

To end this part, a gold nanoparticle can gain energy by absorbing photons when it is exposed to incident light in the visible spectral domain. This energy is released in the form of heat, modifying the temperature of the AuNP environment (photothermal capacity). This explains the dramatic increase about in the study and applications of AuNPs [1,16].

## 3. Synthesis of Gold Nanoparticles

Synthesis methods to obtain nanoparticles can be classified into two types: a “top-down” approach or a “bottom-up” approach. In the top-down approach, nanoparticles are obtained by decreasing the size of the bulk material. This reduction is carried out through different physical and chemical treatments, e.g., mechanical milling and laser ablation [17]. However, this method gives rise to imperfections

in the surface structure of nanomaterial [18]. On the other hand, bottom-up synthesis frequently considers chemical and biological methods. Nanoparticles are generated by joining atoms and/or molecules, e.g., chemical vapor deposition, the sol–gel method, colloidal synthesis, and microemulsion synthesis [17,19–21]. A common and simple synthesis of metallic nanoparticles is performed by chemical reduction of metal salts in solution phase [22]. The main components for AuNPs production are gold precursors, reducing agents, the reaction medium and capping agents [21]. Kimling et al. [23] proposed a mechanism for the growth of AuNPs when following the Turkevich method, using X-ray scattering and electron microscopy. Through a series of experiments, these authors observed that there is a change in the oxidation state of the gold ions Au(III) and Au (I) immediately after the addition of the reducing agent to the gold precursor solution. They also observed that after a certain time, some gold atoms (Au (0)) agglomerated (nucleation process) to form a cluster material. The clusters were very small (<5 nm) and uniformly dispersed in the liquid. Later, when clusters were compacted, they formed nanoparticles. Unfortunately, because these nanoparticles were unstable, they formed larger particles [18,23]. Furthermore, Polte et al. [24] explored the evolution of gold nanoparticles during citrate synthesis. This synthesis was carried out at 75 and 85 °C with different concentrations of gold precursor. The authors obtained, by means of small angle X-ray scattering (SAXS), the shape, size, polydispersity, and number of particles formed, while the in-situ oxidation state of AuNPs was determined by X-ray absorption near edge spectroscopy (XANES). With the use of these techniques, it was possible to determine different phases in the formation of nanoparticles. The first phase took place between 0 and 25 min. During this time, the gold precursor was transformed into nuclei (2 nm) that later merged and aggregated (4 nm). The second phase took place at between 25 and 50 min. Here, the change in concentration of the Au(III) precursor was slow, leading to a continuous grow (5.2 nm). During the third phase, at between 50 and 70 min, the remaining Au(III) was rapidly consumed, with an increase in particle size to 7.6 nm. It was also observed that an increase in temperature and/or concentration of the gold precursor significantly accelerated the formation process of AuNPs without changing the mechanism. On the other hand, Köth et al. [25] synthesized AuNPs in the presence of oligosaccharide-modified hyperbranched poly(ethyleneimines) PEI. The polymer acted simultaneously as a reducing and a stabilizing agent. These authors utilized different techniques, such as DLS and SAXS, among others, for characterization purposes. Using DLS, it was possible to determine the particle size not only of the polymer coils but also of the nanoparticles themselves. The authors observed that the size of polymer coils decreased due to the formation of nanoparticles immediately after mixing the PEI solution with the gold precursor solution. It was possible to obtain the radius of the core (1.5 nm) and of the thickness of the shell (3.3 nm) by means of SAXS and SANS measurements. In the same line, Polte et al. [26] studied the synthesis of AuNPs using employing Pluronic F127 triblock copolymer as both reducing and colloidal stabilizer. The one-step method was carried out at room temperature. The authors suggested the following mechanism for the formation of AuNPs. It essentially consisted of a typical “burst” nucleation. When Au(III) was trapped in the polymer cavities (pseudo ether crown complex), it was reduced to Au(0), followed by continuous particle growth. Figure 1 shows a schematic illustration for mechanism of AuNPs formation.

The representative structure of AuNPs synthesized in solution considers the following three parts: (1) central atoms with a closed packed crystalline structure; (2) surface atoms exposed on outer layers, and (3) capping agents that protect the surface of the nanomaterials, sometimes providing surface functionality [1].

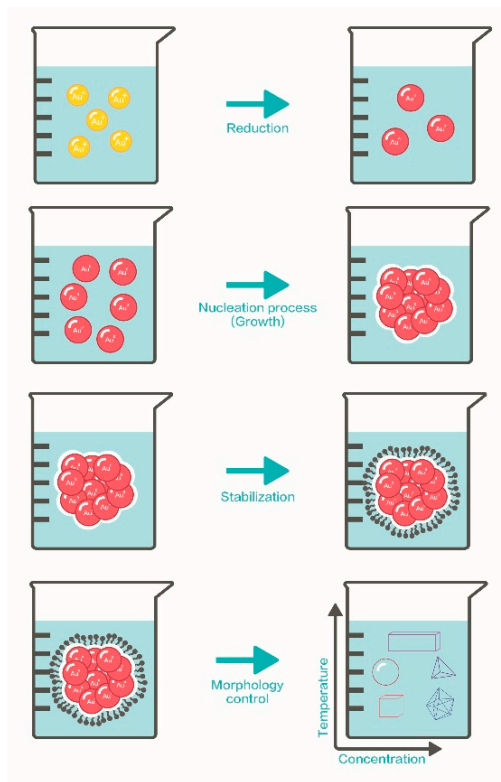


**Figure 1.** Schematic illustration for mechanism of AuNPs formation.

### 3.1. Toward Green Synthesis

Turkevich in 1951 provided the first reproducible synthesis of gold metal colloids (20 nm) by the reduction of  $AuCl_4^-$  using sodium citrate [27]. Sodium citrate acts as both reducing and capping agent and remains one of the best candidates to prepare AuNPs because it has advantages such as: it is economical, non-toxic, soluble in water, and has little contamination in the reaction. However, the use of sodium citrate has the disadvantage that low yields are obtained in the synthesis of AuNPs (approximately 0.005 wt.%), which also require large amounts of water for its preparation and consume large amounts of energy [28]. In addition, small AuNPs are obtained and aggregated to form larger particles that are not desired for applications [2]. Currently, AuNPs must be stable and completely dispersed in a solvent for their later application; for this reason, polymers have been widely used as stabilizers. Shan and Tenhu [29] analyzed the performance of polymers in the synthesis of AuNPs. The authors found that polymers increase the stability of AuNPs even at very long times. They can adjust the solubility of NPs, and can also modify their properties, compatibility, and processability [29,30]. Two major synthetic routes to prepare hybrid metal/polymer NPs include the “grafting to” and “grafting from” techniques. In the “grafting to” method, synthesis of AuNPs is carried out by the attachment of polymers onto the Au surface. In the “grafting from” method, initiators are needed to carry out polymerization on the Au surface [30]. This research is being developed because it is viable to prepare hybrid nanocomposites using non-toxic reagents with a simple synthetic route [31]. A new era in nanomaterial synthesis methods is emerging with the purpose of contributing to the development of materials science and clean technology [32]. Green synthesis attempts to produce nanomaterials with the least possible number of components (economical), using ideal solvents such as water, with efficient and rapid reactions. In other words, the goal of green synthesis is to protect the environment. The use of polymers and block copolymers has opened a “green” opportunity in nanomaterial surface engineering [19].

### 3.2. The Behavior of Polymers in Gold Nanoparticle Synthesis

“Naked” AuNPs have a tendency to aggregate because of their high surface energy, decreasing their performance. Therefore, stabilizers or capping agents are necessary to avoid aggregates during their synthesis, thus ensuring their high performance. Trisodium citrate was the first stabilizer used in the synthesis of AuNPs. There are other stabilizers, such as tetraalkyl ammonia salts, e.g., cetyltrimethyl ammonium bromide. Even ligands such as thiols are utilized as stabilizers [9]. However, polymers are broadly used in the green synthesis of AuNPs. Polymers employed as AuNPs stabilizers consider homopolymers such as poly(*N*-vinyl-2-pyrrolidone) PVP and poly(acrylic acid) PAA, block copolymers such as poly(ethylene oxide)-*b*-poly(propylene oxide)-*b*-poly(ethylene oxide) PEO-PPO-PEO, and polyethylene glycol-*g*-polyvinyl alcohol PEG-*g*-PVA, among others [3,33–37]. Stabilization of metal surfaces using polymers, offers the possibility of tuning the optical properties, functionality, and surface reactivity of metal nanoparticles [31]. This surface adjustment permits AuNPs to be used in different applications [2].

#### 3.2.1. Polymers as Reducing and Stabilizing Agents

The most common application of polymers in nanoparticle synthesis is as stabilizing or capping agents, in order to avoid the aggregation of metal nanoparticles. However, the use of polymers in the chemical reduction of metal ions in solution has recently emerged, attracting the attention of many scientists. In this context, the chemical nature of polymers is a very important consideration in carrying out redox reactions between polymers and metal salts [31,35]. Moreover, at present, with the need to have green synthesis and good care of the environment, the use of biodegradable polymers as reducing and stabilizing agents for AuNPs synthesis has increased. The use of less toxic molecules, such as natural polysaccharides, chitosan, sodium alginate, and starch, among others, has been studied considerably [38–40]. Table 1 summarizes some current reports on the synthesis of AuNPs with both synthetic and natural homopolymers.

**Table 1.** Examples of some AuNPs synthesized with different polymers.

| Polymers   | Function               | Size [nm] * | Morphology *               | Reference |
|--|------------------------|-------------|----------------------------|-----------|
| Synthetic Polymer  |                        |             |                            |           |
| Poly( <i>N</i> -vinyl-2-pyrrolidone) (PVP) and Polydiallyldimethylammonium chloride (PDAC)   | Stabilizer             | ~8          | Spherical                  | [33]      |
| Poly (acrylic acid) (PAA)  | Reducer and stabilizer | ~7          | –                          | [34]      |
| di- or tri-carboxylate- polyethylene glycol (PEG); Citrate-PEG (CPEG); malate-PEG (MAP); tartrate-PEG (TAP)                          | Reducer and stabilizer | 9–14        | Spherical                  | [41]      |
| Natural Polymer  |                        |             |                            |           |
| Alginate polymer   | Stabilizer             | 10–15       | spherical                  | [42]      |
| Sodium alginate (Natural polyhydroxylated polymer)   | Reducer and stabilizer | < 100       | Spherical and agglomerates | [39]      |
| Mung bean starch (MBS) (Natural polysaccharides)   | Reducer and stabilizer | ~10         | Spherical                  | [40]      |
| Chitosan, acylated chitosan (hydrophobically modified chitosan with acyl groups) and chitosan oligosaccharide (short chain chitosan) | Reducer and stabilizer | 3–16        | Spherical                  | [38]      |
| Chitosan oligosaccharide (COS)   | Reducer and stabilizer | ~61         | Spherical                  | [43]      |

\* the size and the morphology were obtained by TEM analysis.

In a colloidal solution, a good stabilizer permits access to the active sites of AuNPs. Amphiphilic polymers (polymers composed of hydrophilic and hydrophobic parts) are good candidates. In solution, they possess high stability, and due to their composition and structure, their affinity for AuNPs can be adjusted [9]. For the first time, Sakai et al. [3] in 2004 reported a single-step synthesis of AuNPs using PEO-PPO-PEO block copolymers (Pluronic). These copolymers acted as reductants and stabilizers. The formation of AuNPs was controlled by the molecular weight and block length of the copolymer. One year later, the same group of researchers [35] studied nanoparticle formation (growth), size control, and colloidal stability in the green synthesis of AuNPs again utilizing aqueous Pluronic solutions. Sakai et al. reported three essential steps in AuNPs formation: “(1) reduction of metal ions by the block copolymer in solution, (2) absorption of block copolymer on gold clusters and reduction of metal ions on the surface of these gold clusters, and (3) growth of metal particles stabilized by block copolymers”. Finally, the reported synthesis procedure was environmentally benign and inexpensive [35]. Table 2 summarizes some reports about the green synthesis of AuNPs with both synthetic and natural block copolymers.

**Table 2.** Examples of some AuNPs synthesized with synthetic or natural block copolymers.

| Synthetic/Natural Block Copolymer   | Size [nm] *     | Morphology *   | Reference |
|---|-----------------|--|-----------|
| Pluronic L64, P65, P84, P103, P104, P105, P123, and F127  | ~10             | Spherical  | [3]       |
| Pluronic L43, L44, L62, L64, P65, F68, P84, P85, F88, P103, P104, P105, F108, P123, and F127                          | 7–20            | Spherical  | [35]      |
| Polyethylene oxide-polystyrene oxide block copolymers   | -               | Spherical, quasispherical, and anisotropic shapes (nanoplates) | [44]      |
| Pluronic P85  | -               | Spherical and quasispherical                                   | [45]      |
| Block copolymers containing a poly (ε-caprolactone) central block and poly(N-vinyl 2-pyrrolidone) arms<br>PVP-PCL-PVP | 80–200          | Spherical, triangular, hexagonal, and multi-armed shapes       | [46]      |
| Pluronic F127   | ~20             | Spherical and quasispherical                                   | [47]      |
| Pluronic L121   | ~100            | Platelike, triangular and hexagonal shapes                     | [48]      |
| Poly(ethylene glycol)-block-linear polyethylenimine-block-poly(ε-caprolactone)<br>PEG-PEI-PCL                         | ~8              | Spherical  | [49]      |
| Polyethylene glycol-g-polyvinyl alcohol<br>PEG-g-PVA  | ~23, 44, 62, 79 | Spherical  | [37]      |
| Pluronic F127   | ~18.5           | Polygonal  | [50]      |
| Pluronic F127   | ~5<br>10–70     | Quasi-spherical<br>Mixture of morphologies                     | [51]      |
| [hydroxyethyl starch-g-poly (methylacrylate-co-sodium acrylate)] (PHES)   | 16–20           | Spherical  | [52]      |
| Pyromellitic dianhydride-p-phenylene diamine-PPDDs  | 11–170          | Spherical and nanoflowers (multi branched)                     | [53]      |

\* the size and the morphology were obtained by TEM analysis.

### 3.2.2. Polymers as Soft Template

Block copolymers have been known to form micelles. A micelle is an ordered structure that possesses hydrophobic and hydrophilic domains. The temperature at which micelles are formed is known as the critical micelle temperature (CMT). The size and shape of the micelle can be changed with modifications in copolymer molecular characteristics, solvent quality, and temperature. Copolymers, such as diblock or triblock, can form micelles of nanometric size. These structures can act as nanoreactors or soft templates for gold nanoparticle synthesis [1,48,54,55]. AuNPs can be homogeneously distributed

inside whole micelles, or located on the peripheral surface of the polymeric particles [56]. For this reason, block copolymers have recently been used as versatile templates for synthesizing AuNPs [57]. The formation of NPs using block copolymers presents benefits such as favorable particle-polymer interactions and control over morphology [58]. For example, Spatz et al. [59] generated a surface nanopattern (regular arrangement of isolated gold particles) employing self-assembled diblock copolymer poly (styrene)-block-poly(2-vinylpyridine) (PS-*b*-P2VP) with a different molecular weight. Polymeric micelles acted as a template where the AuNPs were loaded. This hybrid material was then deposited onto a substrate. The copolymer was later removed by oxygen plasma, leaving behind regularly arranged AuNPs of uniform size, with distances of 1–140 nm between them. The size of the Au dots was controlled by the amount of inorganic precursor present. However, the inter-particle distance (the distance from the edge of each gold core to that of another adjacent particle [60]) was related to the molecular weight of the block copolymer. Other authors have also reported that the inter-particle distance of AuNPs increases with the increase in molecular weight of protecting polymers [60]. In addition, in 2015, Yin et al. [56] decorated mixed shell polymeric micelles (MSPM) with AuNPs. For this purpose, the authors utilized poly (3-caprolactone) -block- (ethylene glycol) (PCL-*b*-PEG) and poly (3-caprolactone) -block-poly (*N*-isopropylacrylamide) (PCL-*b*-PNIPAM). The self-assembly of the two-block polymers generated micelles with a PCL core having a mixed shell of PEG and PNIPAM. Additionally, thiol groups were introduced at the end of each PNIPAM chain, in order to reduce the gold precursor and limit the location of AuNPs on the micellar surface. Yin et al. observed that if the amount of thiol groups in the shell decreased, the number of AuNPs on the micellar surface also decreased, exhibiting in consequence an increased inter-particle distance. On the other hand, when the system was heated, PNIPAM chains collapsed and AuNPs approached each other, which led to a shorter inter-particle distance. In this case, the color of the hybrid micellar suspension changed from red to deep purple, corroborating a change in the inter-particle distance.

Following green synthesis, in 2006, Bakshi et al. [61] observed AuNPs of 2–3 nm uniformly distributed on the surface of Pluronic P123 and P84 triblock copolymer (TBC) micelles. These authors reported that micelles showed large surface areas covered by small surface cavities that provided nucleation sites for AuNPs formation. Four years later, Khullar et al. [54] produced AuNPs using Pluronic F68 (predominantly hydrophilic) and Pluronic P103 (predominantly hydrophobic). Khullar et al. found that the reduction of gold ions was carried out by small surface cavities present in the micelles. TEM studies helped to elucidate the interaction between AuNPs and micellar assemblies. The study demonstrated that spherical micelles of F68 at 40 °C were loaded with a low quantity of small NPs. However, at the same temperature, the Pluronic P103 system revealed micelles completely loaded with tiny NPs. The authors concluded that the excessive hydration of surface cavities leads to a poor reduction process. In the same line, Khullar et al. [48] also synthesized tiny AuNPs in hydrophobic Pluronic L121 micelles. Furthermore, Tepale et al. [36] prepared hybrid gold nanomaterials using Pluronic P103 micelles as soft template. The results concluded that micellar assemblies control the final morphology of hybrid materials. Table 3 summarizes some reports on AuNPs synthesis with block copolymers as soft templates.

**Table 3.** Examples of some AuNPs synthesized with soft templates.

| Block Copolymer   | Size [nm] * | Reference |
|---|-------------|-----------|
| Pluronic P103, P84, P123, and F127                                  | 2–3         | [61]      |
| Pluronic F68 and P103   | 2–3         | [54]      |
| Pluronic L121   | 3–6         | [48]      |
| Poly ( <i>N</i> -isopropyl acrylamide)/polyethyleneimine PNIPAm/PEI | <10         | [62]      |
| Pluronic P103   | 2–6         | [36]      |
| Pluronic F127   | -           | [63]      |
| Pluronic F127   | <5          | [51]      |

\* the size and the morphology were obtained by TEM analysis.

### 3.3. Biosynthesis

The synthesis of nanoparticles can be carried out by means of different physicochemical methods [64]. However, biological methods are attractive due to their low toxicity and biocompatibility [18]. A promising ecological method comprises biosynthesis using plant extracts. Recently, it was reported that extracts serve as reducing agents due to the presence of molecules such as phenols, amino acids, flavones, terpenoids, vitamins, polysaccharides, proteins, and enzymes among others [19]. However, it has also been reported that plant extracts may act as stabilizing agents in AuNPs synthesis [18]. As previously mentioned, the stability of nanoparticles is a key issue to consider. Although biosynthesis with plants offers advantages, there are many challenges to overcome before it can be applied. The diversity of plants renders the task complicated. An important challenge is the ability to control the size, shape, and crystallinity of NPs. In biosynthesis, far more experiments are required to understand the stability of the NPs [65]. Different plants can be used to reduce and stabilize AuNPs (Figure 2); some of these are presented in Tables 4 and 5.



**Figure 2.** Different plants are used in AuNPs biosynthesis.

**Table 4.** Examples of some AuNPs synthesized with plant extracts.

| Plant Origin                                 | Size [nm] * | Morphology *  | Applications   | Reference |
|--|-------------|---|--|-----------|
| <i>Aloe vera</i>                             | 50–350      | Triangular  | Cancer hyperthermia, optical coatings                              | [66]      |
| <i>Coriandrum sativum</i> (coriander leaves) | 6.7–57.9    | Spherical, triangular, truncated triangular, decahedral | Non-linear optics, biomedical and biotechnological applications    | [67]      |
| Apiin (henna leaves)                         | 39          | Spherical, triangular, and Quasispheroidal              | Hyperthermia of cancer cells and IR-absorbing optical coatings     | [68]      |
| <i>Camellia sinensis</i> (black tea leaf)    | 20          | Spherical, prism  | Catalysts, sensors   | [69]      |
| <i>Cassia fistula</i> (stem bark)            | 55–98       | Rectangular and triangular                              | Diabetes mellitus  | [70]      |
| Mentha and Pelargonium                       | 34–33       | Spherical, triangular and polygonal shapes              | Medical applications   | [71]      |
| <i>Artemisia capillaris</i>                  | 20–30       | Spherical, triangular and rod                           | Catalytic activity   | [72]      |
| Onion peel                                   | 45          | Spherical, and triangular shapes                        | Antibacterial, anticandidal, antioxidant and proteasome inhibitory | [73]      |
| <i>Plumeria alba</i> flower                  | 15–28       | Spherical   | Antibacterial activity and catalytic activity                      | [74]      |

\* the size and the morphology were obtained by TEM analysis.

**Table 5.** Examples of AuNPs synthesized with plant extracts plus a polymer or block copolymer.

| Plant Origin  | Size [nm] * | Morphology *  | Applications               | Reference |
|---|-------------|---|----------------------------|-----------|
| <i>Zingiber Officinale</i> and Poloxamer 188  | 10–35       | Spherical   | Anti-bacterial activity    | [75]      |
| <i>Leucas Aspera</i> and poly lactic acid-co-poly ethylene glycol-co-poly lactic acid (PLA-PEG-PLA) copolymer | 25          | Spherical   | Anti-inflammatory activity | [76]      |
| <i>Nigella sativa</i> and zein biopolymer   | 50–80       | Nanospherical and nanoplates (hexagons and triangles) | Antimicrobial activity     | [77]      |

\* the size and the morphology were obtained by TEM analysis.

#### 4. Characterization of Hybrid Gold/Polymer Nanomaterials

Different techniques have been used for characterizing gold nanoparticles stabilized with block copolymers, which lead to a better distribution and orientation of the metal particles, for example, surface characterization microscopy, spectrophotometry, X-ray spectroscopy, and flux properties.

##### 4.1. Surface Characterization Microscopy

Recently, research has been directed to the synthesis of AuNPs through green methods by employing polymers due to their capacity in terms of reduction and stabilization of gold. The utilization of polymers includes, for example, the following: (1) biopolymers, i.e., starch, chitosan, polypeptides, sodium alginate, etc.; (2) block copolymers, i.e., Pluronics, and (3) amide type polymers, i.e., acrylamide, *N*-isopropyl acrylamide, etc. Nazirov et al. [78] reported that the size of AuNPs synthesized with biopolymers is controlled by the rates of crystal growth and the balance of nucleation centers, which in turn it determined of the concentration and strength of the polymer and their reductant power.

On the other hand, the amphiphilic nature of block copolymers allow them to form micelles in aqueous media, acting as nanoreactors or templates for the three-dimensional organization of NPs. The size and morphology of the embedded AuNPs depends on the size and shape of the micelles, which also depends on the temperature variation, pH, solvent quality, solvent composition, and polymer concentration [55]. In order to study the roles of the precursors and the block copolymers micelles involved in the formation of AuNPs, surface characterization has been essential. With TEM and AFM, it is possible to observe the morphology of micelles and AuNPs, but also how they interact collectively. Thus, the electrostatic nature can be elucidated of the self-assemble arrangement in hybrid gold/polymer nanomaterials.

##### 4.1.1. Transmission Electron Microscopy, (TEM)

TEM is used to study the morphology and size of AuNPs and the nanostructures formed with homopolymers and block copolymers, which act as reducing agents, stabilizers, and/or soft templates for AuNPs synthesis. Micellar assemblies formed with triblock copolymers act as soft templates due to the large surface cavities of micelles, which leads to the formation of tiny AuNPs, resulting in micelle-AuNPs hybrid assemblies [55].

The sample preparation is a critical point at present to obtain a representative image of the non-agglomerate micellar systems formed by the block copolymer and AuNPs. Zhang et al. [79] synthesized an amphiphilic block copolymer, poly (2-methacryloyloxyethyl ferrocenecarboxylate)-block-poly(*N*-isopropylacrylamide) with AuNPs to produce the PMAEFc-*b*-PNIPAM-AuNPs system via reversible addition fragmentation chain transfer (RAFT) and in-situ reduction of tetrachloroauric acid (HAuCl<sub>4</sub>). Figure 3 presents the TEM images of PMAEFc25-*b*-PNIPAM130, which depicts a regular globular core-shell micelle copolymer nanoparticles with particle sizes of ca. 75–105 nm (Figure 3a). The inset in Figure 3a shows the size distribution, where a mean size of ca. 90 nm is

observed. Figure 3b presents AuNPs attached to the spherical micelles of PMAEFc25-b-PNIPAM130 forming a hybrid nanomaterial of AuNPs-PMAEFc-b-PNIPAM by complexation between mercapto groups and AuNPs. Here, the PMAEFc-b-PNIPAM micelles acts as soft template. The mean size of AuNPs-PMAEFc-b-PNIPAM hybrid copolymer micelles is ca. 110 nm (inset, Figure 3b). Zhang attribute the increase in size of the AuNPs-PMAEFc-b-PNIPAM to increased PNIPAM interchain repulsion and consequently the swelling of PNIPAM shells, and not to the accumulation of AuNPs. Moreover, from Figure 3c, the mean size of the AuNPs is ca. 13.5 nm, whereas the AuNPs attached to the micelles have a mean diameter of ca. 7.2 nm. Figure 3d lists DLS measurements, where the hydrodynamic diameter ( $D_h$ ) is ca. 189 nm and 200 nm for PMAEFc-b-PNIPAM micelles and AuNPs-PMAEFc-b-PNIPAM hybrid copolymer micelles, respectively. Additionally, the TEM images of their hybrids demonstrated the formation of core-shell structures in solvents such as: aqueous solution, a mixture of n-hexane and methanol with THF.

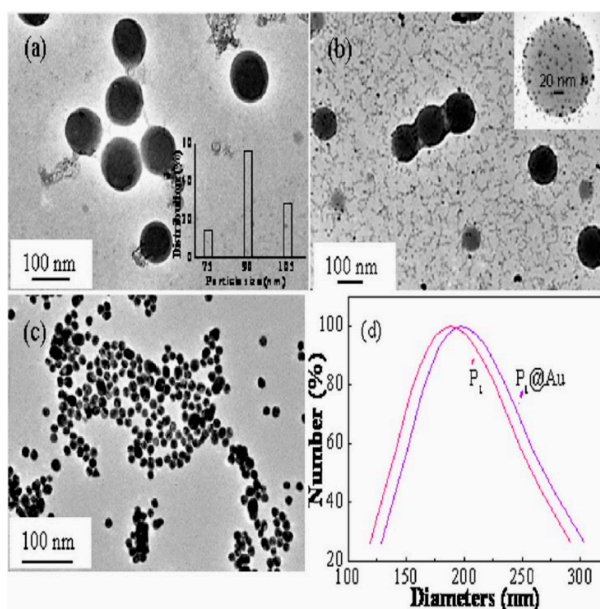


**Figure 3.** TEM images of (a) typical P1 micelles (Inset: size distribution histogram); (b) P1@Au micelles; (c) Au NPs; and (d) hydrodynamic diameters and particle size distribution of typical P1 and P1@Au copolymer micelles (All the micelles have a concentration of  $0.5 \text{ mg mL}^{-1}$  in aqueous solution). Reproduced from Reference [79] with permission from the Elsevier B.V. © 2018.

In order to prepare thermally stable AuNPs, azide groups ( $-N_3$ ) have been introduced into polymeric ligands formed by cross-linked polystyrene (PS) and azido-polystyrene (PS- $N_3$ ) blocks (P(S-b-S- $N_3$ )-AuNPs). The P(S-b-S- $N_3$ )-AuNPs were dispersed in PS and PS/Poly(methyl methacrylate) blends. TEM images indicated that, as the wt.% of AuNPs increases, the interfacial width of the AuNPs layer increases. The investigation also showed that the P(S-b-S- $N_3$ )-AuNPs were localized at the interface of PS and PMMA, which reduced the interfacial tension; this suggests that the function of AuNPs as compatibilizer in polymer blends [80]. Recently, di-block copolymer micelles formed between benzyl alcohol and poly- $\epsilon$ -caprolactone (BenzA)-b-(PCL) assembled core-shell structures to house the particular shape of AuNPs. The pH-sensitive system was applied in the release of the anticancer drug doxorubicin hydrochloride (DOX) [81]. Another method for preparing AuNPs is with a polymer cross-linked network, where the amide groups of polyacrylamide (PAAm) acted as reductant and template. AuNPs were in-situ synthesized into spherical PAAm cross-linked microgels [82]. The procedure consisted of a two-stage synthesis process: (1) the PAAm microgels were first synthesized by the semi-continuous inverse heterophase polymerization (SIHP) process under monomer-starving

conditions, which allowed to obtain a controlled molecular weight, a low particle size, and a high solids content, and (2) dried microgels were loaded with aqueous solutions of  $\text{HAuCl}_4$  at different concentrations and the reduction took place inside the microgels at 25 °C. These authors reported particles sizes, as observed by TEM, of 17–19 nm, where the diameter increases with  $\text{HAuCl}_4$  concentration, whereas the microgels exhibited a quasi-spherical shape with diameters of  $102 \pm 11$  nm. Table 6 summarizes some reports on particle sizes in AuNPs systems by TEM.

**Table 6.** Summary of particle sizes in block-copolymer and homopolymer template/AuNPs systems by TEM.

| Block Copolymer and Homopolymer                 | Template Size [nm] | AuNPs Size [nm] | Additional Techniques Analyzed in Particle Size | Reference |
|---|--------------------|-----------------|---|-----------|
| <sup>a</sup> PMAEFc- <i>b</i> -PNIPAM           | 90 ± 15            | 5.5–14.0        | DLS   | [79]      |
| <sup>b</sup> P(S- <i>b</i> -S-N <sub>3</sub> )  | 2.5 ± 1.5          | -               | -   | [80]      |
| <sup>c</sup> P4VP- <i>b</i> -PS- <i>b</i> -P4VP | 440 ± 80           | 7.61–11.6       | DLS   | [83]      |
| <sup>d</sup> BenzA- <i>b</i> -PCL               | 36 ± 9             | ~18.0           | -   | [81]      |
| <sup>e</sup> PS- <i>b</i> -PVP                  | 29 ± 6             | 2.0–6.0         | AFM   | [84]      |
| <sup>f</sup> PI- <i>b</i> -PEO                  | 34 ± 3             | -               | DLS   | [85]      |
| <sup>g</sup> PCL- <i>b</i> -PEO                 | 40.2 *             | 15.3 ± 1.4      | DLS   | [86]      |
| <sup>h</sup> HES-g-PMA                          | -                  | 16–20           | -   | [52]      |
| <sup>i</sup> COS-PTX                            | -                  | 42–76           | DLS   | [43]      |
| <sup>j</sup> PAAm                               | 102 ± 11           | 17–19           | -   | [82]      |

\* Calculated after a stain treatment.

<sup>a</sup> Poly(2-methacryloyloxyethyl ferrocenecarboxylate)-block-poly(*N*-isopropylacrylamide).

<sup>b</sup> Polystyrene-block-azido-polystyrene.

<sup>c</sup> Poly(4-vinylpyridine)-block-polystyrene-block-poly(4-vinylpyridine)

<sup>d</sup> Benzyl alcohol-block-poly-ε-caprolactone.

<sup>e</sup> Poly(styrene)-block-poly(vinylpyridine)

<sup>f</sup> Poly(isoprene)-block-poly(ethylene oxide).

<sup>g</sup> Poly(caprolactone)-block-poly(ethylene oxide).

<sup>h</sup> Hydroxyl ethyl starch-g-poly(methylacrylate).

<sup>i</sup> Chitosan oligosaccharide (COS)-Paclitaxel.

<sup>j</sup> Polyacrylamide.

#### 4.1.2. Atomic Force Microscopy, (AFM)

It remains a challenge to optimize the shape and size of AuNPs by employing block copolymers. Atomic Force Microscopy (AFM) has been used to obtain imaging the surface of the atoms and molecules, and even perform the sample, which was conductive, semi-conductive or nonconductive [87]. Sabir et al. [88] demonstrated the formation of polydisperse gold nanoparticle in AFM images. AuNPs directly depend on copolymer molecular weight, in that the authors analyzed by the addition to the systems of Pluronic L31 and F68 mixtures; AFM measurements identified compact aggregates below 10 nm with mean height. On the other hand, the traditional approaches using AuNPs as fillers of block copolymers continues to be renovated as presented in a recent study, in which the authors synthesized polystyrene-block-poly(ethylene oxide) (PS-*b*-PEO) di-block copolymer (BCP) and AuNPs via solvent-based processing for preparing the following: (1) BCP copolymerized with poly(ethylene oxide) (PEO) and AuNPs in order to assemble the (BCP-Au-PEO) system, and (2) BCP copolymerized with polystyrene (PS) and AuNPs (BCP-Au-PS). In order to observe these systems with AFM, the authors prepared toluene-solution films of copolymers with spin-coating technique in a toluene solution. The images showed that both composites exhibit cylindrical morphology, the BCP-Au-PEO system presents a hexagonal arrangement, whereas for the BCP-Au-PS system, the AuNPs were selectively localized at the center [89]. In this work, the goal was to analyze the topographic surface of thin films after plasma O<sub>2</sub> etching exposure to a greater degree extent than monitoring the location of the nanoparticles.

The control of AuNPs size at a specific location is now possible with oriented phases of block copolymers. AuNPs were synthesized using poly(styrene)-*b*-poly(vinylpyridine) (PS-*b*-PVP) with a process in which a substrate was used perpendicularly or parallel to the copolymer in the reduction of gold. This method promised the achievement of anisotropic geometries of valuable interest for optics [84].

Dendronized structures formed by copolymerization are the subject of recent research in Materials Science, since the application of smart materials such as sensor and catalyst have increased. Recently Liu et al. [90] synthesized bulky hydrophilic triethylene glycol (TEG) and hydrophobic ferrocenyl (Fc) (TEG-*b*-Fc), later employed as stabilizers of gold and silver nanoparticles. AFM images were used to analyze the formation of micelles in Tetrahydrofuran (THF) and Dimethyl sulfoxide (DMSO) as solvents.

An innovative sensor application of a nano-thin block copolymer brush-layer film was recently developed by Zhu et al. [91]. AuNPs were deposited onto polystyrene-block-poly(4-vinylpyridine) (PS-*b*-P4VP) films, which was previously adsorbed on glass nanofibers. AFM analyzed the roughness and thickness of the PS-*b*-P4VP. AFM results showed that there is not surface pattern after coating the glass nanofiber and the height profile of the block, with a copolymer layer thickness of 3 nm. In comparison, particle sizes of AuNPs and hybrid block copolymer micelles with AuNPs obtained by AFM are presented in Table 7.

**Table 7.** Summary of particle sizes in block-copolymer template/AuNPs systems by AFM.

| Template                          | Template Size [nm]                | AuNPs Size Range [nm] | Additional Techniques Analyzed in Particle Size | Reference |
|-----------------------------------|-----------------------------------|-----------------------|---|-----------|
| <sup>a</sup> PS- <i>b</i> -PVP    | 29 ± 6                            | 2–10                  | TEM   | [84]      |
| <sup>b</sup> L31-F68              | 9 ± 2<br>59 ± 8                   | 2–5                   | FESEM, STEM, TEM, DLS, SLS                      | [88]      |
| <sup>c</sup> PS- <i>b</i> -PEO    | ~11                               | 5                     | -   | [89]      |
| <sup>d</sup> TEG- <i>b</i> -Fc    | 110 ± 30 (DMSO)<br>150 ± 35 (THF) | -                     | SEM, DLS  | [90]      |
| <sup>e,*</sup> PS- <i>b</i> -P4VP | -                                 | 46–52 **              | -   | [91]      |

\* AuNPs were deposited on PS-*b*-P4VP films. \*\* Measurement done by UV-Vis spectroscopy and SEM. <sup>a</sup> Poly(styrene)-block-poly(vinylpyridine). <sup>b</sup> Pluronic L31 (EO2–PO16–EO2) and Pluronic F68 (EO78–PO30–EO78) mixtures. <sup>c</sup> Polystyrene-block-poly (ethylene oxide). <sup>d</sup> Triethylene glycol-block-ferrocenyl. <sup>e</sup> Polystyrene-block-poly(4-vinylpyridine).

#### 4.2. Spectroscopic Method: UV-Visible Spectroscopy, (UV-Vis)

The driving forces of the electronic level in individual atoms and their interaction with other species can be elucidated with spectroscopic techniques. Optical-based spectroscopy is substantiated in the Bohr-Einstein frequency relationship, which establishes relations in the electronic states of species, due to that they absorbing or emitting radiation at a specific wavelength [92].

UV-Vis spectrophotometry measures the absorption spectra of the individual gold nanoparticles, which are related with surface plasmon resonance, because of the strong interaction between the beam and the delocalized electrons on the nanoparticles surface [93]. The formation of AuNPs may be followed by the shift of the plasmon in UV-Vis spectroscopy. Gold nanoparticles synthesized in a liquid solution of 2-anthracene sulfonate (2-AS) presented a surface plasmon band at ca. 535, and ca. 530 nm in the presence of water-soluble micelles of Pluronic P123 and Pluronic F127; this hybrid material was obtained by Rakshit et al. [94]. The intermediate species formed during the reduction process of the AuNPs precursor were identified by Ray and Aswal. These authors identified a peak at ca. 230 nm, indicating the presence of non-associated Au ions; a peak at ca. 310 nm corresponds to the presence of Au atoms coexisting with AuNPs in Pluronic P85 block copolymer micelles. The presence of AuNPs was confirmed with a peak located at 540 nm [95]. On the other hand, Pluronic F127 micelles functionalized with thiol groups were cross-linked with AuNPs at different ratios to form a core-shell structure. In order to measure the binding degree of AuNPs onto the thiol-functionalized F127-SH micelles by UV-Vis measurements, it was added to the solutions cysteamine as precipitator. Results exhibited that the addition of cysteamine to the system led to aggregate unbounded gold nanoparticles. UV-Vis absorption spectra revealed decreased absorbance as a consequence of cysteamine addition, in which

the red-shift occurred at 508–540 nm [96]. It is worth mentioning that gold nanoparticle aggregation seriously affects the plasmon absorption band. An investigation conducted by Kuo and Yang [97] concluded that AuNPs aggregation turned into a red shift on the absorption band because neighbor particles affect the coupling of electronic interactions. These authors synthesized a hybrid material formed by epoxidated poly(styrene-block-vinyl oxirane) di-block copolymer and gold nanoparticles (PS-*b*-PBO/AuNPs) at different concentrations. Kuo and collaborator studied different concentrations of the curing agent Poly(ethylene oxide bisamine) (D230), in order to control the crosslinking degree of PS-*b*-PBO/AuNPs, for studying the inter-particle distance of AuNPs in the copolymer. As shown in Figure 4, the lower concentration of the D230 into the PS-*b*-PBO/AuNPs composite permitted intimate contact among the gold nanoparticles, causing a red-shift plasmon band.

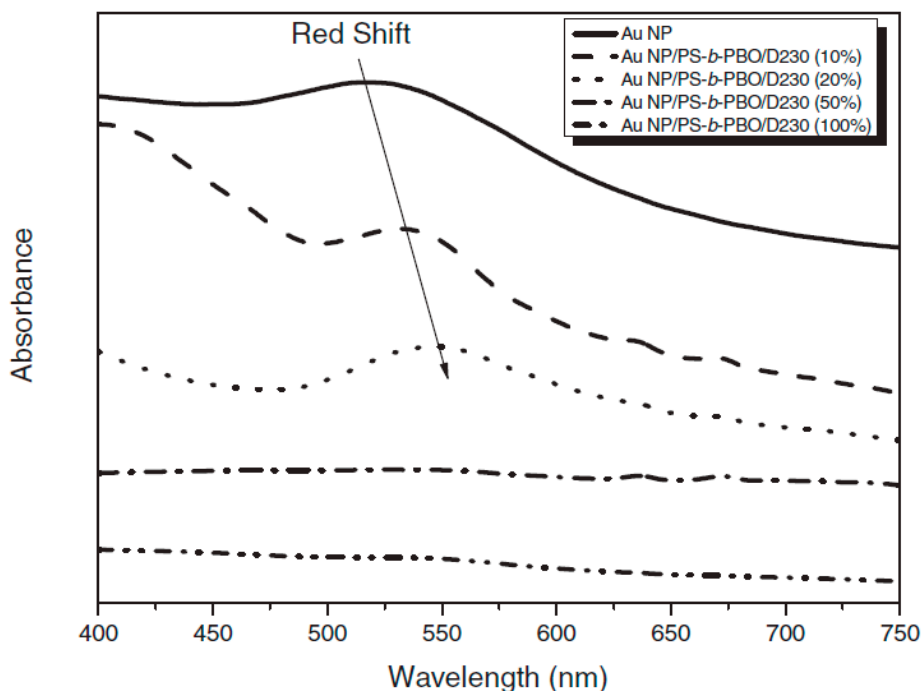


**Figure 4.** UV-Vis spectra of Au NP/PS-*b*-PBO composites with different amounts of D230 curing agent at 3 wt.% of AuNPs. Reproduced from Reference [97] with permission from the WILEY-VCH Verlag GmbH & Co. KGaA, Weinheim © 2011.

The growth process of AuNPs in individual micelles from nanosheets to large sheets is a commonly faced problem. Coating AuNPs with poly(caprolactone)-*b*-poly(ethylene oxide) (PCL-*b*-PEO) di-block copolymers is a proposed strategy that undergoes the growth process. UV-Vis spectra analyzed how PCL crystallization directly affect the AuNPs growth, where absorption bands at 520, 620, 680, and 710 nm were identified for AuNPs, clusters, cylinders, and sheet morphologies in the growth of gold systems [86]. On the other hand, Tepale et al. [36], analyzed the structural behavior of P103-AuNPs at different block copolymer concentrations (10, 15 and 20 wt.%), and different synthesis temperatures (30, 35 and 50 °C). Figure 5 describes how AuNPs size is affected by the wt.% of Pluronic P103. At 30 °C, the maximum intensity absorbance ( $I_{max}$ ) measured at 540 nm, increased with increasing the Pluronic P103 concentration, and a slight shift on the absorption band to larger wavelength is observed in inset an in Figure 5. On the other hand, increasing the synthesis temperature to 35 °C and at 10 wt.% of Pluronic P103, an absorption band at ca. 548 nm was observed, indication the presence of AuNPs (inset b in Figure 5). Moreover, increasing the Pluronic P103 concentration at 15 wt.%, a second absorption band was observed at ca. 740 nm which the authors attribute to the self-aggregation of independent large colloidal AuNPs produced by the increase of nucleation centers. This behavior

was related to the formation of polymer-like micelles of Pluronic P103, where its aggregation number increases which allowed the formation of cavities and subsequently AuNPs. At temperature reduction of 50 °C (inset c in Figure 5), the authors demonstrated the non-dependency between the polymer concentration and the maximal intensity absorbance band, maintaining the nucleation centers of AuNPs constant. Table 8 presents a summary of the variation of plasmon band location in the UV-Vis spectroscopy measurements of AuNPs stabilized with different block copolymers.

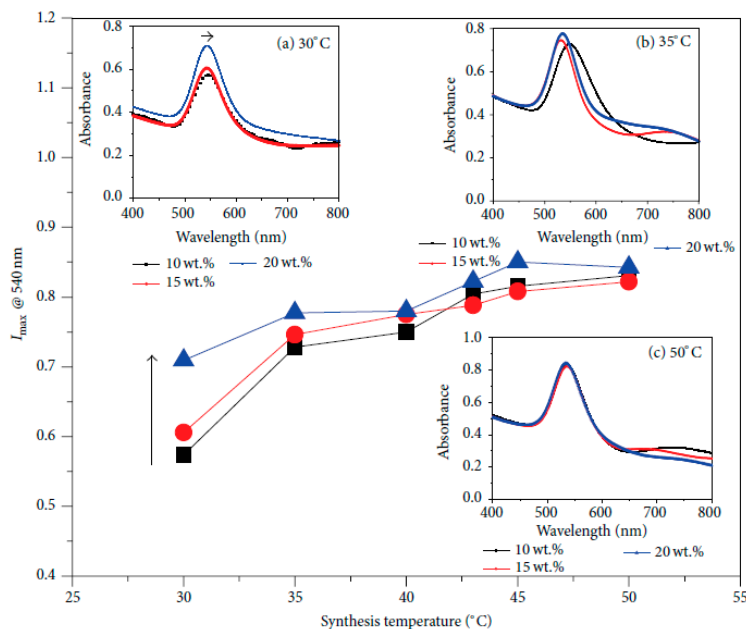


**Figure 5.** Intensity of the UV-Vis absorbance peak measured at 540 nm versus synthesis temperature for HAuCl<sub>4</sub> and P103 aqueous solutions at different concentrations: (■) 10wt.%; (●) 15wt.%; and (▲) 20wt.%. Insets show UV-visible scans of HAuCl<sub>4</sub>-P103 aqueous solutions. Reproduced from Reference [36] with permission from the Hindawi Publishing Corporation.

**Table 8.** UV-Vis plasmon band location of AuNPs for different block-copolymer templates.

| Copolymer Template                                    | Plasmon Band Location of AuNPs [nm] | Reference |
|---|-------------------------------------|-----------|
| <sup>a</sup> P123                                     | ~535                                | [94]      |
| <sup>b</sup> F127                                     | ~530                                |           |
| <sup>c</sup> P85                                      | ~540                                | [95]      |
| F127  | ~508                                | [96]      |
| <sup>d</sup> PS- <i>b</i> -PBO                        | ~521                                | [97]      |
| <sup>e</sup> MPEG- <i>b</i> -PNIPAAm- <i>b</i> -PN(+) | ~550                                | [98]      |
| <sup>f</sup> PEG- <i>b</i> -PDEAEM                    | ~534                                | [99]      |
| <sup>g</sup> PVEIM- <i>b</i> -PNIPAM                  | ~525                                | [100]     |

<sup>a</sup> Pluronic P123 (PEO<sub>19</sub>PPO<sub>69</sub>PEO<sub>19</sub>). <sup>b</sup> Pluronic F127 (PEO<sub>100</sub>PPO<sub>65</sub>PEO<sub>100</sub>). <sup>c</sup> Pluronic P85 (EO<sub>26</sub>PO<sub>39</sub>EO<sub>26</sub>). <sup>d</sup> Poly(styrene-*b*-butadiene). <sup>e</sup> Methoxy-poly (ethylene glycol)-*b*-poly(*N*-isopropylacrylamide)-*b*-poly((3-acrylamidopropyl) trimethyl ammonium chloride). <sup>f</sup> Polyethyleneglycol-*b*-poly (*N,N'*-diethylaminoethyl methacrylate). <sup>g</sup> Poly(1-vinyl-3-ethylimidazolium bromide)-*b*-poly(*N*-isopropylacrylamide).

#### 4.3. Light Scattering Method: Dynamic Light Scattering, (DLS)

An important technique to determine particle size in solutions is with dynamic light scattering (DLS). DLS encompasses all of the light scattering methods that inform concerning molecule movement between those can be found the photon correlation spectroscopy (PCS) and the quasielastic light scattering (QLS) [101]. An important approach in the formation of hybrid AuNPs-block copolymer

materials is based in the synthesis of “smart” materials, which responds to certain stimuli, for example, changes in pH or temperature. Shi et al. [102] measured the hydrodynamic diameter ( $D_H$ ) as a function of the temperature of hybrid AuNPs assembled with poly(*N*-isopropylacrylamide)-block-poly(2-succinyloxyethyl methacrylate) (PNIPAM-*b*-PSEMA). The  $D_H$  of hybrid AuNPs decreased from ca. 207 to ca. 182 nm, while the temperature rose from 25 to 40 °C at a constant pH, due to a second-order broad phase transition of the PNIPAM block.

New hybrid thermo-responsive material formed by methoxy-poly(ethylene glycol)-block-poly(*N*-isopropylacrylamide)-block-poly((3-acrylamidopropyl) trimethyl ammonium chloride) (MPEG-*b*-PNIPAAM-*b*-PN(+)) and AuNPs tend to self-associate by increasing the temperature, where a decrease in the hydrodynamic radius was reported [98]. The solvents used in DLS measurements of hybrid nanomaterials reflect important changes in the values obtained. The alcoholic medium formed by ethanol and isopropanol and copolymer poly(ethylene glycol)-block-poly(*N,N'*-diethylaminoethyl methacrylate) (PEG-*b*-PDEAEM) were used for the synthesis of AuNPs [99], where the  $D_H$  of micelles resulted as stimulated by differences in the alcoholic medium. Bio-applications of AuNPs encounter important limitations, and research efforts are being engaged in find the mechanism of biocompatibility for absorption. Scarabelli et al. [85] presented a protocol for control AuNPs encapsulation covered by a block polymer shell with high stability in oxidizing and ionic environments. AuNPs were directly synthesized using the poly(isoprene)-block-poly(ethylene oxide) (PI-*b*-PEO) copolymer. In addition, Pluronic F127 has been used to prepare AuNPs with different morphologies, i.e., Pluronic F127 core-shell AuNPs and Pluronic F127-Au nanohybrid particles. Simon et al. [103] prepared Pluronic F127 core-shell AuNPs with a hydrodynamic diameter of ca. 35 nm by employing a two-step synthesis method. These authors utilized DLS to demonstrate the formation of core-shell type structures, where the Pluronic F127 shell was attached to the AuNPs surface by hydrophobic interactions. The authors reported that the hydrodynamic diameter of oleylamine-capped AuNPs and Pluronic F127 core-shell AuNPs were 13.48 nm ± 0.24 nm and 34.75 nm ± 1.56 nm, respectively, where the size difference of ca. 10 nm was attributed to the Pluronic F127 shell, whereas, others have reported the formation of AuNPs inside of Rhodamine B (Rh B) doped F127 nanohybrids. Their DLS results are shown in Figure 6, where it is observed that the  $D_H$  of F127-AuNPs nanohybrids prepared with 5 wt.% of Pluronic F127 was ca. 24 nm at 25 °C, and the average diameter of Pluronic F127 micelles increased with the concentration of the gold solution. The authors attributed this result to the formation of F127-AuNPs nanohybrids and the increase in their size of micellar aggregates [63].

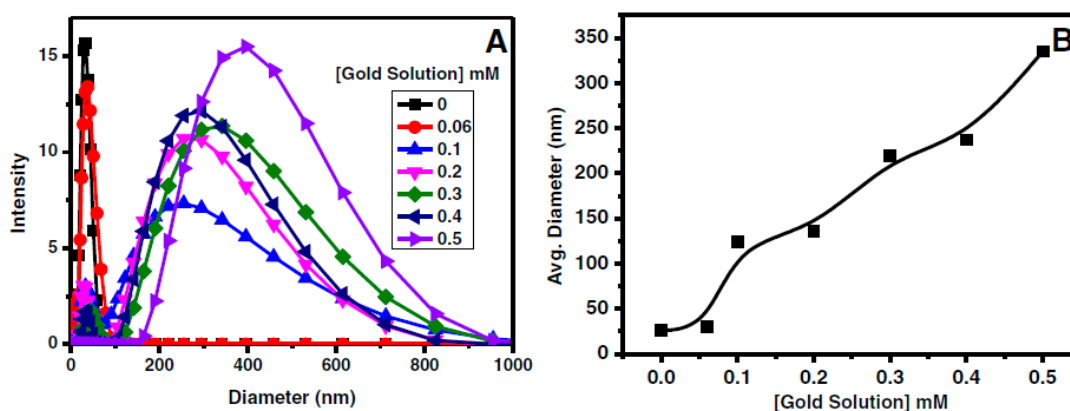


**Figure 6.** (A) DLS plot for distribution of hydrodynamic diameter of F127-AuNPs nanohybrid system with increase in concentration of gold solution; (B) DLS plot for the variation of mean diameter of F127-AuNPs nanohybrid system vs. gold concentration in solution (F127 of 5 wt.%). Reproduced from Reference [63] with permission from the Elsevier B.V. © 2016.

On the other hand, the use of polymers such as chitosan as a reducing and stabilizing agent has been reported. For instance, Manivasagan et al. [43] reported the hydrodynamic particle size of  $61.86 \pm 3.01$  measured by DLS for AuNPs prepared with chitosan oligosaccharide (COS). Also, Parveen and Tremiliosi-Filho reported the environment-friendly synthesis of AuNPs using crude glycerol (CG), Polyvinylpyrrolidone (PVP), and Polydiallyldimethylammonium chloride (PDAC), for which particle sizes were  $7 \pm 2$ , 6.1, and  $8 \pm 2$  nm, respectively [33]. Table 9 compares the hydrodynamic radii and diameters of the previously discussed hybrid nanomaterials. The hydrodynamic radii was calculated using the Stokes-Einstein equation, which is related with the diffusion coefficient [104].

**Table 9.** Summary of particle sizes in block-copolymer and homopolymer template/AuNPs systems by DLS.

| Template   | Hybrid Particle Size $R_h$ <sup>†</sup> [nm] | AuNPs Size $R_h$ [nm] | Hybrid Particle Size $D_H$ <sup>††</sup> [nm] | AuNPs Size $D_H$ [nm] | Reference |
|--|--|-----------------------|---|-----------------------|-----------|
| <sup>a</sup> PI- <i>b</i> -PEO (1:2.5) *               | -  | -                     | 112 ± 45                                      | 19 ± 2.0              | [85]      |
| <sup>b</sup> TEG- <i>b</i> -Fc                         | -  | -                     | 288 (THF)<br>219 (DMSO)                       | -                     | [90]      |
| <sup>c</sup> AuNPs- F127 (Core-shell)                  | -  | -                     | 34.75 ± 1.56                                  | 13.48 ± 0.24          | [103]     |
| F127- AuNPs  | -  | -                     | 24  | -                     | [63]      |
| <sup>d</sup> MPEG- <i>b</i> -PNIPAAm- <i>b</i> -PN (+) | 200 ± 100.0                                  | 22 ± 0.0              | -   | -                     | [98]      |
| <sup>e</sup> PEG- <i>b</i> -PDEAEM                     | -  | -                     | 45 (ethanol)<br>74 (isopropanol)              | 27 ± 3.0              | [99]      |
| <sup>f</sup> PNIPAM- <i>b</i> -PSEMA                   | -  | -                     | 208 (20 °C)<br>182 (40 °C) **                 | 14.1 ± 1.3            | [102]     |
| <sup>g</sup> COS-PTX                                   | -  | -                     | -   | 61.86 ± 3.01          | [43]      |
| <sup>h</sup> CG  | -  | -                     | -   | 7 ± 2                 | [33]      |
| PVP  | -  | -                     | -   | 6.1                   |           |
| PDAC   | -  | -                     | -   | 8 ± 2                 |           |

<sup>†</sup> Hydrodynamic ratio, calculated with the Stokes-Einstein equation. <sup>††</sup> Hydrodynamic diameter. \* The study analyzed different proportions of block copolymers. \*\* The value in parenthesis corresponds to a specific temperature measurement. <sup>a</sup> Poly(isoprene)-block-poly(ethylene oxide). <sup>b</sup> Triethylene glycol-block-ferrocenyl. <sup>c</sup> Pluronic F127 (PEO<sub>100</sub>PPO<sub>65</sub>PEO<sub>100</sub>). <sup>d</sup> Methoxy-poly(ethyleneglycol)-block-poly(*N*-isopropylacrylamide)-block-poly((3-acrylamidopropyl) trimethyl ammonium chloride). <sup>e</sup> Polyethyleneglycol-block-poly (*N,N'*-diethylaminoethyl methacrylate). <sup>f</sup> Poly(*N*-isopropylacrylamide)-block-poly (2-succinyloxyethyl methacrylate). <sup>g</sup> Chitosan oligosaccharide (COS)-Paclitaxel. <sup>h</sup> Crude glycerol.

#### 4.4. X-ray Spectroscopy: X-Ray Diffraction, XRD

The study of crystalline structures in solid materials provides evidence on the manner in which their physicochemical states behave. Techniques based on X-ray spectroscopy aid in elucidating properties such as electronic chemical states or the structural arrangement by detecting the dispersed energy from a sample irradiated with X-rays [105].

Das et al. [52] prepared AuNPs by means of an environmentally friendly process using a biodegradable copolymer synthesized by the graft polymerization of hydroxyl ethyl starch (HES) and methylacrylate (MA). The authors reported the characteristic peaks of AuNPs at  $2\theta$  values of  $38.48^\circ$ ,  $44.54^\circ$ , and  $64.88^\circ$ , which corresponds to the (111), (200), and (220) planes, respectively, indicating that AuNPs had the structural type of face centered cubic (fcc). Others have showed diffraction peaks at  $2\theta = 38.23^\circ$ ,  $44.58^\circ$ ,  $64.89^\circ$ , and  $77.81^\circ$  which corresponds to the planes of (111), (200), (220), and (311), respectively, for AuNPs synthesized using chitosan oligosaccharide (COS) loaded with Paclitaxel (PTX) used as anticancer drug [43]. Parveen and Tremiliosi-Filho [33] reported the environmentally friendly synthesis of AuNPs using crude glycerol (CG) extracted from a plant

that produces biodiesel. These authors found diffraction peaks at  $2\theta = 38.2^\circ, 44.3^\circ, 64.6^\circ, 77.6^\circ,$  and  $81.7^\circ$ , corresponding to the (111), (200), (220), (311), and (320) planes, indicating an fcc structure of Au, respectively. The authors compared the size of AuNPs prepared with the CG extracted from the biodiesel plant and commercial CG using the Scherrer equation, where the size of both AuNPs was  $13 \pm 3$  nm. On the other hand, several shapes of AuNPs have been reported, among these attention has been paid recently to the multi-branched nanoflowers (AuNFs). Kariuki et al. [53] in 2017 synthesized AuNFs with the polymer pyromellitic dianhydride-p-phenylene diamine (PPDDs) as a precursor. The authors found that the sizes of AuNFs depended on the PPDDs concentration, i.e., at a medium concentration of PPDDs, spherical NPs were formed. From the XRD results, AuNFs XRD patterns showed peaks of (111), (200), (220), (311), and (222), which was characteristic of fcc and polycrystalline structures. Moreover, the intensity ratio between the peaks (111)/(200) was 2.21, which is larger than that of spherical AuNPs (1.9), the latter attributed to a preferential growth of AuNFs (111) [53]. Furthermore, Feng et al. [106] obtained crystalline AuNPs by centrifuging aqueous solutions of poly (*N*-isopropylacrylamide)-*b*-poly(ethyl acrylate) (PNIPAM-*b*-PEA) and poly(2-(dimethylamino)ethyl acrylate) (PDMAEA) to form PNIPAM-*b*-(PEA-*g*-PDMAEA)-AuNPs. In this work, the authors obtained the typical gold nanoparticles diffraction pattern at  $2\theta = 38.3^\circ, 44.3^\circ, 64.8^\circ, 77.9^\circ,$  and  $81.8^\circ$ , and they also compared the size of gold nanoparticles from data using the Scherrer equation (5.6 nm) with the value obtained by TEM (6.1 nm). Sanches et al. [107] reported the formation of hybrid composites containing polyaniline and AuNPs by using sodium citrate (CITRATE) as reducing agent and polyaniline emeraldine-salt form (ES-PANI) as stabilizer. The XRD pattern exhibited an amorphous structure where broad peaks centered at  $2\theta = 11.9^\circ$  and  $23.4^\circ$  were observed due to ES-PANI, and peaks at  $2\theta = 38, 44^\circ,$  and  $65^\circ$  were attributed to the presence of AuNPs (Figure 7). These authors suggested the formation of a complex between the AuNPs and ES-PANI (ES-PANI/Au-CITRATE), where the polyaniline molecules coated the Au-CITRATE NPs, due to attractive electrostatic interactions between the opposite charges [107].

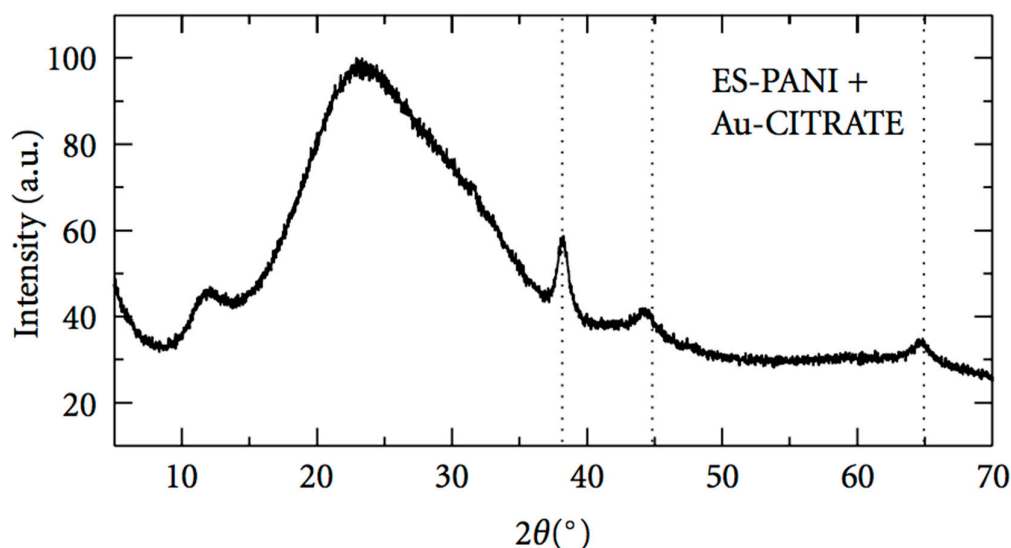


**Figure 7.** XRD patterns of complex of ES-PANI/Au-CITRATE NPs. Reproduced from Reference [107] with permission from the Hindawi Publishing.

#### 4.5. Electron Spectroscopy: X-Ray Photoelectron Spectroscopy, XPS

X-ray photoelectron spectroscopy (XPS) has been used to study the composition and the oxidation state of surfaces of AuNPs [40]. The green synthesis of luminescent AuNPs using *N*-(4-imidazolyl) methylchitosan (IMC), and the chitosan derivative biopolymer was reported by Nazirov et al. [78]. These authors followed the kinetics of  $\text{Au}^{+3}$  reduction by means of IMC with XPS. The authors found

that the reduction of  $\text{Au}^{+3}$  proceeds very slowly, in which the conversion to  $\text{Au}^0$  is not completed in 1 week. The XPS spectra showed broad peaks of Au  $4f_{7/2}$  and Au  $4f_{5/2}$  in the Au/IMC solution, indicating that gold is present in numerous oxidation states. Moreover, the XPS spectra deconvolution of Au  $4f_{7/2}$  in Au/IMC was 85.3–84.9 eV. The authors argued, that due to the ultra-small size of the AuNPs (2.3 nm), it was not possible to assign a lower oxidation state solely to the gold ions. The apparent binding energy of ultra-small AuNPs was found to be 1 eV higher than the bulk gold value of 84 eV. Thus, the authors suggest the possibility of the existence of  $\text{Au}^+$ -IMC complexes on the surface of AuNPs; these results suggest that the materials possess luminescent properties.

Biodegradable polymers such as mung bean starch (MBS) have been employed in the eco-friendly synthesis of AuNPs. Chairam et al. [40] utilized XPS spectra to explore the oxidation state values of AuNPs. Figure 8 presents the XPS spectra of MBS-AuNPs, where the survey spectrum of MBS-AuNPs demonstrated the existence of O1s, C1s, and Au4f (Figure 8A). Moreover, in Figure 8B, the Au4f core-level spectrum revealed one peak related to the core level of  $4f_{7/2}$  at 87.3 eV, attributed to the external surface of the atoms of Au of AuNPs bound to MBS. Another peak was observed at 83.7 eV, related to the spin-orbital splitting of  $4f_{5/2}$ , attributed to the inner atoms of Au of AuNPs. Also, the authors reported the presence of little  $\text{Au}^{+3}$  ions present in MBS, which were not reduced by the starch support. The authors found that the peaks shifted as compared with other works reported previously by Wu et al. [108], in which the authors attributed the accumulation of  $\text{Au}^0$  in the starch [40].

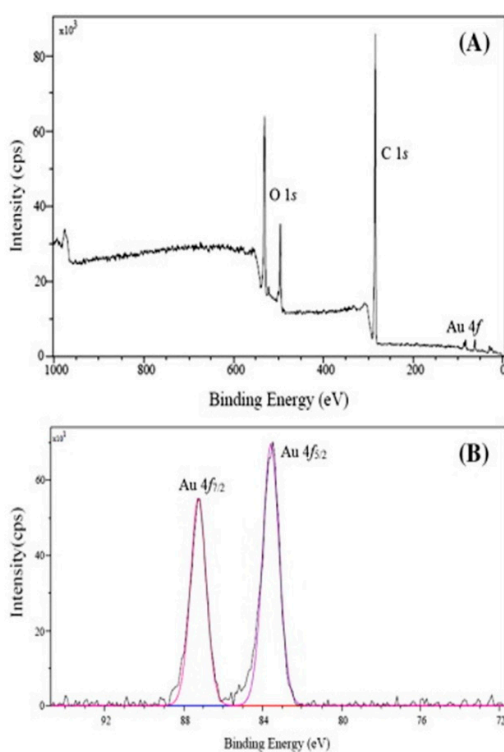


**Figure 8.** XPS spectra of MBS-AuNPs, (A) Survey scan spectrum; (B) Au 4f core-level spectrum. Reproduced from Reference [40] with permission from the CC BY-NC-ND. ©2015 King Saud University. Production and hosting by Elsevier B.V.

Other authors have synthesized AuNPs with polymers of di-or-tri-carboxylate-polyethylene glycol (PEG) accordingly the following combinations: (1) citrate-PEG (CPEG); (2) malate-PEG (MAP), and tartrate-PEG (TAP). XPS spectra were used to investigate AuNPs interactions with the CPEG, MAP and TAP polymers. The XPS spectra showed the existence of atoms of C, O, and Au for all of the systems studied. For the CPEG-AuNPs system, Au4f core-levels exhibited the spin-orbital splitting

of  $4f_{7/2}$  at 83.9 eV and  $4f_{5/2}$  at 87.5 eV; whereas for the MAP-AuNPs system, it presented the  $4f_{7/2}$  at 83.9 eV and  $4f_{5/2}$  at 87.5 eV. Moreover, the deconvolution confirmed the  $\pi$  conjugation of AuNPs with the oxygen of the C–O–C and –C=O functional groups of CPEG, MAP, and TAP polymers [41].

On the other hand, XPS analysis can also be accomplished in thin films, carried out by Liu et al. [109] did. These authors used polystyrene-block-poly (methyl methacrylate) (PS-*b*-PMMA) as templates to produce AuNPs compactly packed in arrays of one and two dimensions. In this work, carbon bonds were significantly modified after plasma etching demonstrated with a decrease in intensity of the peaks. In addition, nano-porous membranes of poly (2-dimethylaminoethyl methacrylate) and polystyrene (PDMAEMA-*b*-PS) were employed to immobilize the anchoring by AuNPs of Au precursors by tertiary amine groups. This anchoring was possible due to the tortuous channels into the block copolymer membranes. A notable phenomenon occurred during the swelling process with AuNPs precursor. PDMAEMA chains enriched the surface of pore-wall membranes shown by an increase in N content in pores during the swelling process, which is accompanied by attaching spots for AuNPs immobilization. XPS measurements evidence the phenomena that involves the change of surface composition during the swelling treatment, where the observation of one peak at 400 eV was related to N 1s in the PDMAEMA chains [110]. The use of block copolymer as AuNPs stabilizer has been extensively studied; however, innovative studies have been recently approached in the stabilization of complex systems such as the use of graphene oxide and AuNPs. Chen et al. [100] utilized poly(1-vinyl-3-ethylimidazolium bromide) and poly(*N*-isopropylacrylamide) (PVEIM-*b*-PNIPAM) block copolymer to form well distributed AuNPs on the surface of reduced graphene oxide. The hybrid system was catalytically thermo-responsively active for the reduction of 4-nitrophenol. The XPS spectra demonstrated the binding interaction of each component of the hybrid system. On the other hand, Polystyrene-block-poly-2-vinylpyridine (PS-*b*-P2VP) was employed as template to obtain AuNPs of 5 nm in a system used in bio-medics for DNA origami attachment. XPS spectra revealed a highly oxidized gold state in 87.5 eV; a displacement to the lower binding energy of Au  $4f_{7/2}$  electrons indicated that the reduced gold continued to remain in the copolymer micelle after plasma etching, resulting in a selective behavior of AuNPs attached to the modified DNA [111]. Binding energy values of the hydrocarbon constituents is summed up in Table 10.

**Table 10.** Summary of binding energy values in block-copolymer and homopolymer AuNPs systems from XPS.

| Template                             | Au (4f) [eV] | N (1s) [eV] | O (1s) [eV] | C (1s) [eV] | Carbon in the Methoxy Group [eV] | Carbon in the Ester Group [eV] | Aromatic Rings [eV] | Reference |
|--------------------------------------|--------------|-------------|-------------|-------------|----------------------------------|--------------------------------|---------------------|-----------|
| <sup>a</sup> PVEIM- <i>b</i> -PNIPAM | ~80          | ~400        | ~540        | ~290        | -                                | -                              | -                   | [100]     |
| <sup>b</sup> PS- <i>b</i> -PMMA      | -            | -           | -           | 284.6       | 286.8                            | 289.0                          | 291.7               | [109]     |
| <sup>c</sup> PDMAEMA- <i>b</i> -PS   | -            | ~400        | -           | -           | -                                | -                              | -                   | [110]     |
| <sup>d</sup> PS- <i>b</i> -P2VP      | 84.5         | -           | -           | -           | -                                | -                              | -                   | [111]     |
| <sup>e</sup> MBS                     | 83.7         | -           | -           | -           | -                                | -                              | -                   | [40]      |
| <sup>f</sup> TAP-PEG                 | 83.9         | -           | -           | -           | -                                | 288.1                          | -                   | [41]      |

<sup>a</sup> Poly(1-vinyl-3-ethylimidazolium bromide)-block-poly(*N*-isopropylacrylamide). <sup>b</sup> Polystyrene-block-poly (methyl methacrylate). <sup>c</sup> Poly(2-dimethylaminoethyl methacrylate)-block-polystyrene. <sup>d</sup> Polystyrene-*b*-poly-2-vinylpyridine.

<sup>e</sup> Mung bean starch. <sup>f</sup> Tartare-polyethylene glycol.

#### 4.6. Synchrotron X-Ray: Small-Angle X-Ray Scattering, (SAXS)

Structural characterization is fundamental to understanding the mechanism of particle nucleation and growth. At present, there is little information of the mechanism of reaction, including how nucleation and growth are, mainly in studies on nanoparticles immersed in a liquid. The SEM and TEM techniques are very efficient in dried samples; however, synchrotron X-ray beams are more compatible with liquid-phase reactions due to the penetration power of X-rays in liquids and air [112]. SAXS allows

the investigation of the different factors that affect the mechanism of nucleation of nanoparticles, such as the concentration and types of reducing agents and the synthesis temperature [113]. Particle nucleation and growth can be analyzed from seconds to microseconds [114] in order to provide information on the evolution of shape, size, and growth kinetics as a function of time [115]. The shape and size of AuNPs, as well as the reagents used to synthesize them, possess low toxicity in humans, permitting their use in medical and biological systems [116]. SAXS has been utilized to analyze the structural conformations of AuNPs synthesized by low-toxicity reagents. Poly(ethylenglicol) (PGE), chitosan, urea, choline chloride and a variety of pluronics comply with the requirements described previously. The kinetic synthesis of AuNPs through the reduction of Au with diluted acid solutions of chitosan was studied by SAXS [117]. The following two synthesis stages were observed: (1) at short times, scattering intensity changed considerably due to the formation of AuNPs and their consequently growth in size from 2.9 to 4.5 nm. Here, the amount of atoms is high and they are combined to form clusters. Then, the coalescence of the cluster takes place, followed of their coagulation, and (2) growth is slowed by insertion into formed particles [117]. Also, the effect has been investigated by SAXS of the  $\text{HAuCl}_4$ /chitosan molar ratio on the size of AuNPs [118]. The authors observed a subsequent increase in the size and heterogeneity of AuNPs as the concentration and ratio of  $\text{HAuCl}_4$ /chitosan increased [118]. SAXS analysis was employed by Dunlop et al. (2014) to demonstrate the formation of AuNPs stabilized with PEG in the presence of 2-diethylamino methacrylate (DEAMA). The authors reported the synthesis of AuNPs in one step, with a constant increase in total intensity during the reduction reaction in order to prepare nanoparticles with high polydispersity values [119]. Another mechanism of the reduction of AuNPs with trisodium citrate was analyzed by SAXS, where the complete reduction and the presence of intermediates were performed in four steps, consists of the following: (1) particle nucleation; (2) growth by aggregation; (3) slow particle growth, and (4) complete consumption of the precursor species [24]. Another important phenomenon can be explained by SAXS, in terms of studying how the polymeric matrix is structured among the nanoparticles. Köth et al. [25] demonstrated that the Au core is surrounded by a polymer shell; thus, synthesis must be conformed of functional polymers to stabilize these electrostatically or sterically and to avoid NPs aggregation or agglomeration.

#### 4.7. Flow Property Characterization: Rheology

In that the addition of metal nanoparticles to a liquid alters the way it flows, flow properties in hybrid nanomaterials have attracted attention for analyzing the flow behavior of these engineered nanomaterials, the latter used in important applications such as drug delivery systems in humans. Rheology principles are based on the application of a shear rate to a steady state system and measuring the shear stress, which results in viscosity variations [120]. Some additional variables can seriously affect the system's viscosity, such as temperature, nanoparticle morphology, size, and concentration, polymer concentration, etc., which modified the colloidal forces formed among the nanoparticles dispersed in the polymeric medium, especially in the semi-diluted regimen [121,122].

New applications of AuNPs such as drug delivery systems require a controlled release of the drug. Recently, studies have related the influenced on the rheological behavior of semi-diluted aqueous micellar solutions as a function of temperature and concentration. Tepale et al. [36] reported that viscosity in hybrid nanomaterials in aqueous solution was directly proportional to the block copolymer concentration utilized. In this study, AuNPs were synthesized, varying the synthesis temperature (30–50 °C), using  $\text{HAuCl}_4$  (2.0 mM) in block copolymer Pluronic P103 aqueous solutions (10, 15, and 20 wt.%); the mixing ratio of  $\text{HAuCl}_4$  to P103 was 1/9. Rheological measurements performed on hybrid gold/P103 nanomaterials in aqueous solutions were carried out at 30, 34, 37, and 40 °C. Figure 9 revealed that, when the polymer concentration diminished, the viscosity decreased. However, at 40 °C, viscosity exhibited an increase of nearly two orders of magnitude (Inset (a) in Figure 9). In all cases, the fluids presented a Newtonian fluid behavior. The changes were attributed to the modification in shape and sizes of the nanostructures caused by the synthesis temperature [36].

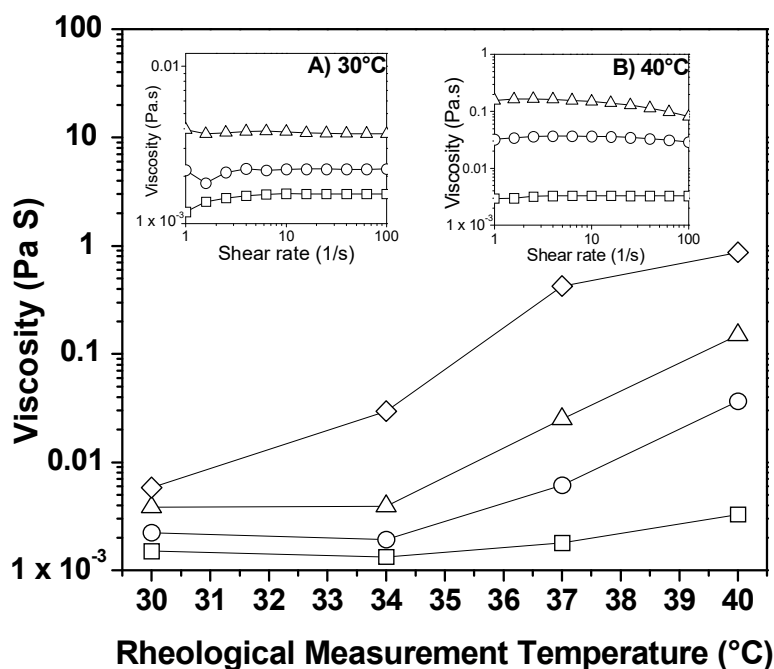


**Figure 9.** Zero-shear-rate viscosity vs. rheological measurement temperature of aqueous solution of 20 wt.% of P103 as reference ( $\diamond$ ), and solutions of hybrid nanomaterials with: ( $\Delta$ ) 20 wt.% of P103, ( $\circ$ ) 15 wt.% of P103 and ( $\square$ ) 10 wt.% of P103. All synthesized at 30 °C. Insets: viscosity vs. shear rate for the hybrid nanomaterials at the rheological measurement temperature of (a) 30 °C and (b) 40 °C. The line is a guide for the eye. Reproduced from Reference [36] with permission from the Hindawi Publishing Corporation.

Few studies have been conducted to describe how AuNPs affect the flow behavior of block copolymer systems [123,124]. Mendoza et al. [124] compared the rheology of the polystyrene-block-poly-4-vinylpyridine (PS-*b*-P4VP) di-block copolymer with and without AuNPs to analyze the macroscopic response under shear rate measurements, in order to obtain highly ordered 3-D patterns. In an initial work, Mendoza et al. [124] incorporated the HAuCl<sub>4</sub> precursor into the block copolymer system at three different ratios with respect to the number of pyridine groups (PS-*b*-(P4VP:HAuCl<sub>4</sub>)): 1:1; 4:3, and 2:1. Samples were prepared with THF under stirring at 40 °C for 24 h to ensure homogenization. Then the THF was evaporated and the powder was pressed between PTFE disks to obtain cylindrical tablets. Rheological measurements were performed at 1 Hz of angular frequency, 200–250 °C, and at a strain of 0.5%. The measurements were carried out using large amplitude shear (LAOS). The results demonstrated that nanoparticles affected the glass transition temperature ( $T_g$ ) and the order-disorder transition temperature ( $T_{ODT}$ ) of the block copolymer system. After application of the LAOS process, the AuNPs became arranged homogeneously within the P4VP phase [124]. In an additional work Mendoza et al. [123] carried out a systematic study to find the optimal temperature of AuNPs alignment, applying different shear stresses to the samples. Table 11 summarizes some rheological parameters of the hybrid systems discussed herein.

**Table 11.** Summary of the rheological parameters in block-copolymers and AuNPs systems.

| Hybrid AuNPs  | Copolymer                        | Elastic Modulus<br>G'<br>[Pa] | Temperature<br>[°C] | Viscosity<br>[Pa·s] | Reference |
|---|----------------------------------|-------------------------------|---------------------|---------------------|-----------|
| <sup>a</sup> AuNPs-P103<br>(20 wt.%) *                |                                  | -                             | 30.0<br>40.0        | 0.003832<br>0.1497  | [36]      |
|   | <sup>c</sup> P103<br>(20 wt.%) * | -                             | 30.0<br>40.0        | 0.005809<br>0.8743  |           |
| <sup>b</sup> PS- <i>b</i> -(P4VP/HAuCl <sub>4</sub> ) |                                  | 3 × 10 <sup>5</sup>           | 200                 | -                   | [124]     |
|   | <sup>d</sup> PS- <i>b</i> -P4VP  | 6 × 10 <sup>5</sup>           | 200                 | -                   |           |
| PS- <i>b</i> -(P4VP/HAuCl <sub>4</sub> )              |                                  | 10 <sup>5</sup>               | 130.0               | -                   | [123]     |

\* In this study the block copolymer concentrations were varied and the values showed correspond to a 20 wt.%.

<sup>a</sup> Pluronic (PEO<sub>17</sub>PPO<sub>60</sub>PEO<sub>17</sub>)/AuNPs. <sup>b</sup> Polystyrene-block-(poly-4-vinylpyridine/HAuCl<sub>4</sub>) at the ratio of 1:1.

<sup>c</sup> Pluronic (PEO<sub>17</sub>PPO<sub>60</sub>PEO<sub>17</sub>). <sup>d</sup> Polystyrene-block-(poly-4-vinylpyridine).

## 5. Technological Applications of Hybrid Gold/Polymer Nanomaterials

AuNPs find use in different areas, such as the biomedical, pharmaceutical, catalytic, cosmetic, energy, and environmental. Due to the potential of this technology, there has been a worldwide increase in investment in nanotechnology research and development. Major emphasis is also being placed on societal improvements and sustainable development. Green synthesis will doubtlessly help to achieve this purpose.

### 5.1. Antibacterial

Recent research in the medical area has allowed the creation of new medicines and cures for nearly any disease. However, the excessive use of multiple drugs has modified the resistance of some microorganisms generating a serious public health problem. Thus, there is a strong need to create new bactericides. Certainly, the design of NPs with controllable chemical properties comprises a promising alternative [73,125,126]. The large surface area of NPs permits a better interaction with microbes such as bacteria [77]. Different mechanisms have been proposed to explain the antibacterial activity of NPs as follows: (1) antibacterial activity is associated with the action of the ions released by the nanoparticles, and (2) when NPs penetrate the bacterial cell membrane, it dies [13,126]. Therefore, the size, shape, concentration, and stability of NPs are crucial parameters [52,126].

In comparison with silver, few studies have investigated the antimicrobial abilities of gold, although it has been reported that adequate amounts of gold and silver nanoparticles do not cause negative effects on the human body [127].

Zhang et al. [13] studied the antibacterial effect of AuNPs in various publications. Zhang found that AuNPs are normally not bactericidal unless they are present at high concentrations. However, Dasari et al. [128] proposed that AuNPs exhibit various degrees of antibacterial activity. These authors prepared AuNPs by conventional synthesis using sodium citrate as a reducing agent, and removed residual ions by centrifugation. The authors demonstrated that both Au (I) and Au (III) ions inhibited the bacterial growth of some organisms (*Escherichia coli*, *Staphylococcus typhimurium* DT104, and *Staphylococcus aureus*). In addition, the authors concluded that the washing of AuNPs to remove impurities could help to clarify the differences that exist in some reports on the antibacterial effect of AuNPs. It should be noted that, in many reports, the purification of nanomaterials is not mentioned.

As mentioned previously, antibacterial properties depend on the size and morphology of the NPs. Therefore, it is recommendable to avoid aggregation. Consequently, polymers are used to protect and provide stability to nanoparticles. Metal/polymer hybrid NPs are a great promise due to the opportunity of combining the functionality of both components [129]. Until a few years ago, hybrid AuNPs were based mainly on synthetic polymers. These materials were not biocompatible and exhibited some toxicity. Hence, they were not to be used for biomedical applications [130]. However, the synthesis of

NPs by green methods has allowed consideration of the possibility [52]. Das et al. [52] synthesized AuNPs with a graft copolymer (hydroxyl ethyl starch (HES)-g-methylacrylate (MA) HES-g-PMA). AuNPs were spherical with a mean diameter of 16–20 nm. Das and collaborators observed that AuNPs interacted easily with the cell membrane of bacteria causing damage on their surface and, eventually, their death. Thus, AuNPs demonstrated good antibacterial activity against two Gram-positive bacteria (*Bacillus cereus* and *Bacillus subtilis*). On the other hand, Wang et al. [129] prepared hybrid AuNPs utilizing a polymer (PAA/Chitosan) as soft template. TEM images revealed spherical PAA/Chitosan particles of 150 nm on which small AuNPs were deposited (5–10 nm). Additionally, Rose Bengal (RB) was employed as photosensitizer to transfer light energy to the surrounding oxygen and to form reactive oxygen species (ROS). These species are cytotoxic and can be used to destroy pathogens. RB molecules did not affect the morphology of hybrid nanomaterials. This hybrid material improved the ability to produce ROS, exhibiting high antibacterial efficacy towards Gram-negative *Escherichia coli*.

Fortunately, the antimicrobial efficacy of NPs has improved with the development of green synthesis methods. It has even been suggested that this is the result of the inherent bactericidal activity of natural sources combined with NPs [131]. In this respect, Khan et al. [132] obtained AuNPs from the aqueous extract of *Acer pentapomicum* leaves, which was used as a reducing and stabilizing agent. The authors reported that *A. pentapomicum* has a medicinal importance. SEM micrographs revealed spherical morphology with sizes between 18 and 25 nm. The antibacterial bioassays showed potent antimicrobial activity against pathogenic bacterial such as *Klebsiella pneumonia*, *Pseudomonas aeruginosa*, *B. subtilis*, *E. coli*, *S. aureus* and *X. campestris*. In addition, Otari et al. [42] developed AuNPs in an alginate polymer utilizing antimicrobial peptides. The peptide *Nisin*, a food preservative, acted as the reducing agent, while the alginate polymer was the stabilizing agent. Although synthesis was performed at 121 °C, the peptides retained their antimicrobial activity. TEM micrographs exhibited spherical NPs (10–15 nm) with peptides on their surface. Results revealed that Au-peptide-alginate hydrogel was more efficient than peptide-alginate hydrogel against the pathogens studied (*S. aureus*, *B. cereus*, and *E. faecalis*). Furthermore, Suganya et al. [77] reported a green synthesis of AuNPs from *Nigella sativa* using the zein (Ze) biopolymer as a capping agent (Ze-AuNPs). The Ze biopolymer incorporates a complex mixture of storage proteins that enrich maize seeds. This new material was evaluated against Gram-positive (*Bacillus pumilus* and *Bacillus subtilis*), Gram-negative (*Shigella sonnei* and *Pseudomonas aeruginosa*) bacteria and *Aedes aegypti* larvae. SEM and TEM micrographs showed nanoparticles with spherical, hexagonal, and triangular shapes with sizes between 50 and 80 nm. The authors evaluated the antibacterial activity of Ze-AuNPs, but also of zein and HAuCl<sub>4</sub>. Among these, only zein did not show important antibacterial activity. Ze-AuNP exhibited an excellent antibacterial effect, and interestingly, it also demonstrated a great capability to control the larval populations of *A. aegypti* mosquitoes. On the other hand, Borah et al. [133] detailed the synthesis of flower-like AuNPs utilizing the extract of *Syzygium cumini* and starch as reducing agent and template, respectively. This plant has showed beneficial health effects in antidiabetic, anticancer, and antioxidant activities [134]. When synthesis was carried out exclusively with the plant extract, TEM micrographs revealed spherical and a few non-spherical NPs with sizes of approximately 10 nm. Nonetheless, if the same reaction was developed with starch (0.3% w/v), TEM analysis confirmed flower-like morphology with sizes ranging from 30–110 nm. Furthermore, the antimicrobial activities of AuNPs were investigated against four Gram-positive bacterial strains (*Staphylococcus aureus* MTCC 121), two Gram-negative bacterial strains (*Escherichia coli* MTCC 40 and *Pseudomonas aeruginosa* MTCC 4673), and one fungus (*Candida albicans* MTCC 227). The results revealed that antibacterial activity was better when nanoflowers were used. The efficiency of nanoflowers could be attributed to their colloidal stability and their large, multi-branched surface area. It is important to mention that antimicrobial activity was tested for both solutions: HAuCl<sub>4</sub> and plant extract. Neither of these showed activity against the microbes-under-study.

New experiments suggest that AuNPs can penetrate the skin of rats and humans. These mechanisms have even been studied by molecular dynamics simulations. These novel studies have provided a huge opportunity to create nanoparticles for use in the cosmetic field and for transdermal

drug delivery [135]. Recently, the photothermal-based antibacterial activity of gold nanorods (AuNRs) coated with cholesterol-PEG and phospholipid-PEG were tested on human skin. The use of the PEG polymer promoted excellent colloidal stability, improving the ability to disperse in water. Lipids, phospholipids, and cholesterol allowed the addition of AuNRs to the skin layers. TEM analysis showed rod-shaped NPs free of aggregation. Previous studies have shown that compared with spherical shapes, AuNRs exhibit greater penetration through the skin [136]. In summary, these novel nanomaterials exhibited feasible photothermal-based bactericidal activities against *S. aureus*, the most common skin pathogen. Therefore, they could truly be useful treating skin diseases [137].

In this section, we have shown the use of AuNPs as antibacterial agents. Hybrid AuNPs especially synthesized by green methods resulted as a great promise in antimicrobial therapies. However, more studies are required to find clear interactions between biosynthesized AuNPs and bacteria. There remain many variables and parameters to study in order to reach optimal antimicrobial efficacy.

## 5.2. Catalysis

Catalysts are used in the chemical industry worldwide. Thanks to catalysts, society makes use of different products, such as medicines, paints, fuels, and lubricants, among others. If catalysts are in the same phase as reactants, they exhibit homogeneous catalysis. Homogeneous catalysis presents advantages such as high selectivity and better yield. However, their separation causes economic and/or environmental problems. To solve this obstacle, new strategies such as heterogeneous catalysis have been proposed. In this approach, an active component has been or not immobilized on a solid support with the disadvantage that only sites located on the surface are available for catalysis, decreasing their catalytic activity. Therefore, new catalyst systems with excellent performance and ease of recovery are required. NPs appear to be a sustainable alternative to conventional materials. In the catalysis area, NPs increase the exposed surface area of the active component, improving contact between reagents and the catalyst. At this scale, NPs appear to be similar to homogeneous catalysts. However, since they are insoluble, they can be easily separated from the reaction mixture, like heterogeneous catalysts [1,138,139]. Due to environmental concerns, innovative, ecological, and sustainable processes are needed. Therefore, a simple catalytic reaction that requires minimal energy and produces minimal waste of byproduct is highly desirable, for instance, liquid phase oxidations at room temperature with atmospheric pressure using air as oxidant, replacement of toxic organic solvents with aqueous media, and mild reactions. In addition, green catalysis requires easy removal from the reaction media, as well as good recycling while maintaining very high efficiency [139–141]. Traditionally, gold was considered chemically inert, thus a poor catalyst. No dissociative adsorption of both molecular hydrogen and oxygen took place over the smooth surfaces of Au at low temperatures (200 °C), suggesting that Au should be catalytically inactive for hydrogenation and oxidation reactions. However, Haruta et al. [142] prepared AuNPs of around 5 nm on an oxide support material in 1987. Surprisingly, it became a highly active oxidation catalyst for CO oxidation and propylene epoxidation in the gas phase. This finding modified the science of gold. On the other hand, it is known that once aggregation occurs, the catalytic activity of AuNPs decreases considerably. Therefore, small, stable AuNPs are needed. Organic polymers are definitely useful for stabilizing them. In 2005, Tsunoyama et al. [143] published the aerobic oxidation of benzylic alcohols catalyzed by gold nanoclusters stabilized by poly (*N*-vinyl-2-pyrrolidone) PVP. Tsunoyama and collaborators found that small nanoclusters (1.3 nm) exhibited better catalytic activity than larger ones (9.5 nm). This process is eco-friendly because reactions were carried out at room temperature and utilized air as oxidant. Furthermore, Miyaruma et al. [144] developed a reusable catalyst (gold nanoclusters stabilized by polystyrene) for the aerobic oxidation of alcohols at room temperature under atmospheric conditions. TEM analysis showed small nanoclusters (around 1 nm) that worked efficiently. The catalyst was recovered by simple filtration and reused without significant loss of activity. In these reactions, the sole co-product was water. Similarly, Han et al. [145] studied the formation of AuNPs employing hollow poly (*o*-phenylenediamine) PoPD microspheres as both reductant and template/stabilizer. AuNPs with an average size of 3 nm were used

in the aerobic oxidation of alcohols in aqueous phase at room temperature. The new material revealed high catalytic activity. This behavior suggested that the system of these authors could have good results in organic catalytic reactions. In this regard, the reduction of 4-nitrophenol (4-NP) to 4-aminophenol (4-AP) is an important key for the environment and industry. 4-AP is less toxic and it is utilized as industrial raw material [146,147]. Different researchers have studied this subject. Wang et al. [148], for example, proposed a simple synthesis to obtain AuNPs inside polymer nanospheres, specifically resorcinol–melamine–formaldehyde resin RMF, which acted as a soft template. Through TEM analysis, it was possible to observe spherical RMF nanospheres with sizes between 250 and 300 nm, in which tiny AuNPs (2–6 nm) were finely dispersed on their surfaces. The hybrid nanostructure was then used for the reduction of 4-NP to 4-AP with high efficiency, even after successive cycles. In this case, the polymer demonstrated an important role in the reduction of 4-NP because it stabilized NPs and increased catalytic activity. Dai et al. [49] also prepared AuNPs employing ABC triblock copolymer (poly(ethylene glycol)–block-linear polyethylenimine–block-poly( $\epsilon$ -caprolactone) PEG–PEI–PCL) as stabilizer in 2015. The size of AuNPs was < 10 nm and exhibited a spherical shape. Synthesis carried out at room temperature and using water as a solvent was reproducible. This system was efficient in a well-known catalytic reduction from 4-NP to 4-AP. It was even possible to prepare large quantities of AuNPs solution (4 L) while retaining its catalytic activity, making it promising at the industrial level. Again, in 2017, Dai et al. prepared AuNPs but this time using poly(ethylene oxide-*b*-2-vinyl pyridine-*b*-styrene) PEO-*b*-P2VP-*b*-PS [146]. This nanomaterial (of approximately 7 nm) exhibited high catalytic activity for the chemical reduction of 4-NP. In addition, Santos et al. [51] presented the synthesis of AuNPs using Pluronic F127 as stabilizer. The polymer concentration was a fundamental parameter in the growth of the nanoparticle. Santos and collaborators selected the larger and smaller (<5 nm) particles for the catalytic reduction of 4-NP to 4-AP. Smaller particles revealed better catalytic activity due to their larger contact surface. This system exhibited higher catalytic performance compared with AuNPs prepared using sodium citrate, the classical reduction method.

### 5.2.1. Catalysis of Biosynthesis Routes

Certainly science and technology must shift toward sustainable ecological resources and processes. Therefore, many researchers are preparing AuNPs with biomaterials to study their behavior in catalysis. Gupta et al. [140] formed AuNPs using green tea-leaf extract. Reduction was carried out by the polyphenols, catechins, flavonoids, and phytochemicals present in the tea extract. Compounds of the extract also acted as stabilizers. Particles of approximately 20 nm were predominantly spherical with fcc structure. They were employed for the reduction of Methylene Blue (MB) in the presence of Sn(II), in water and in micellar media (anionic surfactant: sodium dodecyl sulphate, SDS, and cationic surfactant, CTAB). Gupta et al. showed that chemicals produced by plants did not significantly reduce MB. The catalysts were SnCl<sub>2</sub> and AuNPs. In addition, the reduction rate in the micellar media was more efficient compared with water due to the electrostatic interaction between MB and SDS, as well as to the hydrophobic interaction between MB and CTAB. On the other hand, Nazirov et al. [78] prepared and characterized small AuNPs reduced by biocompatible chitosan derivative (*N*-(4-imidazolyl) methylchitosan, BMI). This polymer also acted as a stabilizer. The size of the NPs was less than 5.5 nm. These were used in quasi-homogeneous catalysis in a *p*-nitrophenol reduction reaction. System performance was efficient in that *p*-aminophenol was obtained in a few minutes. In addition, Yan et al. [149] studied the synthesis of AuNPs utilizing cellulose nanocrystal (CNC). The resulting CNC-AuNPs exhibited good catalytic activity for the reduction of 4-NP. Since the latter is an eco-friendly synthesis, the system has great potential for medical and industrial applications. Chairam et al. [40] produced AuNPs using mung bean starch (MBS). The starch acted as a reducing and stabilizing agent. TEM analysis revealed spherical particles of 10 nm. This material was used in the reduction of 4-NP with good performance. The authors proposed that their procedure could be extended to other starch-rich polymers, potentiating their applications.

As previously mentioned, polymers are used in the stabilization of AuNPs. Although polymers can restrict access to catalytically active sites, they also can act as active or selective promoters, increasing the catalytic effect [150]. Additionally, a critical factor in catalytic processes comprises the size of the AuNPs. Nanoclusters gold promise great potential as more active and selective catalysts because a large percentage of their atoms lie on the surface [139,151,152].

### 5.2.2. Heterogeneous Catalysis

On the other hand, materials widely used in heterogeneous photocatalysis are semiconductor oxides, among which TiO<sub>2</sub> and ZnO are prominent due to characteristics such as low toxicity, physical and chemical stability, high abundance, and low price. The main disadvantage of these materials is that their bandgap (3.2 eV) causes them to be activated only by UV radiation, which corresponds to solely 4–5% of sunlight. One of the most studied lines of research is the modification of these semiconductor materials in such a way that they can make use of a wider range of the solar spectrum. Complementing them with metal nanoparticles appears to be one of the most viable options, since there are two advantages in the formation of a heterostructure with these semiconductor oxides as follows: (i) the presence of SPR, which gives rise to a greater amount of electrons for taking part in the photocatalytic reduction reaction, and (ii) the formation of a Schottky barrier, which acts as a scavenger of the electrons that reach the surface of the semiconductor. Thus, the Schottky barrier increases the lifetime of the structure by decreasing the process of the recombination of electron-hole pairs on the surface of the semiconductor oxide, which is consequently accompanied by an increase in its photocatalytic activity [153]. Several researchers have focused on obtaining a heterostructure that improves interaction between the nanoparticles and the semiconductor oxide in order to enhance photocatalytic activity. Heterogeneous photocatalysis using AuNPs has generally been employed for the degradation of dyes [154–156], organic synthesis [157–159], and the generation of energy sources, particularly the production of hydrogen and methane [160–163].

Chen et al. [164] synthesized an Au-TiO<sub>2</sub> heterostructure using tetrabutyl titanate and chloroauric acid as precursors for TiO<sub>2</sub> and Au, respectively. Synthesis was carried out in two steps, obtaining TiO<sub>2</sub> nanoparticles by microwave-solvothermal synthesis complemented with photodeposited AuNPs by UV radiation. The results revealed particle sizes of 30–40 nm for TiO<sub>2</sub> and of 4.8 nm for AuNPs. This system was used for the selective oxidation of benzyl alcohol into benzaldehyde at 30 °C under an oxygen atmosphere. It was considered that the oxidation of benzyl alcohol was carried out by charge transfer between the metal-bonding of the complex formed on the surface of the nanostructure when benzyl alcohol was adsorbed on TiO<sub>2</sub>. The increase in photoactivity is the result of the increase in absorbance of visible light caused by the AuNPs. This provides additional energy to the electrons, which then overcome the Schottky barrier, giving rise to an injection of “hot” electrons into the conduction band of the TiO<sub>2</sub>, improving the benzaldehyde yield.

Mondal et al. [155] synthesized an Au-ZnO nanocomposite using a modified hydrothermal methodology. Morphologically, the nanocomposite is a ZnO petal-like complemented with AuNPs in a range of 5–10 wt.%. The synthesized Au-ZnO material was utilized in the degradation of Rhodamine B, Methylene Blue, Methyl Orange, Congo Red and Rose Bengal under the application of direct sunlight irradiation. In the case of Rhodamine B, the authors employed several catalyst loads, obtaining a nearly complete degradation within 60–270 min for the lowest and highest photocatalyst load, respectively. Furthermore, according to the monitoring of the degradation mechanism by UV-vis spectroscopy, Rhodamine B degraded when the conjugated xanthene ring was destroyed. The high photocatalytic activity was attributed to the strong electronic interaction between AuNPs and ZnO. This promoted a rapid transfer of electrons from the surface of the ZnO to the AuNPs, thus avoiding recombination of electron-hole pairs and promoting the reaction with adsorbed O<sub>2</sub> on the surface of the AuNPs, generating highly reactive oxygen radicals [O<sup>2-</sup>]. Due to the presence of AuNPs on the surface of ZnO, the lifetime of the charge carriers increased. Consequently, there was a considerable increase in the formation of hydroxyl radicals by the reaction of the holes in the valence band of ZnO with the

adsorbed water on their surface. These hydroxyl radicals were responsible for the degradation of the dye. Therefore, the higher the number the hydroxyl radicals, the greater the photocatalytic activity of the nanocomposite.

Another type of nanostructure being studied is the core-shell type. Sun et al. [165] obtained heterostructures with high photocatalytic activity, associated with AuNPs, in the degradation of dyes. This was the result of an improvement in the SPR utilizing sunlight radiation. The AuNPs obtained had octahedral morphology coated with ZnO, resulting in structures of the core-shell type. These structures were employed for the degradation of dyes (Rhodamine B, Methyl Orange and Methylene Blue). The results of these authors demonstrated that core-shell structures are highly active in the degradation of dyes using sunlight radiation, maintaining their high activity for several cycles. The high photocatalytic activity of these core-shell structures is attributed to the quick electron transfer from ZnO to Au through its interface, increasing the density of the electrons on the surface of the AuNPs, improving their plasmonic absorption. Thus, the SPR effect is enhanced by the formation of the ZnO shell on AuNPs. In addition to the fact that the formation of a Schottky barrier near the Au/ZnO interface prevents the return of electrons from Au to ZnO, it also facilitates the migration of the holes in the valence band from ZnO to Au.

Pougin et al. [166] synthesized a core-shell type heterostructure, in which Au nanoparticles (20 nm) were coated with a TiO<sub>2</sub> shell (8 nm thick). In addition, more Au nanoparticles were deposited on the surface of the shell. These structures were used to reduce CO<sub>2</sub> in order to produce methane. Methane production is proportional to the thickness of the TiO<sub>2</sub> shell, due to its influence on the absorption of the Au central-core plasmon (to a thicker shell corresponding a longer wavelength). The authors greatly increased the production of methane by having a TiO<sub>2</sub> shell on the AuNPs, compared to the same core-shell structure without AuNPs. In this respect, the improvement is not only attributed to the injection of "hot" electrons from the central Au core to the TiO<sub>2</sub> shell, but also to the activity of the AuNPs on the TiO<sub>2</sub> shell, their plasmonic effect, and their surface exposure.

Gavade et al. [167] synthesized a ternary nanostructure formed by Cu<sub>x</sub>O/ZnO ( $x = 1$  or  $2$ ) modified with AuNPs. This nanostructure possesses two characteristics. On the one hand, it has a p-n junction in the interface of the Cu<sub>x</sub>O/ZnO. Therefore, the generated electron-hole pairs do not recombine due to the electric field naturally produced by the p-n junction. On the other hand, the impact of the SPR effect due to the presence of the AuNPs renders it possible for the heterostructure to be sensitive to visible light. The combination of these two characteristics exerts an effect on the photocatalytic activity of the ternary nanostructure. In addition, the presence of Cu<sub>x</sub>O together with AuNPs extends the absorption range of the visible spectrum of the ternary nanostructure. Additionally, AuNPs can acquire some incident photons from the energy around the plasmonic "hot" point and "hot" electrons during the process of SPR excitation. This ternary nanostructure was used to degrade Methyl Orange, achieving 98% degradation in 30 minutes compared to the binary Cu<sub>2</sub>O/ZnO nanostructure, which reached 93% when using UV radiation. This increase in photocatalytic activity is attributed to that in the presence of AuNPs, there is an increase in the oxidation process due to the formation of OH radicals, which are responsible for the degradation of the organic dye. Under conditions of sunlight radiation, the charge transfer mechanism indicates the transfer of photogenerated electrons from the Cu<sub>2</sub>O conduction band to the ZnO conduction band, because the recombination process is avoided due to the p-n junction. Electrons in the conduction band of the ZnO react with the adsorbed oxygen on their surface to generate O<sup>2-</sup>. Furthermore, holes of the valence band of the ZnO migrate to the valence band of the Cu<sub>2</sub>O, reacting with the OH-terminals of the structure and the adsorbed water to generate -OH and HO<sub>2</sub>, respectively. At the same time, AuNPs capture photons that induce the SPR effect, causing the photoexcited electrons to be immediately injected into the conduction band of the ZnO and the Cu<sub>x</sub>O. SPR originates a local electromagnetic field around the AuNPs that facilitates the excitation of the electrons and improves the dynamic transfer in such a way that a greater quantity of electrons participate in the degradation of the dye, improving the efficiency of the photocatalytic activity.

Due to the aforementioned, with the synergy generated between the Au NPs and the semiconductor oxides employed in photocatalysis, as well as the understanding, mainly, of the mechanisms of charge transfer arising between them, continuous improvement in the efficiency of their applications is possible. Therefore, in the near future, applications such as environmental improvement and the generation of sustainable energy, on a larger scale than that of the laboratory will be possible.

In this section, we reviewed the photocatalytic properties of Au, either only as a nanoparticle or producing synergy with other materials. This feature has allowed Au to have a wide range of application. First, by itself or by modifying its surface, it becomes an attractive option in the area of health, particularly in environmental remediation (degradation of organic compounds), and in medicine (drug nanocarrier, treatment, and diagnosis of cancer, diabetes, among others). Second, when Au nanoparticles are deposited on the surface of larger molecules, in particular, semiconductor oxides, the catalytic capacity of this new heterostructure becomes potentially greater, beyond its individual properties. This results in the more efficient use of charge carriers generated by absorbing electromagnetic radiation utilized for the catalytic activation of the heterostructure, enhancing its catalytic activity.

### 5.3. Medical Applications

Nanomedicine is a relatively new multidiscipline, that is based on designing, developing, and/or improving current techniques to solve problems of modern medicine, using NPs made of different materials. Specifically, AuNPs are excellent candidates for biomedical applications thanks to their physicochemical and optical properties, which are dependent on their size, shape, adaptability, subcellular size, and biocompatibility. These NPs offer an adequate alternative for transporting small molecules and biomacromolecules to diseased cells and tissues [168]. Due to the diversity of available techniques to synthesize NPs, AuNPs can be synthesized in a variety of presentations that include nanospheres, nanorods (NRs), nanocages, nanoprisms, nanocubes, and nanostars [169]. AuNPs are potentially useful for imaging, the thermotherapy of biological targets, and as drug carriers, due to the easy functionalization of their surface, which renders them universal substrates to bound molecules [170,171]. They also possess good stability against oxidation. Therefore, they will play a significant role in the development of diagnostic and therapeutic nanomedicines [172]. AuNPs can manipulate light at the nanoscale based on their LSPR, leading to strong electromagnetic fields on the particle surface, enhancing their radiative properties such as absorption and scattering. In addition, strongly absorbed light is converted into heat rapidly through non-radiative processes. After light excitation, gold nanoparticles absorb or scatter light in the NIR region, enabling them to be useful as imaging and therapeutic agents [171,173].

To design applicable AuNPs treatments, the conjugation of AuNPs is necessary. The surface must be functionalized with ligands such as drugs, biomolecules, and biopolymers [174,175]. More specifically, NPs created for biomedical applications are frequently coated with polymers containing reactive functional groups, in order to conjugate targeting ligands or drugs [176]. During recent years, polymers have been studied for their applications in nanomedicine. Polymers employed in nanomedicine must be non-toxic, biocompatible, and biodegradable [177].

PEG is the most widely used polymer in biomedical applications and the first PEGylated product that has been on the market for more than 20 years. It inhibits the response of the immune system. It is hydrophilic. Therefore, it is able to stabilize NPs by steric, and not ionic effects, especially in water [177]. For instance, densely packed repeating chains of polymers such as PEG are capable of decreasing non-specific reactions [178]. PEG is commonly used to coat the surface of AuNPs to improve their stability in vivo and to prevent phagocytosis [179]. However, PEG can also decrease the effectiveness of cell internalization and binding with targets, which significantly reduces the potential for utilizing AuNPs as therapeutic agents [180]. Because of this, other alternatives have been sought for functionalization; e.g., it has been shown that AuNPs coated with glutathione do not cause morbidity

at concentrations up to 60  $\mu\text{M}$ , suggesting that glutathione may be an alternative to PEG in the design of therapies [180].

During the most recent years, much of nanomedicine research has been aimed at improving the diagnosis and treatment of cancer. In the following sections, we have focused mainly on works related to cancer. We divided these into three main applications: drug nanocarriers; photodynamic and photothermal therapy, as well as nanotheranostics, which combines the diagnosis and treatment of diseases in single doses.

### 5.3.1. Drug Nanocarriers

The main side effects of drugs used in the treatment of cancer are related to the lack of target specificity and uncontrolled release [181]. Therefore, many research works focus on the design of drug nanocarriers that are able to increase the specificity of the drug and the control of its release.

In this context, polyaspartic acid (PAsp), a biodegradable polymer, was used for the synthesis of AuNPs. These NPs were loaded with doxorubicin (DOX), a drug commonly used in cancer chemotherapy. AuNPs with polyaspartic acid showed no cytotoxicity in in-vitro assays. However, NPs loaded with DOX exhibited a significant decrease in the tumor size (fibrosarcoma) of the mice-under-study in in-vivo assays. In addition, a greater decrease in the body weight of the mice was observed when they were treated with free DOX compared to mice treated with DOX bound to the NPs. This confirms the greater efficacy and lower toxicity of AuNPs functionalized with polyaspartic acid [182]. On the other hand, AuNPs were synthesized using the following three polymers as reducing and stabilizing agents: citrate-PEG; malate-PEG, and tartrate-PEG, this resulting in three different nanoparticle systems to which folate (a cancer cell targeting agent) and the drug 5-fluorouracil (5FU) were added. The nanosystems demonstrated a sustained release of 5FU up to 27 days in breast cancer cells and inhibited cell proliferation with lower concentrations of the drug than those reported in previous studies [41]. In line with the concept of “green synthesis”, AuNPs stabilized with alginate were synthesized. Similarly, drug-conjugated NPs were created using a “green solvent”: water. Curcumin and Methotrexate (an antifolate, a drug used in treatment of some types of cancer) were the drugs utilized for conjugation with NPs. These NPs exerted a cytotoxic effect on C6 glioma and MCF-7 cancer-cell lines and were found to be hemocompatible. Their active targeting against MCF-7 cancer cells was due to the presence of the Methotrexate [183]. In the case of polysaccharides, chitosan is one of the most used of these biomedical applications due to its biocompatibility and biodegradability. For instance, Salem et al. [184] synthesized AuNPs using chitosan as a reducing agent and stabilizer. These NPs were designed with the aim of reducing the adverse effects of the anticancer drug 5FU and were evaluated in hepatocellular carcinoma cells (HepG2). The authors showed that the concentration of chitosan is an important parameter for enhancing the dispersion of nanocomposites for a prolonged time. In a cytotoxic assay, greater inhibition of cell growth was observed with 5FU when it was bound to gold NPs as compared to free 5FU. Cai and Yan et al. [185] developed a complex system formed by AuNPs, which were trapped inside nanogels. These nanogels were made of lysozyme-dextran. The new system was loaded with DOX. Through in vitro assays with HEK293 cells, it was demonstrated that nanogels have the same antitumor activity as DOX alone. The researchers proposed that nanogels can be employed as a contrasting agent in optical cell imaging. This could be a promising system for simultaneous drug delivery and biomedical imaging. Pullulan is another polysaccharide that possesses great potential for its use in nanomedicine due to its stability, biocompatibility, hydrophilic nature, and the availability of reactive sites for chemical modification [186]. Using Pullulan as a reducing and stabilizing agent, AuNPs have been synthesized for drug delivery systems to increase the safety and efficacy of these systems. These AuNPs exhibited high cellular uptake, biocompatibility, and non-cytotoxicity for normal cells. NPs were loaded with novel cassiarin A chloride derivatives (3d and 3i) as candidate anticancer drugs. They exhibited cytotoxicity up to 10 times more against gastric cancer cells (KATO-III) compared to free compounds and Cisplatin, a drug commonly used to treat some types of cancer [187]. The same group also utilized

modified para-aminobenzoic acid-quat-pullulan (PABA-QP) for the synthesis of AuNPs. These NPs were used as nanocarriers of DOX, revealing greater toxicity against cancer cells and, simultaneously, less toxicity against normal cells compared with free DOX [188]. In addition, AuNPs stabilized with Pullulan were functionalized with 5FU and folic acid for their potential use in drug administration. The authors found that the amount of 5FU required to obtain a 50% increase in inhibition was lower in 5FU conjugated with folic acid and AuNPs than in free 5FU [189].

In the case of copolymers, AuNPs were coated with the copolymer thiolated methoxy-poly(ethylene glycol)-b-poly((2-dimethylamino) ethyl methacrylate-co-itaconic acid) mPEG-b-p(DMAEMA-co-IA). In addition, Methotrexate was attached to the NPs. Analysis of cellular uptake, internalization of AuNPs, cellular cytotoxicity, and analysis of drug release times demonstrated that these nanoparticles show promise in terms of the active and passive targeting abilities of anti-cancer agents [190]. Furthermore, the formation of micelles based on di-block copolymer systems and their role in the synthesis of AuNPs with hollow core-shell morphology is a novel approach in the biomedical field for its application in drug administration. Di-block copolymer formed by benzyl alcohol and poly- $\epsilon$ -caprolactone was synthesized, achieving the formation of micelles, which act as a complement to assemble the AuNPs of a specific morphology. Hollow core-shell capsules were loaded with DOX (charge efficiency, ~74%) and released in a controlled and prolonged manner by a change in pH [81]. In addition, AuNPs loaded with Amphotericin B was evaluated in an *in vivo* test with rabbits. It was concluded that NPs are efficient carriers of drugs, enhancing the oral bioavailability of Amphotericin B in a controlled manner [191].

On the other hand, the green synthesis of AuNPs utilizing plant extracts for medical applications, offers the advantage of having extracts with known medicinal effects that can potentiate the effect of NPs in treatments as reducing and/or stabilizing agents. Additionally, this type of synthesis uses water as a reducing medium, minimizing human exposure to other hazardous reducing agents [192]. Mukherjee et al. [193] developed a method for the synthesis of AuNPs using an extract of *Eclipta Alba* (an Indian medicinal plant) as a reducing and stabilizing agent. DOX was bound to these AuNPs. Their effect on breast-cancer cells (MCF-7 and MDA-MB-231) was tested. A significant inhibitory effect on cell proliferation compared to the effect of DOX alone was observed. Therefore, the authors proposed that these AuNPs can be used as efficient vehicles for drug delivery in the treatment of cancer.

### 5.3.2. Photodynamic and Photothermal Therapy

Photothermal and photodynamic therapy employs photo-absorbing agents to generate heat from the optical energy, which triggers the death of the tumor cells [194]. AuNPs and Indocyanine green encapsulated chitosan hybrid nanomaterials were used for photothermal and photodynamic therapy with single irradiation (808 nm laser). During the *in-vivo* assay, nanohybrids were able to produce hyperthermia and ROS, which caused cell death and disappearance of the tumor in the majority of the treated mice [195]. With the intention of developing a new phototherapeutic agent for oncotherapy, a nanosystem of mesoporous silica coated AuNPs was synthesized. Indocyanine green, beta-Cyclodextrin, and a specific peptide (RLA) were attached directly to the NPs. A 2,3-dimethylmaleic anhydride-modified chitosan oligosaccharide-block-poly (ethylene glycol) polymer was used to functionalize the surface of the nanosystem. When the nanosystem extravasates to tumor tissue, the change of pH in the tumor microenvironment could induce the dissociation of the polymer and re-exposure of the peptide. This could help with the selective accumulation of the nanosystem in the cell. In addition, after irradiation of the NPs for 5 minutes with a laser at 808 nm, the temperature increases more than 30 °C [196]. On the other hand, Gum Arabic encapsulated AuNPs were synthesized and their effectiveness was evaluated in the photothermal treatment of lung cancer and hepatocarcinogenesis. The NPs did not show cytotoxicity in the absence of irradiation in the case of lung cancer. However, when the NPs were excited with the irradiation, they induced cell death in lung-tumor tissues with a reduction in inflammation and angiogenesis, as observed. In the case of hepatocarcinogenesis during *in-vivo* studies with a mouse model, with or without laser irradiation, the NPs induced cancer-cell

apoptosis. These results suggested the potential use of these functionalized NPs as a promising photothermal treatment [197,198]. With the intention of designing AuNPs for photothermal therapy, Silva et al. [199] synthesized AuNPs using aqueous extracts of *Plectranthus saccatus*. The authors obtained AuNPs with absorption in the NIR region (800 nm). These AuNPs exhibited good biocompatibility when analyzed in-vitro in human keratinocytes. Additionally, AuNPs were incorporated into an agar phantom. Their temperature was increased using an ultrasound water bath (frequency: 45 kHz) and a pulsed laser (532 nm). These results suggested that these NPs may be potentially useful for photothermal cancer therapy.

### 5.3.3. Nanotheranostics

The promising results obtained with monofunctional nanomedicine have directed research efforts toward the creation of “nanotheranostics”, which simultaneously integrates the diagnosis and non-invasive treatment of diseases in a single platform, with the possibility of controlling the distribution and release of medicines in real time [200]. Systems have been developed that integrate therapeutic and diagnostic capabilities, exploiting the synergies among NPs, the drug, and hyperthermia [181].

Gold nanoshells were synthesized and functionalized with glycol chitosan for their use in imaging and photothermal treatment. The biocompatibility of the NPs was evaluated in mouse fibroblast cells (L929). Cell death was evaluated after irradiation for 4 minutes in breast-cancer cells (MCF-7). The results validated the efficacy of these NPs for the treatment of cancer, since 80% cell death was obtained. In addition, these authors showed that these NPs have potential for use in computed tomography (CT) [201]. On the other hand, a system was designed for the combined treatment of chemotherapy and hyperthermia, while allowing magnetic resonance imaging (MRI). The system was made up of poly (lactic-co-glycolic acid) NPs loaded with AuNPs and Docetaxel. In-vitro (MCF-7 human breast cancer cell line) and in-vivo (subcutaneous S-180 tumor model) tests were performed. Results indicated that the system could be used for nanotheranostic applications [202]. Following this approach, Baek et al. [181] utilized AuNPs as the core of a complex formed by AuNPs mesoporous silica shell-DOX. Pores of the mesoporous silica shell were then capped with poly (*N*-isopropylacrylamide)-based *N*-butyl imidazolium copolymer (poly (NIPAAm-co-BVIm)), a temperature-sensitive copolymer. The transition of the polymer was achieved after 5 min of exposure to NIR irradiation, which triggered the release of the drug by opening the pores and an increase in temperature to above 43 °C. DOX is also released by a drop in pH, which permits the controlled release of the drug when the cancer cells capture the NPs. In addition, the authors also proposed the use of these NPs as contrast agents employing CT [181].

Hollow-structure NPs composed of CuS, Cu<sub>2</sub>S, and Au as multifunctional drug carriers were synthesized and coated with a thermosensitive copolymer (poly oligo (ethylene oxide) methacrylate-co-2-(2-methoxyethoxy) ethyl methacrylate), and azobenzene-modified arginylglycylaspartic acid. The copolymers formed a large cavity and a mesoporous shell for drug loading and release. This cavity was loaded with DOX, which resulted in an improvement in the efficacy of the antitumor therapy by combining chemotherapy and photothermal therapy. The results obtained allowed these NPs to appear to be attractive for use as new vehicles for drug administration and as photothermal agents for cancer therapy. In addition, these NPs reduced off-target toxicity and non-specific absorption. Furthermore, the authors suggested that these NPs can also be employed for real-time imaging [203]. With the intention of designing a nanosystem that could be utilized simultaneously for diagnosis, imaging, and treatment, Simon et al. [204] synthesized AuNPs coated with the copolymer Pluronic (F127), which conferred stability on NPs. This nanosystem was loaded with Methylene Blue, an optical labelling and photosensitizing drug. The authors demonstrated the effectiveness of NPs for providing optical imaging and for enhancing photodynamic therapeutic activity of Methylene Blue against murine colon carcinoma cells (C-26), compared with the free drug. On the other hand, a chitosan-stearic acid copolymer was employed to encapsulate hollow AuNPs, and a near-infrared (IR) fluorescent tracer was attached to these NPs. Additionally, the surface of

the NPs was functionalized with a small peptide (TNYL) to facilitate EphB4-positive tumor-targeting delivery. After irradiation, the NPs induced greater cell death in EphB4-positive tumors than in EphB4-negative tumors. This is attributed to the enhanced accumulation of NPs in EphB4-positive tumors. In addition, the authors were able to monitor the biodistribution of NPs [194].

A copolymer poly (epsilon-caprolactone)-*ss*-poly (2-(dimethylamino) ethyl methacrylate) was synthesized. This copolymer was then utilized to create a system that combines chemotherapy and diagnosis through CT. The drug DOX was loaded into the core of the micelle and AuNPs were attached to the shell. Drug-release profiles suggested the effectiveness of NPs for controlled release through a change in pH- or redox-triggered. Through a colorimetric assay for assessing cell metabolic activity, the inhibition of HepG2 and MCF-7 cells in the presence of micelles loaded with DOX was observed. The CT imaging assay indicated the potential of the micelles for the diagnosis of tumors [205].

A theranostic agent for use in MRI, CT imaging, and photothermal therapy in hepatocellular carcinoma was synthesized. The system was formed by AuNPs attached to polydopamine as inner core, Indocyanine green as photothermal therapeutic agent, and lipids modified with gadolinium-1,4,7,10-tetraacetic acid and lactobionic acid as shell. The system demonstrated specificity in the hepatocellular-carcinoma cell line, dual-mode imaging ability (enhanced magnetic resonance and CT imaging), and significant photothermal cytotoxicity after NIR irradiation [206].

In order to implement a system that performs diagnosis and the treatment of cancer in a single agent, folic acid-conjugated block polymers composed of PEG and poly-beta-benzyl-L-aspartate were bound to AuNPs. Afterward, a hydrophobic photosensitizer (Verteporfin) was incorporated onto the surfaces of the NPs. An in-vitro cell study (HeLa cells) revealed high intracellular uptake of NPs and marked phototoxicity after laser irradiation (0.4 mW/cm<sup>2</sup>, 708 nm) compared with a free photosensitizer. These results suggested that NPs synthesized and bound to the photosensitizer could be useful as an effective theranostic agent for photodynamic tumor imaging and therapy [207].

For photothermal-chemotherapy and photoacoustic imaging, a pH-sensitive diblock copolymer (2-(diisopropylamino) ethylamine-grafted poly (L-aspartic acid) and 2-mercaptoethylamine-grafted poly (L-aspartic acid)) was synthesized and self-assembled into micelles loaded with DOX. Later, a gold nanocage was formed and PEG was grafted onto the nanocage in order to increase the stability of the NPs. In-vitro and in-vivo tests were carried out to evaluate the effectiveness of the nanosystem in human ovarian cancer. This nanosystem has the ability to deactivate the release of DOX into the bloodstream and activate it within the tumor tissue, mainly due to changes in pH and NIR irradiation. In addition, stimulation with NIR irradiation of AuNPs could generate hyperthermia, which causes the death of tumor cells. Consequently, tumor growth was inhibited and the survival of mice with human SKOV-3 ovarian tumor was prolonged. Tumor accumulation and intratumor diffusion of the NPs were easily located using photoacoustic imaging [208].

Another example is the use of cocoa extract as a reducing and stabilizing agent to synthesize anisotropic gold nanoparticles with maximal absorbance in the NIR. AuNPs synthesized by aqueous route revealed good biocompatibility in non-cancerous (L929 and NIH-3T3) and cancerous (A431 and MDA-MB231) cell lines. Cell death induced in epidermoid carcinoma (A431) was observed during an in-vitro assay when cells were in contact with AuNPs and were irradiated with a femtosecond laser (800 nm, 6 W/cm<sup>2</sup>). In addition, AuNPs were also tested as contrast agent in CT, exhibiting a good X-ray contrast. These results demonstrated the potential use of these AuNPs for photothermal therapy and as contrast agents [209].

#### 5.3.4. Treatment of Other Diseases

The use of AuNPs for applications in nanomedicine focuses mainly on the treatment and diagnosis of cancer. However, research has also been directed toward tuberculosis, diabetes, Alzheimer disease, atherosclerosis, obesity, human virus immunodeficiency (HIV), influenza, among others.

In the case of diabetes, research has focused on AuNPs as insulin nanocarriers to increase release time, and in possessing sensing functions to measure the number of antibodies employed for diabetes

control. In order to explore the use of AuNPs as drugs carriers, they were coated with Dextran and loaded with insulin. This system was capable of increasing insulin activity [210]. In addition, AuNPs were synthesized using chitosan as a reducing agent. In this case, chitosan promoted the stability of NPs for 6 months. Through in-vivo studies in diabetic male Wistar rats, it was demonstrated that oral and nasal administration of AuNPs loaded with insulin improved pharmacodynamic activity [211]. AuNPs on polypyrrole film have been synthesized. This system was utilized as immunosensors capable of detecting levels of hemoglobin and hemoglobin-A1c in blood, enabled as a sensor with potential use in the monitoring of diabetes [212,213]. Similarly, AuNPs with polypyrrole were synthesized. The new material was used for the local delivery of insulin and revealed considerable response to electrical and pH changes. The research group considered that their system had great potential for the treatment of diabetes mellitus [214].

On the other hand, atherosclerosis is another disease in which nanomedicine has attempted to improve treatment and diagnosis. Atherosclerosis is characterized by chronic inflammation of the arteries and lipid accumulation in the blood vessel walls. This behavior causes many cardiovascular diseases [215]. For example, 5-aminolevulinic acid (ALA) AuNPs functionalized with PEG (ALA-AuNPs-PEG) were synthesized and administered to rabbits to evaluate their use in clinical practice as therapeutic agents for atherosclerosis [216]. ALA is used to differentiate between healthy and diseased tissue in the diagnosis of tumors. This technique has been adapted to detect atherosclerotic plaques [217]. Additionally, ALA is a potentially useful photosensitizer for use in photodynamic therapy. In the same line, protoporphyrin IX (PPIX), a derivative of hematoporphyrin, can accumulate in tumors and atherosclerotic plaques [217]. Peng et al. [218] showed that PPIX was detected in atheromatous plaques after the intravenous administration of ALA in rabbits. Similarly, Oliveira et al. [216] measured the fluorescence of porphyrin extracted from the blood and feces of rabbits after administration of ALA-AuNPs-PEG, detecting an increase in porphyrin emission and the high stability of ALA when attached to the AuNPs-PEG. These results suggested that this method can aid in the diagnosis and treatment of atherosclerosis with good sensitivity. AuNPs entrapped in dendrimers made of polyamidoamine were coated with PEG and fluorescein Isothiocyanate. They were tested as contrast agents for use in the CT imaging of macrophages in atherosclerotic lesions. Molecular imaging of macrophages may improve the detection and characterization of atherosclerosis. These NPs are non-cytotoxic even at high concentrations and can be absorbed by murine macrophage cells. In addition, the results obtained during in-vivo tests suggested that NPs exhibited great potential in the detection of atherosclerotic lesions [219]. AuNPs functionalized with PEG have also been employed in the photodynamic and sonodynamic therapies of atherosclerosis [220]. Diseases such as Mycobacterium tuberculosis, obesity, and liver heart disease have also been targeted by nanomedicine for treatment and diagnosis. For example, AuNPs coated with chitosan have been used to detect Mycobacterium tuberculosis. Differentiation between positive and negative Mycobacterium tuberculosis samples was possible by a color change in the system [221].

Furthermore, polypyrrole-coated hollow gold nanoshells were synthesized and tested in a treatment for obesity (photothermal lipolysis). NPs were injected into porcine adipose tissue and irradiated with an NIR laser. The temperature of the adipose tissue was monitored. A temperature increase to 47.7 °C was detected. This increment induced the death of the adipocytes. These results suggested that NPs could be used as a potential photothermal agent for the treatment of obesity [222].

In the case of liver disease, a glycogen and an AuNPs nanosystem was designed to increase the effectiveness of Silymarin, a potential hepatoprotective drug. AuNPs were synthesized from the *Annona reticulata* leaf extract and Silymarin. They were deposited in a glycogen biopolymer. Results showed that nano-systems provided significant protection against CCl<sub>4</sub>-induced hepatic injury in Wistar rats. In addition, it was shown that the Silymarin-AuNPs-glycogen complex had higher bioavailability compared to that of free Silymarin or Silymarin-AuNPs [223].

AuNPs have also been utilized to measure the anti-inflammatory effect. Reena et al. [76] synthesized AuNPs using a *Leucas aspera* extract and a poly lactic acid-co-poly ethylene glycol-co-poly lactic acid

copolymer. The cytotoxicity of the NPs was evaluated in South African green-monkey kidney cells. The NPs exhibited excellent anti-inflammatory activity when compared with pure the *Leucas aspera* extract. In another example, the use of AuNPs as a protective agent in heart disease was evaluated. The cardioprotective function of AuNPs synthesized with proanthocyanidin, extracted from grape seeds, was evaluated. Myocardial injury was induced in rats by Isoproterenol, in order for them to be treated with AuNPs. These NPs demonstrated cardioprotective action in myocardial lesion induced by Isoproterenol. A cytotoxicity assay with peripheral blood mononuclear cells exhibited a non-toxic effect of the NPs [224].

Nanomedicine offers innovative and promising approaches to improve the diagnosis and treatment of many diseases, focusing mainly on cancer. However, although many research projects are in progress, the majority of the advances have not yet been approved for use in humans. Current research is focused mainly on personalized nanomedicine and theranostics with more effective and innocuous NPs. Throughout this section, we have presented some of the most recent advances in the area of nanomedicine, focusing mainly on the use of AuNPs synthesized under the concept of “green synthesis”, using polymers/copolymers as reducing agent and/or stabilizer. In addition, polymers are also being employed to improve or enhance the properties of AuNPs. It is necessary to train experts in nanomedicine, promote interdisciplinarity, and increase regulations on the use of nanodrugs.

#### 5.4. Sensors

A sensor is a device designed to receive information of a certain magnitude from the outside and transform it into another magnitude, normally electrical, that could be quantified. Since the SPR was introduced as a sensor, a large number of sensors have been developed in several fields, such as biochemistry and analytical chemistry. Conventional sensors are not sensitive to the detection of small molecules. However, researchers have improved the sensitivity of sensors up to 1000 times when combining macromolecules with AuNPs [225]. Therefore, AuNPs have been widely used in different sensors.

For example, the mechanism to determine the presence of an analyte has been studied. It has been proposed that chitosan is adsorbed on the surface of Au, due to the affinity of an amine group, in a system where the 2,6-pyridinedicarboxylic (PDA) chelating agent is aggregated for determination of  $Hg^{2+}$ . PDA contains a pyridine nitrogen atom that possess great affinity to  $Hg^{2+}$ , causing giving rise to the formation of coordination complexes. Thus, AuNPs/Chitosan/PDA would bind and form complexes with  $Hg^{2+}$ . This behavior results in a color change of the solution: from red to blue. In this case, the authors obtained excellent results in the range of 300 nM–5  $\mu$ M, revealing excellent selectivity toward  $Hg^{2+}$  [226].

Table 12 corresponds to AuNPs using a polymer during synthesis. In the table, we find mentioned the type of synthetic or natural polymer, block copolymer, size, and morphology of AuNPs, and their corresponding application as a sensor.

**Table 12.** Examples of AuNPs synthesized with different polymers and their use as sensors.

| Synthetic/Natural Polymer or Block Copolymer                  | Size [nm] | Morphology | Application   | Reference |
|---|-----------|------------|---|-----------|
| Chitosan  | 23        | Spherical  | Detection of $Hg^{2+}$  | [226]     |
| Polystyrene-block-poly(2-vinyl pyridine)                      | 16–20     | Spherical  | Detection of 5,5'-dithiobis(2-nitrobenzoic acid)                    | [227]     |
| Poly(amidoamine) PAMAM  | 55        | Spherical  | Detection of $Hg^{2+}$  | [228]     |
| Poly(4-vinylpyridine) and polystyrene-b-poly(4-vinylpyridine) | -         | Hexagonal  | No is specify   | [229]     |
| Polystyrene-block-poly(methyl methacrylate) (PS-b-PMMA)       | 20        | Spherical  | Benzenethiol  | [230]     |
| Poly(4-vinylphenol) (PVP)                                     | -         | Variable   | Detection of $Hg^{2+}$  | [231]     |
| Poly(styrene-b-4-vinylpyridine) (PS-b-P4VP)                   | 10–92     | Nanodisk   | Human gamma globulin (IgG) and affini-pure goat anti-human IgG(H+L) | [232]     |

The use of sensors utilizing gold nanoparticles combined with green synthesis possesses the advantage of being inexpensive, simple, a fast procedure, friendly, and handy. All of these characteristics enables the use of these materials as perfect for sensing purposes.

## 6. Conclusions

AuNP exhibit interesting optical, electronic, and catalytic properties, among others. The exploitation of these properties has been carried out for the development of synthetic routes that are benign for the environment, making rendering AuNPs most versatile, therefore being able to be used in different technological applications. In an outstanding manner, if the synthesis is green, toxic effects are minimized, costs are reduced, and there will be high probabilities of production on a larger scale. As mentioned in this review, stabilization of AuNPs with polymers offers the possibility of adjusting their surface properties, functionality, and catalytic activity either alone, superficially modified, or decorating other materials such as semiconductor oxides. Consequently, understanding the interaction of protective agents with AuNPs, through different characterization techniques will help design new morphologies efficiently for use in novel applications.

**Author Contributions:** N.T. conceived the idea and was main responsible for resources and editing. J.A. and V.V.A.F.-E. contributed to the drafting of the characterization section. N.T., C.C.-A., V.J.G.-C., A.C.-A. and A.L.-F. collaborated in the writing of the application section. All the authors contributed in the preparation of the manuscript.

**Funding:** This research received no external funding.

**Conflicts of Interest:** The authors declare no conflict of interest.

## References

1. Louis, C.; Pluchery, O. *Gold Nanoparticles for Physics, Chemistry and Biology*; World Scientific: Singapore, 2012; ISBN 978-1-84816-806-0.
2. Mingos, D.M.P. Historical Introduction to Gold Colloids, Clusters and Nanoparticles. In *Gold Clusters, Colloids and Nanoparticles I. Structure and Bonding*; Springer: Cham, Switzerland, 2014; Volume 161, ISBN 978-3-319-07848-9.
3. Sakai, T.; Alexandridis, P. Single-Step Synthesis and Stabilization of Metal Nanoparticles in Aqueous Pluronic Block Copolymer Solutions at Ambient Temperature. *Langmuir* **2004**, *20*, 8426–8430. [[CrossRef](#)] [[PubMed](#)]
4. Habashi, F. *Handbook of extractive metallurgy*; Wiley-VCH: Weinheim, Germany, 1997; ISBN 3-527-28792-2.
5. Schmid, G.; Corain, B. Nanoparticulated Gold: Syntheses, Structures, Electronics, and Reactivities. *Eur. J. Inorg. Chem.* **2003**, *2003*, 3081–3098. [[CrossRef](#)]
6. Laguna, A. *Modern Supramolecular Gold Chemistry*; Wiley: Weinheim, Germany, 2008; ISBN 9783527320295.
7. Pyykkö, P. Theoretical Chemistry of Gold. *Angew. Chem. Int. Ed.* **2004**, *43*, 4412–4456.
8. Kretsinger, R.H.; Uversky, V.N.; Permyakov, E.A. (Eds.) *Encyclopedia of Metalloproteins*; Springer New York: New York, NY, USA, 2013; ISBN 978-1-4614-1532-9.
9. Dai, Y.; Zhang, X. Recent Advances in Amphiphilic Polymers as the Stabilizers of Colloidal Gold Nanoparticles. *Macromol. Mater. Eng.* **2018**, *303*, 1800105. [[CrossRef](#)]
10. Johal, M.S.; Johnson, L.E. *Understanding Nanomaterials*, 2nd ed.; CRC Press: Boca Raton, FL, USA, 2018; ISBN 9780815354383.
11. Bond, G. The early history of catalysis by gold. *Gold Bull.* **2008**, *41*, 235–241. [[CrossRef](#)]
12. Bond, G.C.; Louis, C.; Thompson, D.T. *Catalysis by Gold*; Catalytic Science Series; Gold Bull, World Scientific: Singapore, 2006; ISBN 978-1-86094-658-5.
13. Zhang, Y.; Shareena Dasari, T.P.; Deng, H.; Yu, H. Antimicrobial Activity of Gold Nanoparticles and Ionic Gold. *J. Environ. Sci. Heal. Part C* **2015**, *33*, 286–327. [[CrossRef](#)]
14. Schatz, G.C. Electrodynamics of nonspherical noble metal nanoparticles and nanoparticle aggregates. *J. Mol. Struct. THEOCHEM* **2001**, *573*, 73–80. [[CrossRef](#)]
15. Willets, K.A.; Van Duyne, R.P. Localized Surface Plasmon Resonance Spectroscopy and Sensing. *Annu. Rev. Phys. Chem.* **2007**, *58*, 267–297. [[CrossRef](#)]

16. Capek, I. Polymer decorated gold nanoparticles in nanomedicine conjugates. *Adv. Colloid Interface Sci.* **2017**, *249*, 386–399. [[CrossRef](#)]
17. Tantra, R. *Nanomaterial Characterization: An Introduction*; Tantra, R., Ed.; John Wiley & Sons, Inc.: Hoboken, NJ, USA, 2016; ISBN 9781118753460.
18. Mittal, A.K.; Chisti, Y.; Banerjee, U.C. Synthesis of metallic nanoparticles using plant extracts. *Biotechnol. Adv.* **2013**, *31*, 346–356. [[CrossRef](#)]
19. Singh, J.; Dutta, T.; Kim, K.-H.; Rawat, M.; Samddar, P.; Kumar, P. 'Green' synthesis of metals and their oxide nanoparticles: Applications for environmental remediation. *J. Nanobiotechnol.* **2018**, *16*, 84. [[CrossRef](#)] [[PubMed](#)]
20. Mukherjee, P.; Ahmad, A.; Mandal, D.; Senapati, S.; Sainkar, S.R.; Khan, M.I.; Parishcha, R.; Ajaykumar, P.V.; Alam, M.; Kumar, R.; et al. Fungus-Mediated Synthesis of Silver Nanoparticles and Their Immobilization in the Mycelial Matrix: A Novel Biological Approach to Nanoparticle Synthesis. *Nano Lett.* **2001**, *1*, 515–519. [[CrossRef](#)]
21. Kumar, C.S.S.R. *Nanomaterials for the Life Science; Metallic Nanomaterials*; Wiley-VCH: Weinheim, Germany, 2009; Volume 1, ISBN 978-3-527-32151-3.
22. Lin, L.; Wang, W.; Huang, J.; Li, Q.; Sun, D.; Yang, X.; Wang, H.; He, N.; Wang, Y. Nature factory of silver nanowires: Plant-mediated synthesis using broth of Cassia fistula leaf. *Chem. Eng. J.* **2010**, *162*, 852–858. [[CrossRef](#)]
23. Kimling, J.; Maier, M.; Okenve, B.; Kotaidis, V.; Ballot, H.; Plech, A. Turkevich Method for Gold Nanoparticle Synthesis Revisited. *J. Phys. Chem. B* **2006**, *110*, 15700–15707. [[CrossRef](#)] [[PubMed](#)]
24. Polte, J.; Ahner, T.T.; Delissen, F.; Sokolov, S.; Emmerling, F.; Thünemann, A.F.; Kraehnert, R. Mechanism of Gold Nanoparticle Formation in the Classical Citrate Synthesis Method Derived from Coupled In Situ XANES and SAXS Evaluation. *J. Am. Chem. Soc.* **2010**, *132*, 1296–1301. [[CrossRef](#)]
25. Köth, A.; Tiersch, B.; Appelhans, D.; Gradzielski, M.; Cölfen, H.; Koetz, J. Synthesis of Core-Shell Gold Nanoparticles with Maltose-Modified Poly(Ethyleneimine). *J. Dispers. Sci. Technol.* **2012**, *33*, 52–60. [[CrossRef](#)]
26. Polte, J.; Emmerling, F.; Radtke, M.; Reinholz, U.; Riesemeier, H.; Thünemann, A.F. Real-Time Monitoring of Copolymer Stabilized Growing Gold Nanoparticles. *Langmuir* **2010**, *26*, 5889–5894. [[CrossRef](#)]
27. Nalwa, H.S. (Ed.) *Encyclopedia of Nanoscience and Nanotechnology*; American Scientific Publishers: Valencia, CA, USA, 2005; Volume 42, ISBN 1588830012.
28. Li, C.; Li, D.; Wan, G.; Xu, J.; Hou, W. Facile synthesis of concentrated gold nanoparticles with low size-distribution in water: Temperature and pH controls. *Nanoscale Res. Lett.* **2011**, *6*, 440. [[CrossRef](#)]
29. Shan, J.; Tenhu, H. Recent advances in polymer protected gold nanoparticles: Synthesis, properties and applications. *Chem. Commun.* **2007**, 4580. [[CrossRef](#)]
30. Zhao, P.; Li, N.; Astruc, D. State of the art in gold nanoparticle synthesis. *Coord. Chem. Rev.* **2013**, *257*, 638–665. [[CrossRef](#)]
31. Saldías, C.; Bonardd, S.; Quezada, C.; Radić, D.; Leiva, A. The Role of Polymers in the Synthesis of Noble Metal Nanoparticles: A Review. *J. Nanosci. Nanotechnol.* **2017**, *17*, 87–114. [[CrossRef](#)] [[PubMed](#)]
32. Alexandridis, P. Gold Nanoparticle Synthesis, Morphology Control, and Stabilization Facilitated by Functional Polymers. *Chem. Eng. Technol.* **2011**, *34*, 15–28. [[CrossRef](#)]
33. Parveen, R.; Tremiliosi-Filho, G. A step ahead towards the green synthesis of monodisperse gold nanoparticles: The use of crude glycerol as a greener and low-cost reducing agent. *RSC Adv.* **2016**, *6*, 95210–95219. [[CrossRef](#)]
34. Kumar, A.; Bhatt, M.; Vyas, G.; Bhatt, S.; Paul, P. Sunlight Induced Preparation of Functionalized Gold Nanoparticles as Recyclable Colorimetric Dual Sensor for Aluminum and Fluoride in Water. *ACS Appl. Mater. Interfaces* **2017**, *9*, 17359–17368. [[CrossRef](#)]
35. Sakai, T.; Alexandridis, P. Mechanism of Gold Metal Ion Reduction, Nanoparticle Growth and Size Control in Aqueous Amphiphilic Block Copolymer Solutions at Ambient Conditions. *J. Phys. Chem. B* **2005**, *109*, 7766–7777. [[CrossRef](#)]
36. Tepale, N.; Fernández-Escamilla, V.V.A.; Álvarez, C.; Flores-Aquino, E.; González-Coronel, V.J.; Cruz, D.; Sánchez-Cantú, M. Morphological and Rheological Characterization of Gold Nanoparticles Synthesized Using Pluronic P103 as Soft Template. *J. Nanomater.* **2016**, *2016*, 45. [[CrossRef](#)]

37. Alkilany, A.M.; Bani Yaseen, A.I.; Kailani, M.H. Synthesis of Monodispersed Gold Nanoparticles with Exceptional Colloidal Stability with Grafted Polyethylene Glycol-*g*-polyvinyl Alcohol. *J. Nanomater.* **2015**, *2015*, 1–9. [[CrossRef](#)]
38. Abrica-González, P.; Zamora-Justo, J.A.; Sotelo-López, A.; Vázquez-Martínez, G.R.; Balderas-López, J.A.; Muñoz-Diosdado, A.; Ibáñez-Hernández, M. Gold nanoparticles with chitosan, N-acylated chitosan, and chitosan oligosaccharide as DNA carriers. *Nanoscale Res. Lett.* **2019**, *14*, 258. [[CrossRef](#)]
39. Valdez, J.; Gómez, I. One-Step Green Synthesis of Metallic Nanoparticles Using Sodium Alginate. *J. Nanomater.* **2016**, *2016*, 1–7. [[CrossRef](#)]
40. Chairam, S.; Konkamdee, W.; Parakhun, R. Starch-supported gold nanoparticles and their use in 4-nitrophenol reduction. *J. Saudi Chem. Soc.* **2017**, *21*, 656–663. [[CrossRef](#)]
41. Gajendiran, M.; Jo, H.; Kim, K.; Balasubramanian, S. Green synthesis of multifunctional PEG-carboxylate  $\pi$  back-bonded gold nanoconjugates for breast cancer treatment. *Int. J. Nanomed.* **2019**, *14*, 819–834. [[CrossRef](#)]
42. Otari, S.V.; Patel, S.K.S.; Jeong, J.-H.; Lee, J.H.; Lee, J.-K. A green chemistry approach for synthesizing thermostable antimicrobial peptide-coated gold nanoparticles immobilized in an alginate biohydrogel. *RSC Adv.* **2016**, *6*, 86808–86816. [[CrossRef](#)]
43. Manivasagan, P.; Bharathiraja, S.; Bui, N.Q.; Lim, I.G.; Oh, J. Paclitaxel-loaded chitosan oligosaccharide-stabilized gold nanoparticles as novel agents for drug delivery and photoacoustic imaging of cancer cells. *Int. J. Pharm.* **2016**, *511*, 367–379. [[CrossRef](#)]
44. Goy-López, S.; Castro, E.; Taboada, P.; Mosquera, V. Block Copolymer-Mediated Synthesis of Size-Tunable Gold Nanospheres and Nanoplates. *Langmuir* **2008**, *24*, 13186–13196. [[CrossRef](#)]
45. Ray, D.; Aswal, V.K.; Srivastava, D. Concentration effect on tuning of block copolymer-mediated synthesis of gold nanoparticles. *J. Nanosci. Nanotechnol.* **2010**. [[CrossRef](#)]
46. Saldías, C.; Leiva, A.; Quezada, C.; Jaque, P.; Gargallo, L.; Radic, D. Structural effects of amphiphilic block copolymers on the gold nanoplates synthesis. Experimental and theoretical study. *Eur. Polym. J.* **2011**, *47*, 1866–1876. [[CrossRef](#)]
47. Simon, T.; Boca, S.C.; Astilean, S. Pluronic-Nanogold hybrids: Synthesis and tagging with photosensitizing molecules. *Colloids Surfaces B Biointerfaces* **2012**, *97*, 77–83. [[CrossRef](#)]
48. Khullar, P.; Singh, V.; Mahal, A.; Kumar, H.; Kaur, G.; Bakshi, M.S. Block Copolymer Micelles as Nanoreactors for Self-Assembled Morphologies of Gold Nanoparticles. *J. Phys. Chem. B* **2013**, *117*, 3028–3039. [[CrossRef](#)]
49. Dai, Y.; Li, Y.; Wang, S. ABC triblock copolymer-stabilized gold nanoparticles for catalytic reduction of 4-nitrophenol. *J. Catal.* **2015**, *329*, 425–430. [[CrossRef](#)]
50. Gomes, D.S.B.; Paterno, L.G.; Santos, A.B.S.; Garay, A.V.; Mertz, D.; Freitas, S.M.; Soler, M.A.G. New insights on the formation of gold nanoparticles and Pluronic nanocomposites: Kinetics and thermodynamics parameters. *J. Mol. Liq.* **2018**, *268*, 181–189. [[CrossRef](#)]
51. Santos, D.C.; de Souza, V.C.; Vasconcelos, D.A.; Andrade, G.R.S.; Gimenez, I.F.; Teixeira, Z. Triblock copolymer-mediated synthesis of catalytically active gold nanostructures. *J. Nanopart. Res.* **2018**, *20*, 105. [[CrossRef](#)]
52. Das, S.; Pandey, A.; Pal, S.; Kolya, H.; Tripathy, T. Green synthesis, characterization and antibacterial activity of gold nanoparticles using hydroxyethyl starch-*g*-poly (methylacrylate-co-sodium acrylate): A novel biodegradable graft copolymer. *J. Mol. Liq.* **2015**, *212*, 259–265. [[CrossRef](#)]
53. Kariuki, V.M.; Hoffmeier, J.C.; Yazgan, I.; Sadik, O.A. Seedless synthesis and SERS characterization of multi-branched gold nanoflowers using water soluble polymers. *Nanoscale* **2017**, *9*, 8330–8340. [[CrossRef](#)] [[PubMed](#)]
54. Khullar, P.; Mahal, A.; Singh, V.; Banipal, T.S.; Kaur, G.; Bakshi, M.S. How PEO-PPO-PEO Triblock Polymer Micelles Control the Synthesis of Gold Nanoparticles: Temperature and Hydrophobic Effects. *Langmuir* **2010**, *26*, 11363–11371. [[CrossRef](#)] [[PubMed](#)]
55. Bakshi, M.S. Colloidal micelles of block copolymers as nanoreactors, templates for gold nanoparticles, and vehicles for biomedical applications. *Adv. Colloid Interface Sci.* **2014**, *213*, 1–20. [[CrossRef](#)] [[PubMed](#)]
56. Yin, T.; Liu, X.; Wang, J.; An, Y.; Zhang, Z.; Shi, L. Thermosensitive mixed shell polymeric micelles decorated with gold nanoparticles at the outmost surface: Tunable surface plasmon resonance and enhanced catalytic properties with excellent colloidal stability. *RSC Adv.* **2015**, *5*, 47458–47465. [[CrossRef](#)]

57. Seo, E.; Kim, J.; Hong, Y.; Kim, Y.S.; Lee, D.; Kim, B.-S. Double Hydrophilic Block Copolymer Templated Au Nanoparticles with Enhanced Catalytic Activity toward Nitroarene Reduction. *J. Phys. Chem. C* **2013**, *117*, 11686–11693. [[CrossRef](#)]
58. Sarkar, B.; Alexandridis, P. Block copolymer–nanoparticle composites: Structure, functional properties, and processing. *Prog. Polym. Sci.* **2015**, *40*, 33–62. [[CrossRef](#)]
59. Spatz, J.P.; Mössmer, S.; Hartmann, C.; Möller, M.; Herzog, T.; Krieger, M.; Boyen, H.-G.; Ziemann, P.; Kabius, B. Ordered Deposition of Inorganic Clusters from Micellar Block Copolymer Films. *Langmuir* **2000**, *16*, 407–415. [[CrossRef](#)]
60. Enomoto-Rogers, Y.; Kamitakahara, H.; Yoshinaga, A.; Takano, T. Radially oriented cellulose triacetate chains on gold nanoparticles. *Cellulose* **2010**, *17*, 923–936. [[CrossRef](#)]
61. Bakshi, M.S.; Kaura, A.; Bhandari, P.; Kaur, G.; Torigoe, K.; Esumi, K. Synthesis of Colloidal Gold Nanoparticles of Different Morphologies in the Presence of Triblock Polymer Micelles. *J. Nanosci. Nanotechnol.* **2006**, *6*, 1405–1410. [[CrossRef](#)] [[PubMed](#)]
62. Tan, N.P.B.; Lee, C.H.; Chen, L.; Ho, K.M.; Lu, Y.; Ballauff, M.; Li, P. Facile synthesis of gold/polymer nanocomposite particles using polymeric amine-based particles as dual reductants and templates. *Polymer (Guildf)* **2015**, *76*, 271–279. [[CrossRef](#)]
63. Antonisamy, J.D.; Swain, J.; Dash, S. Study on binding and fluorescence energy transfer efficiency of Rhodamine B with Pluronic F127-gold nano hybrid using optical spectroscopy methods. *Spectrochim. Acta Part A Mol. Biomol. Spectrosc.* **2017**, *173*, 139–143. [[CrossRef](#)] [[PubMed](#)]
64. Cao, G. *Nanostructures and Nanomaterials: Synthesis, Properties and Applications*; Cao, G., Ed.; World Scientific: Singapore, 2004; ISBN 1-86094-415-9.
65. Gan, P.P.; Li, S.F.Y. Potential of plant as a biological factory to synthesize gold and silver nanoparticles and their applications. *Rev. Environ. Sci. Bio/Technol.* **2012**, *11*, 169–206. [[CrossRef](#)]
66. Chandran, S.P.; Chaudhary, M.; Pasricha, R.; Ahmad, A.; Sastry, M. Synthesis of Gold Nanotriangles and Silver Nanoparticles Using Aloe vera Plant Extract. *Biotechnol. Prog.* **2006**, *22*, 577–583. [[CrossRef](#)]
67. Narayanan, K.B.; Sakthivel, N. Coriander leaf mediated biosynthesis of gold nanoparticles. *Mater. Lett.* **2008**, *62*, 4588–4590. [[CrossRef](#)]
68. Kasthuri, J.; Veerapandian, S.; Rajendiran, N. Biological synthesis of silver and gold nanoparticles using apiin as reducing agent. *Colloids Surfaces B Biointerfaces* **2009**, *68*, 55–60. [[CrossRef](#)]
69. Mondal, S.; Roy, N.; Laskar, R.A.; Sk, I.; Basu, S.; Mandal, D.; Begum, N.A. Biogenic synthesis of Ag, Au and bimetallic Au/Ag alloy nanoparticles using aqueous extract of mahogany (*Swietenia mahogani* JACQ.) leaves. *Colloids Surfaces B Biointerfaces* **2011**, *82*, 497–504. [[CrossRef](#)]
70. Daisy, P. Saipriya Biochemical analysis of Cassia fistula aqueous extract and phytochemically synthesized gold nanoparticles as hypoglycemic treatment for diabetes mellitus. *Int. J. Nanomed.* **2012**, *1189*. [[CrossRef](#)]
71. Jafarizad, A.; Safaei, K.; Gharibian, S.; Omid, Y.; Ekin, D. Biosynthesis and In-vitro Study of Gold Nanoparticles Using Mentha and Pelargonium Extracts. *Procedia Mater. Sci.* **2015**, *11*, 224–230. [[CrossRef](#)]
72. Lim, S.H.; Ahn, E.-Y.; Park, Y. Green Synthesis and Catalytic Activity of Gold Nanoparticles Synthesized by Artemisia capillaris Water Extract. *Nanoscale Res. Lett.* **2016**, *11*, 474. [[CrossRef](#)] [[PubMed](#)]
73. Patra, J.K.; Kwon, Y.; Baek, K.-H. Green biosynthesis of gold nanoparticles by onion peel extract: Synthesis, characterization and biological activities. *Adv. Powder Technol.* **2016**, *27*, 2204–2213. [[CrossRef](#)]
74. Mata, R.; Bhaskaran, A.; Sadras, S.R. Green-synthesized gold nanoparticles from Plumeria alba flower extract to augment catalytic degradation of organic dyes and inhibit bacterial growth. *Particuology* **2016**, *24*, 78–86. [[CrossRef](#)]
75. Chitra, K.; Reena, K.; Manikandan, A.; Antony, S.A. Antibacterial Studies and Effect of Poloxamer on Gold Nanoparticles by Zingiber Officinale Extracted Green Synthesis. *J. Nanosci. Nanotechnol.* **2015**, *15*, 4984–4991. [[CrossRef](#)] [[PubMed](#)]
76. Reena, K.; Balashanmugam, P.; Gajendiran, M.; Arul Antony, S. Synthesis of leucas aspera extract loaded gold-PLA-PEG-PLA amphiphilic copolymer nanoconjugates: In vitro cytotoxicity and anti-inflammatory activity studies. *J. Nanosci. Nanotechnol.* **2016**, *16*, 4762–4770. [[CrossRef](#)]
77. Suganya, P.; Vaseeharan, B.; Vijayakumar, S.; Balan, B.; Govindarajan, M.; Alharbi, N.S.; Kadaikunnan, S.; Khaled, J.M.; Benelli, G. Biopolymer zein-coated gold nanoparticles: Synthesis, antibacterial potential, toxicity and histopathological effects against the Zika virus vector Aedes aegypti. *J. Photochem. Photobiol. B Biol.* **2017**, *173*, 404–411. [[CrossRef](#)]

78. Nazirov, A.; Pestov, A.; Privar, Y.; Ustinov, A.; Modin, E.; Bratskaya, S. One-pot green synthesis of luminescent gold nanoparticles using imidazole derivative of chitosan. *Carbohydr. Polym.* **2016**, *151*, 649–655. [[CrossRef](#)]
79. Zhang, J.-G.; Zhang, X.-Y.; Yu, H.; Luo, Y.-L.; Xu, F.; Chen, Y.-S. Preparation, self-assembly and performance modulation of gold nanoparticles decorated ferrocene-containing hybrid block copolymer multifunctional materials. *J. Ind. Eng. Chem.* **2018**, *65*, 224–235. [[CrossRef](#)]
80. Yoo, M.; Kim, S.; Lim, J.; Kramer, E.J.; Hawker, C.J.; Kim, B.J.; Bang, J. Facile Synthesis of Thermally Stable Core–Shell Gold Nanoparticles via Photo-Cross-Linkable Polymeric Ligands. *Macromolecules* **2010**, *43*, 3570–3575. [[CrossRef](#)]
81. Amgoth, C.; Suman Joshi, D.S.D.; Dharmapuri, G.; Lakavathu, M. Self-assembled block copolymer [(BenzA)-b-(PCL)] micelles to orient randomly distributed AuNPs into hollow core-shell morphology and its role as payload for nanomedicines. *Mater. Sci. Eng. C* **2018**, *92*, 790–799. [[CrossRef](#)]
82. Díaz, M.; Barrera, A.; López-Cuenca, S.; Martínez-Salazar, S.Y.; Rabelero, M.; Ceja, I.; Fernández, V.V.A.; Aguilar, J. Size-controlled gold nanoparticles inside polyacrylamide microgels. *J. Appl. Polym. Sci.* **2016**. [[CrossRef](#)]
83. He, Y.; Zhang, Y.; Yan, N.; Zhu, Y.; Jiang, W.; Shi, D. Self-assembly of block copolymers into sieve-like particles with arrayed switchable channels and as scaffolds to guide the arrangement of gold nanoparticles. *Nanoscale* **2017**, *9*, 15056–15061. [[CrossRef](#)] [[PubMed](#)]
84. Aubrit, F.; Testard, F.; Paquirissamy, A.; Gobeaux, F.; Wang, X.; Nallet, F.; Fontaine, P.; Ponsinet, V.; Guenoun, P. Ligand-free synthesis of gold nanoparticles incorporated within cylindrical block copolymer films. *J. Mater. Chem. C* **2018**, *6*, 8194–8204. [[CrossRef](#)]
85. Scarabelli, L.; Schumacher, M.; Jimenez de Aberasturi, D.; Merkl, J.; Henriksen-Lacey, M.; Milagres de Oliveira, T.; Janschel, M.; Schmidtke, C.; Bals, S.; Weller, H.; et al. Encapsulation of Noble Metal Nanoparticles through Seeded Emulsion Polymerization as Highly Stable Plasmonic Systems. *Adv. Funct. Mater.* **2019**, *29*, 1809071. [[CrossRef](#)]
86. Xu, F.; Zhang, P.; Zhang, J.; Yu, C.; Yan, D.; Mai, Y. Crystallization-Driven Two-Dimensional Self-Assembly of Amphiphilic PCL- b -PEO Coated Gold Nanoparticles in Aqueous Solution. *ACS Macro Lett.* **2018**, *7*, 1062–1067. [[CrossRef](#)]
87. Ikai, A. *The World of Nano-Biomechanics*; Elsevier: Amsterdam, The Netherlands, 2008; ISBN 9780444527776.
88. Sabir, T.S.; Rowland, L.K.; Milligan, J.R.; Yan, D.; Aruni, A.W.; Chen, Q.; Boskovic, D.S.; Kurti, R.S.; Perry, C.C. Mechanistic Investigation of Seeded Growth in Triblock Copolymer Stabilized Gold Nanoparticles. *Langmuir* **2013**, *29*, 3903–3911. [[CrossRef](#)]
89. Jencyk, J.; Woźniak-Budych, M.; Jancelewicz, M.; Jarek, M.; Jurga, S. Structural and dynamic study of block copolymer – Nanoparticles nanocomposites. *Polymer (Guildf)* **2019**, *167*, 130–137. [[CrossRef](#)]
90. Liu, X.; Liu, F.; Astruc, D.; Lin, W.; Gu, H. Highly-branched amphiphilic organometallic dendronized diblock copolymer: ROMP synthesis, self-assembly and long-term Au and Ag nanoparticle stabilizer for high-efficiency catalysis. *Polymer (Guildf)* **2019**, *173*, 1–10. [[CrossRef](#)]
91. Zhu, H.; Lussier, F.; Ducrot, C.; Bourque, M.-J.; Spatz, J.P.; Cui, W.; Yu, L.; Peng, W.; Trudeau, L.-É.; Bazuin, C.G.; et al. Block Copolymer Brush Layer-Templated Gold Nanoparticles on Nanofibers for Surface-Enhanced Raman Scattering Optophysiology. *ACS Appl. Mater. Interfaces* **2019**, *11*, 4373–4384. [[CrossRef](#)]
92. Perkampus, H.-H. *UV-VIS spectroscopy and Its Applications*; Springer: Berlin/Heidelberg, Germany, 1992; ISBN 0387554211.
93. Singh, M.P.; Strouse, G.F. Involvement of the LSPR Spectral Overlap for Energy Transfer between a Dye and Au Nanoparticle. *J. Am. Chem. Soc.* **2010**, *132*, 9383–9391. [[CrossRef](#)]
94. Rakshit, S.; Moulik, S.P.; Bhattacharya, S.C. Deciphering the Role of the Length of the Corona in Controlled NSET within Triblock Copolymers. *J. Phys. Chem. B* **2015**, *119*, 8457–8467. [[CrossRef](#)] [[PubMed](#)]
95. Ray, D.; Aswal, V.K. Step-addition Method for Enhancing the Yield of Gold Nanoparticles in Block Copolymer Solution. *J. Macromol. Sci. Part B* **2010**, *49*, 810–820. [[CrossRef](#)]
96. Xu, J.-P.; Yang, X.; Lv, L.-P.; Wei, Y.; Xu, F.-M.; Ji, J. Gold-Nanoparticle-Stabilized Pluronic Micelles Exhibiting Glutathione Triggered Morphology Evolution Properties. *Langmuir* **2010**, *26*, 16841–16847. [[CrossRef](#)] [[PubMed](#)]
97. Kuo, S.-W.; Yang, H.-Y. Tunable Arrangement of Gold Nanoparticles in Epoxidated Poly(styrene-block-butadiene) Diblock Copolymer Matrices. *Macromol. Chem. Phys.* **2011**, *212*, 2249–2259. [[CrossRef](#)]

98. Pamies, R.; Zhu, K.; Kjøniksen, A.-L.; Nyström, B. Temperature effects on the stability of gold nanoparticles in the presence of a cationic thermoresponsive copolymer. *J. Nanopart. Res.* **2016**, *18*, 319. [[CrossRef](#)]
99. Cortez-Lemus, N.A.; García-Soria, S.V.; Paraguay-Delgado, F.; Licea-Claverie, A. Synthesis of gold nanoparticles using poly(ethyleneglycol)-b-poly(*N,N*-diethylaminoethylmethacrylate) as nanoreactors. *Polym. Bull.* **2017**, *74*, 3527–3544. [[CrossRef](#)]
100. Chen, S.; Xiang, Y.; Peng, C.; Xu, W.; Banks, M.K.; Wu, R. Synthesis of a novel graphene-based gold nanocomposite using PVEIM- b -PNIPAM as a stabilizer and its thermosensitivity for the catalytic reduction of 4-nitrophenol. *Inorg. Chem. Front.* **2019**, *6*, 903–913. [[CrossRef](#)]
101. Schmitz, K.S.; Phillies, G.D.J. *An Introduction to Dynamic Light Scattering by Macromolecules*; American Institute of Physics: Melville, NY, USA, 1991; Volume 44.
102. Shi, Y.; Selin, V.; Wang, Y.; Sukhishvili, S.A. Multiresponsive Block Copolymer-Modified “Hairy” Gold Nanoparticles for Remote Control of Interfaces. *Part. Part. Syst. Character.* **2013**, *30*, 950–957. [[CrossRef](#)]
103. Simon, T.; Boca, S.; Biro, D.; Baldeck, P.; Astilean, S. Gold-Pluronic core-shell nanoparticles: Synthesis, characterization and biological evaluation. *J. Nanopart. Res.* **2013**. [[CrossRef](#)]
104. Fernandez, V.V.A.; Soltero, J.F.A.; Puig, J.E.; Rharbi, Y. Temporal Evolution of the Size Distribution during Exchange Kinetics of Pluronic P103 at Low Temperatures. *J. Phys. Chem. B* **2009**, *113*, 3015–3023. [[CrossRef](#)]
105. Seeck, O.H.; Murphy, B.M. *X-Ray Diffraction: Modern Experimental Techniques*; Taylor & Francis Group: Boca Raton, FL, USA, 2014; ISBN 9780429071898.
106. Feng, C.; Shen, Z.; Li, Y.; Gu, L.; Zhang, Y.; Lu, G.; Huang, X. PNIPAM- b -(PEA- g -PDMAEA) double-hydrophilic graft copolymer: Synthesis and its application for preparation of gold nanoparticles in aqueous media. *J. Polym. Sci. Part A Polym. Chem.* **2009**, *47*, 1811–1824. [[CrossRef](#)]
107. Sanches, E.A.; Soares, J.C.; Iost, R.M.; Marangoni, V.S.; Trovati, G.; Batista, T.; Mafud, A.C.; Zucolotto, V.; Mascarenhas, Y.P. Structural Characterization of Emeraldine-Salt Polyaniline/Gold Nanoparticles Complexes. *J. Nanomater.* **2011**, *2011*, 1–7. [[CrossRef](#)]
108. Wu, H.; Huang, X.; Gao, M.; Liao, X.; Shi, B. Polyphenol-grafted collagen fiber as reductant and stabilizer for one-step synthesis of size-controlled gold nanoparticles and their catalytic application to 4-nitrophenol reduction. *Green Chem.* **2011**, *13*, 651–658. [[CrossRef](#)]
109. Liu, Z.; Huang, H.; He, T. Large-Area 2D Gold Nanorod Arrays Assembled on Block Copolymer Templates. *Small* **2013**, *9*, 505–510. [[CrossRef](#)] [[PubMed](#)]
110. Zhou, J.; Zhang, C.; Wang, Y. Nanoporous block copolymer membranes immobilized with gold nanoparticles for continuous flow catalysis. *Polym. Chem.* **2019**, *10*, 1642–1649. [[CrossRef](#)]
111. Pearson, A.C.; Pound, E.; Woolley, A.T.; Linford, M.R.; Harb, J.N.; Davis, R.C. Chemical Alignment of DNA Origami to Block Copolymer Patterned Arrays of 5 nm Gold Nanoparticles. *Nano Lett.* **2011**, *11*, 1981–1987. [[CrossRef](#)]
112. Sun, Y.; Ren, Y. In Situ Synchrotron X-Ray Techniques for Real-Time Probing of Colloidal Nanoparticle Synthesis. *Part. Part. Syst. Character.* **2013**, *30*, 399–419. [[CrossRef](#)]
113. Chen, X.; Schröder, J.; Hauschild, S.; Rosenfeldt, S.; Dulle, M.; Förster, S. Simultaneous SAXS/WAXS/UV-Vis Study of the Nucleation and Growth of Nanoparticles: A Test of Classical Nucleation Theory. *Langmuir* **2015**, *31*, 11678–11691. [[CrossRef](#)]
114. Abécassis, B.; Testard, F.; Kong, Q.; Francois, B.; Spalla, O. Influence of Monomer Feeding on a Fast Gold Nanoparticles Synthesis: Time-Resolved XANES and SAXS Experiments. *Langmuir* **2010**, *26*, 13847–13854. [[CrossRef](#)]
115. Kikhney, A.G.; Svergun, D.I. A practical guide to small angle X-ray scattering (SAXS) of flexible and intrinsically disordered proteins. *FEBS Lett.* **2015**, *589*, 2570–2577. [[CrossRef](#)]
116. Thakor, A.S.; Jokerst, J.; Zavaleta, C.; Massoud, T.F.; Gambhir, S.S. Gold Nanoparticles: A Revival in Precious Metal Administration to Patients. *Nano Lett.* **2011**, *11*, 4029–4036. [[CrossRef](#)] [[PubMed](#)]
117. Gracheva, T.A.; Kuz'micheva, T.A.; Perevezentsev, V.N.; Smirnova, L.A.; Mochalova, A.E.; Salomatina, E.B. Kinetics and mechanisms of the UV-radiation-assisted formation of gold nanoparticles in H<sub>2</sub>AuCl<sub>4</sub>-doped chitosan solutions. *Tech. Phys.* **2017**, *62*, 1228–1232. [[CrossRef](#)]
118. Yakimovich, N.O.; Smirnova, L.A.; Gracheva, T.A.; Klychkov, K.S.; Bityurin, N.M.; Aleksandrov, A.P. Synthesis of chitosan-stabilized Au nanoparticles with controllable sizes. *Polym. Sci. Ser. B* **2008**, *50*, 238–242. [[CrossRef](#)]

119. Dunlop, I.E.; Ryan, M.P.; Goode, A.E.; Schuster, C.; Terrill, N.J.; Weaver, J.V.M. Direct synthesis of PEG-encapsulated gold nanoparticles using branched copolymer nanoreactors. *RSC Adv.* **2014**, *4*, 27702–27707. [[CrossRef](#)]
120. Macosko, C.W. *Rheology: Principles, Measurements, and Applications*; Wiley VCH: New York, NY, USA, 1994; ISBN 9780471185758.
121. Fernández, V.V.A.; Tepale, N.; Álvarez, J.G.; Pérez-López, J.H.; Macías, E.R.; Bautista, F.; Pignon, F.; Rharbi, Y.; Gámez-Corrales, R.; Manero, O.; et al. Rheology of the Pluronic P103/water system in a semidilute regime: Evidence of nonequilibrium critical behavior. *J. Colloid Interface Sci.* **2009**, *336*, 842–849. [[CrossRef](#)]
122. Abdelhalim, M.A.K.; Mady, M.M.; Ghannam, M.M. Rheological and dielectric properties of different gold nanoparticle sizes. *Lipids Health Dis.* **2011**. [[CrossRef](#)]
123. Mendoza, C.; Gindy, N.; Gutmann, J.S.; Frömsdorf, A.; Förster, S.; Fahmi, A. In Situ Synthesis and Alignment of Au Nanoparticles within Hexagonally Packed Cylindrical Domains of Diblock Copolymers in Bulk. *Langmuir* **2009**, *25*, 9571–9578. [[CrossRef](#)] [[PubMed](#)]
124. Mendoza, C.; Pietsch, T.; Gutmann, J.S.; Jehnichen, D.; Gindy, N.; Fahmi, A. Block Copolymers with Gold Nanoparticles: Correlation between Structural Characteristics and Mechanical Properties. *Macromolecules* **2009**, *42*, 1203–1211. [[CrossRef](#)]
125. Chudasama, B.; Vala, A.K.; Andhariya, N.; Mehta, R.V.; Upadhyay, R.V. Highly bacterial resistant silver nanoparticles: Synthesis and antibacterial activities. *J. Nanopart. Res.* **2010**, *12*, 1677–1685. [[CrossRef](#)]
126. Marta, B.; Jakab, E.; Potara, M.; Simon, T.; Imre-Lucaci, F.; Barbu-Tudoran, L.; Popescu, O.; Astilean, S. Pluronic-coated silver nanoprisms: Synthesis, characterization and their antibacterial activity. *Colloids Surfaces A Physicochem. Eng. Asp.* **2014**, *441*, 77–83. [[CrossRef](#)]
127. Johnston, H.J.; Hutchison, G.; Christensen, F.M.; Peters, S.; Hankin, S.; Stone, V. A review of the in vivo and in vitro toxicity of silver and gold particulates: Particle attributes and biological mechanisms responsible for the observed toxicity. *Crit. Rev. Toxicol.* **2010**, *40*, 328–346. [[CrossRef](#)] [[PubMed](#)]
128. Dasari, T.S.; Zhang, Y.; Yu, H. Antibacterial Activity and Cytotoxicity of Gold (I) and (III) Ions and Gold Nanoparticles. *Biochem. Pharmacol. Open Access* **2015**, *4*. [[CrossRef](#)] [[PubMed](#)]
129. Wang, C.; Cui, Q.; Wang, X.; Li, L. Preparation of Hybrid Gold/Polymer Nanocomposites and Their Application in a Controlled Antibacterial Assay. *ACS Appl. Mater. Interfaces* **2016**, *8*, 29101–29109. [[CrossRef](#)] [[PubMed](#)]
130. Tran, C.D.; Proscenc, F.; Franko, M. Facile synthesis, structure, biocompatibility and antimicrobial property of gold nanoparticle composites from cellulose and keratin. *J. Colloid Interface Sci.* **2018**, *510*, 237–245. [[CrossRef](#)]
131. Ryan, C.; Alcock, E.; Buttimer, F.; Schmidt, M.; Clarke, D.; Pemble, M.; Bardosova, M. Synthesis and characterisation of cross-linked chitosan composites functionalised with silver and gold nanoparticles for antimicrobial applications. *Sci. Technol. Adv. Mater.* **2017**, *18*, 528–540. [[CrossRef](#)]
132. Khan, S.; Bakht, J.; Syed, F. Green synthesis of gold nanoparticles using Acer pentapomicum leaves extract its characterization, antibacterial, antifungal and antioxidant bioassay. *Dig. J. Nanomater. Biostruct.* **2018**, 579–589.
133. Borah, D.; Hazarika, M.; Tailor, P.; Silva, A.R.; Chetia, B.; Singaravelu, G.; Das, P. Starch-templated bio-synthesis of gold nanoflowers for in vitro antimicrobial and anticancer activities. *Appl. Nanosci.* **2018**, *8*, 241–253. [[CrossRef](#)]
134. Liu, F.; Liu, C.; Liu, W.; Ding, Z.; Ma, H.; Seeram, N.P.; Xu, L.; Mu, Y.; Huang, X.; Li, L. New Sesquiterpenoids from Eugenia jambolana Seeds and Their Anti-microbial Activities. *J. Agric. Food Chem.* **2017**, *65*, 10214–10222. [[CrossRef](#)]
135. Gupta, R.; Rai, B. Effect of Size and Surface Charge of Gold Nanoparticles on their Skin Permeability: A Molecular Dynamics Study. *Sci. Rep.* **2017**, *7*, 45292. [[CrossRef](#)]
136. Fernandes, R.; Smyth, N.R.; Muskens, O.L.; Nitti, S.; Heuer-Jungemann, A.; Ardern-Jones, M.R.; Kanaras, A.G. Interactions of Skin with Gold Nanoparticles of Different Surface Charge, Shape, and Functionality. *Small* **2015**, *11*, 713–721. [[CrossRef](#)]
137. Mahmoud, N.N.; Alhusban, A.A.; Ali, J.I.; Al-Bakri, A.G.; Hamed, R.; Khalil, E.A. Preferential Accumulation of Phospholipid-PEG and Cholesterol-PEG Decorated Gold Nanorods into Human Skin Layers and Their Photothermal-Based Antibacterial Activity. *Sci. Rep.* **2019**, *9*, 5796. [[CrossRef](#)] [[PubMed](#)]
138. Polshettiwar, V.; Varma, R.S. Green chemistry by nano-catalysis. *Green Chem.* **2010**, *12*, 743–754. [[CrossRef](#)]

139. Shiju, N.R.; Gulians, V.V. Recent developments in catalysis using nanostructured materials. *Appl. Catal. A Gen.* **2009**, *356*, 1–17. [[CrossRef](#)]
140. Gupta, N.; Singh, H.P.; Sharma, R.K. Single-pot synthesis: Plant mediated gold nanoparticles catalyzed reduction of methylene blue in presence of stannous chloride. *Colloids Surfaces A Physicochem. Eng. Asp.* **2010**, *367*, 102–107. [[CrossRef](#)]
141. Mitsudome, T.; Kaneda, K. Gold nanoparticle catalysts for selective hydrogenations. *Green Chem.* **2013**, *15*, 2636–2654. [[CrossRef](#)]
142. Haruta, M. When gold is not noble: Catalysis by nanoparticles. *Chem. Rec.* **2003**, *3*, 75–87. [[CrossRef](#)]
143. Tsunoyama, H.; Sakurai, H.; Negishi, Y.; Tsukuda, T. Size-specific catalytic activity of polymer-stabilized gold nanoclusters for aerobic alcohol oxidation in water. *J. Am. Chem. Soc.* **2005**. [[CrossRef](#)]
144. Miyamura, H.; Matsubara, R.; Miyazaki, Y.; Kobayashi, S. Aerobic Oxidation of Alcohols at Room Temperature and Atmospheric Conditions Catalyzed by Reusable Gold Nanoclusters Stabilized by the Benzene Rings of Polystyrene Derivatives. *Angew. Chem. Int. Ed.* **2007**, *46*, 4151–4154. [[CrossRef](#)]
145. Han, J.; Liu, Y.; Guo, R. Reactive Template Method to Synthesize Gold Nanoparticles with Controllable Size and Morphology Supported on Shells of Polymer Hollow Microspheres and Their Application for Aerobic Alcohol Oxidation in Water. *Adv. Funct. Mater.* **2009**, *19*, 1112–1117. [[CrossRef](#)]
146. Dai, Y.; Ren, T.; Wang, Y.; Zhang, X. The synergistic effect of nitrogen atoms and triblock structure on stabilizing gold nanoparticles for catalytic reduction of 4-nitrophenol. *Gold Bull.* **2017**, *50*, 123–129. [[CrossRef](#)]
147. Tripathy, T.; Kolya, H.; Jana, S.; Senapati, M. Green synthesis of Ag-Au bimetallic nanocomposites using a biodegradable synthetic graft copolymer; hydroxyethyl starch-g-poly (acrylamide- co -acrylic acid) and evaluation of their catalytic activities. *Eur. Polym. J.* **2017**, *87*, 113–123. [[CrossRef](#)]
148. Wang, S.; Zhang, J.; Yuan, P.; Sun, Q.; Jia, Y.; Yan, W.; Chen, Z.; Xu, Q. Au nanoparticle decorated N-containing polymer spheres: Additive-free synthesis and remarkable catalytic behavior for reduction of 4-nitrophenol. *J. Mater. Sci.* **2015**, *50*, 1323–1332. [[CrossRef](#)]
149. Yan, W.; Chen, C.; Wang, L.; Zhang, D.; Li, A.-J.; Yao, Z.; Shi, L.-Y. Facile and green synthesis of cellulose nanocrystal-supported gold nanoparticles with superior catalytic activity. *Carbohydr. Polym.* **2016**, *140*, 66–73. [[CrossRef](#)] [[PubMed](#)]
150. Kratošová, G.; Holišová, V.; Konvičková, Z.; Ingle, A.P.; Gaikwad, S.; Škrlová, K.; Prokop, A.; Rai, M.; Plachá, D. From biotechnology principles to functional and low-cost metallic bionanocatalysts. *Biotechnol. Adv.* **2019**, *37*, 154–176. [[CrossRef](#)]
151. Aiken, J.D.; Finke, R.G. A review of modern transition-metal nanoclusters: Their synthesis, characterization, and applications in catalysis. *J. Mol. Catal. A Chem.* **1999**, *145*, 1–44. [[CrossRef](#)]
152. Munir, A.; Joya, K.S.; Ul Haq, T.; Babar, N.; Hussain, S.Z.; Qurashi, A.; Ullah, N.; Hussain, I. Metal Nanoclusters: New Paradigm in Catalysis for Water Splitting, Solar and Chemical Energy Conversion. *ChemSusChem* **2019**, *12*, 1517–1548. [[CrossRef](#)]
153. Chiarello, G.L.; Selli, E.; Forni, L. Photocatalytic hydrogen production over flame spray pyrolysis-synthesised TiO<sub>2</sub> and Au/TiO<sub>2</sub>. *Appl. Catal. B Environ.* **2008**, *84*, 332–339. [[CrossRef](#)]
154. Li, W.; Yao, L.; Zhang, Z.; Geng, H.; Li, C.; Yu, Y.; Sheng, P.; Li, S. Tiny Au nanoparticles mediation strategy for preparation of NIR CuInS<sub>2</sub> QDs based 1D TiO<sub>2</sub> hybrid photoelectrode with enhanced photocatalytic activity. *Mater. Sci. Semicond. Process.* **2019**, *99*, 106–113. [[CrossRef](#)]
155. Mondal, C.; Pal, J.; Ganguly, M.; Sinha, A.K.; Jana, J.; Pal, T. A one pot synthesis of Au–ZnO nanocomposites for plasmon-enhanced sunlight driven photocatalytic activity. *New J. Chem.* **2014**, *38*, 2999–3005. [[CrossRef](#)]
156. Padikkaparambil, S.; Narayanan, B.; Yaakob, Z.; Viswanathan, S.; Tasirin, S.M. Au/TiO<sub>2</sub> Reusable Photocatalysts for Dye Degradation. *Int. J. Photoenergy* **2013**, *2013*, 1–10. [[CrossRef](#)]
157. Lakshminarayana, B.; Satyanarayana, G.; Subrahmanyam, C. Bimetallic Pd–Au/TiO<sub>2</sub> Nanoparticles: An Efficient and Sustainable Heterogeneous Catalyst for Rapid Catalytic Hydrogen Transfer Reduction of Nitroarenes. *ACS Omega* **2018**, *3*, 13065–13072. [[CrossRef](#)]
158. Zhang, Q.; Jin, X.; Xu, Z.; Zhang, J.; Rendón, U.F.; Razzari, L.; Chaker, M.; Ma, D. Plasmonic Au-Loaded Hierarchical Hollow Porous TiO<sub>2</sub> Spheres: Synergistic Catalysts for Nitroaromatic Reduction. *J. Phys. Chem. Lett.* **2018**, *9*, 5317–5326. [[CrossRef](#)]
159. Pradhan, S.; Ghosh, D.; Chen, S. Janus Nanostructures Based on Au–TiO<sub>2</sub> Heterodimers and Their Photocatalytic Activity in the Oxidation of Methanol. *ACS Appl. Mater. Interfaces* **2009**, *1*, 2060–2065. [[CrossRef](#)]

160. Martínez, L.; Benito, M.; Mata, I.; Soler, L.; Molins, E.; Llorca, J. Preparation and photocatalytic activity of Au/TiO<sub>2</sub> lyogels for hydrogen production. *Sustain. Energy Fuels* **2018**, *2*, 2284–2295. [[CrossRef](#)]
161. Khore, S.K.; Kadam, S.R.; Naik, S.D.; Kale, B.B.; Sonawane, R.S. Solar light active plasmonic Au@TiO<sub>2</sub> nanocomposite with superior photocatalytic performance for H<sub>2</sub> production and pollutant degradation. *New J. Chem.* **2018**, *42*, 10958–10968. [[CrossRef](#)]
162. Panayotov, D.A.; Frenkel, A.I.; Morris, J.R. Catalysis and Photocatalysis by Nanoscale Au/TiO<sub>2</sub>: Perspectives for Renewable Energy. *ACS Energy Lett.* **2017**, *2*, 1223–1231. [[CrossRef](#)]
163. Ratliff, J.S.; Tenney, S.A.; Hu, X.; Conner, S.F.; Ma, S.; Chen, D.A. Decomposition of Dimethyl Methylphosphonate on Pt, Au, and Au–Pt Clusters Supported on TiO<sub>2</sub> (110). *Langmuir* **2009**, *25*, 216–225. [[CrossRef](#)]
164. Chen, Y.; Wang, Y.; Li, W.; Yang, Q.; Hou, Q.; Wei, L.; Liu, L.; Huang, F.; Ju, M. Enhancement of photocatalytic performance with the use of noble-metal-decorated TiO<sub>2</sub> nanocrystals as highly active catalysts for aerobic oxidation under visible-light irradiation. *Appl. Catal. B Environ.* **2017**.
165. Sun, Y.; Sun, Y.; Zhang, T.; Chen, G.; Zhang, F.; Liu, D.; Cai, W.; Li, Y.; Yang, X.; Li, C. Complete Au@ZnO core-shell nanoparticles with enhanced plasmonic absorption enabling significantly improved photocatalysis. *Nanoscale* **2016**, *8*, 10774–10782. [[CrossRef](#)]
166. Pougín, A.; Dodekatos, G.; Dilla, M.; Tüysüz, H.; Strunk, J. Au@TiO<sub>2</sub> Core-Shell Composites for the Photocatalytic Reduction of CO<sub>2</sub>. *Chem. A Eur. J.* **2018**, *24*, 12416–12425. [[CrossRef](#)]
167. Gavade, N.L.; Babar, S.B.; Kadam, A.N.; Gophane, A.D.; Garadkar, K.M. Fabrication of M@Cu<sub>x</sub>O/ZnO (M = Ag, Au) Heterostructured Nanocomposite with Enhanced Photocatalytic Performance under Sunlight. *Ind. Eng. Chem. Res.* **2017**, *56*, 14489–14501. [[CrossRef](#)]
168. Arvizo, R.; Bhattacharya, R.; Mukherjee, P. Gold nanoparticles: Opportunities and challenges in nanomedicine. *Expert Opin. Drug Deliv.* **2010**, *7*, 753–763. [[CrossRef](#)]
169. Sasidharan, A.; Monteiro-Riviere, N.A. Biomedical applications of gold nanomaterials: Opportunities and challenges. *Wiley Interdiscip. Rev. Nanomed. Nanobiotechnol.* **2015**, *7*, 779–796.
170. Sekhon, B.S.; Kamboj, S.R. Inorganic nanomedicine—Part 2. *Nanomed. Nanotechnol. Biol. Med.* **2010**, *6*, 612–618. [[CrossRef](#)]
171. Dai, Z. (Ed.) *Advances in Nanotheranostics II*; Springer Series in Biomaterials Science and Engineering; Springer Singapore: Singapore, 2016; Volume 7, ISBN 978-981-10-0061-4.
172. Kattumuri, V.; Katti, K.; Bhaskaran, S.; Boote, E.J.; Casteel, S.W.; Fent, G.M.; Robertson, D.J.; Chandrasekhar, M.; Kannan, R.; Katti, K.V. Gum Arabic as a Phytochemical Construct for the Stabilization of Gold Nanoparticles: In Vivo Pharmacokinetics and X-ray-Contrast-Imaging Studies. *Small* **2007**, *3*, 333–341. [[CrossRef](#)]
173. Huang, X.; El-Sayed, M.A. Gold nanoparticles: Optical properties and implementations in cancer diagnosis and photothermal therapy. *J. Adv. Res.* **2010**, *1*, 13–28. [[CrossRef](#)]
174. Harrison, E.; Coulter, J.A.; Dixon, D. Gold nanoparticle surface functionalization: Mixed monolayer versus hetero bifunctional peg linker. *Nanomedicine* **2016**, *11*, 851–865. [[CrossRef](#)]
175. Miao, Z.; Gao, Z.; Chen, R.; Yu, X.; Su, Z.; Wei, G. Surface-bioengineered Gold Nanoparticles for Biomedical Applications. *Curr. Med. Chem.* **2018**, *25*, 1920–1944. [[CrossRef](#)]
176. Chen, H.; Zou, H.; Paholak, H.J.; Ito, M.; Qian, W.; Che, Y.; Sun, D. Thiol-reactive amphiphilic block copolymer for coating gold nanoparticles with neutral and functional surfaces. *Polym. Chem.* **2014**, *5*, 2768–2773. [[CrossRef](#)]
177. Locatelli, E.; Comes Franchini, M. Biodegradable PLGA-b-PEG polymeric nanoparticles: Synthesis, properties, and nanomedical applications as drug delivery system. *J. Nanopart. Res.* **2012**, *14*, 1316. [[CrossRef](#)]
178. Anniebell, S.; Gopinath, S.C.B. Polymer Conjugated Gold Nanoparticles in Biomedical Applications. *Curr. Med. Chem.* **2018**, *25*, 1433–1445. [[CrossRef](#)]
179. Manson, J.; Kumar, D.; Meenan, B.J.; Dixon, D. Polyethylene glycol functionalized gold nanoparticles: The influence of capping density on stability in various media. *Gold Bull.* **2011**, *44*, 99–105. [[CrossRef](#)]
180. Simpson, C.A.; Salleng, K.J.; Cliffl, D.E.; Feldheim, D.L. In vivo toxicity, biodistribution, and clearance of glutathione-coated gold nanoparticles. *Nanomed. Nanotechnol. Biol. Med.* **2013**, *9*, 257–263. [[CrossRef](#)] [[PubMed](#)]
181. Baek, S.; Singh, R.K.; Kim, T.H.; Seo, J.W.; Shin, U.S.; Chrzanowski, W.; Kim, H.W. Triple Hit with Drug Carriers: pH- and Temperature-Responsive Theranostics for Multimodal Chemo- and Photothermal Therapy and Diagnostic Applications. *ACS Appl. Mater. Interfaces* **2016**, *8*, 8967–8979. [[CrossRef](#)] [[PubMed](#)]

182. Khandekar, S.V.; Kulkarni, M.G.; Devarajan, P.V. Polyaspartic acid functionalized gold nanoparticles for tumor targeted doxorubicin delivery. *J. Biomed. Nanotechnol.* **2014**, *10*, 143–153. [[CrossRef](#)]
183. Dey, S.; Sherly, M.C.; Rekha, M.R.; Sreenivasan, K. Alginate stabilized gold nanoparticle as multidrug carrier: Evaluation of cellular interactions and hemolytic potential. *Carbohydr. Polym.* **2016**, *136*, 71–80. [[CrossRef](#)]
184. Salem, D.S.; Sliem, M.A.; El-Sesy, M.; Shouman, S.A.; Badr, Y. Improved chemo-photothermal therapy of hepatocellular carcinoma using chitosan-coated gold nanoparticles. *J. Photochem Photobiol B* **2018**, *182*, 92–99. [[CrossRef](#)]
185. Cai, H.; Yao, P. In situ preparation of gold nanoparticle-loaded lysozyme–dextran nanogels and applications for cell imaging and drug delivery. *Nanoscale* **2013**, *5*, 2892–2900. [[CrossRef](#)]
186. Tiwari, S.; Patil, R.; Dubey, S.K.; Bahadur, P. Derivatization approaches and applications of pullulan. *Adv. Colloid Interface Sci.* **2019**, *269*, 296–308. [[CrossRef](#)]
187. Laksee, S.; Puthong, S.; Teerawatananon, T.; Palaga, T.; Muangsin, N. Highly efficient and facile fabrication of monodispersed Au nanoparticles using pullulan and their application as anticancer drug carriers. *Carbohydr. Polym.* **2017**, *173*, 178–191. [[CrossRef](#)]
188. Laksee, S.; Puthong, S.; Kongkavitoon, P.; Palaga, T.; Muangsin, N. Facile and green synthesis of pullulan derivative-stabilized Au nanoparticles as drug carriers for enhancing anticancer activity. *Carbohydr. Polym.* **2018**, *198*, 495–508. [[CrossRef](#)] [[PubMed](#)]
189. Ganeshkumar, M.; Ponrasu, T.; Raja, M.D.; Subamekala, M.K.; Suguna, L. Green synthesis of pullulan stabilized gold nanoparticles for cancer targeted drug delivery. *Spectrochim. Acta A Mol. Biomol. Spectrosc.* **2014**, *130*, 64–71. [[CrossRef](#)] [[PubMed](#)]
190. Ghorbani, M.; Hamishehkar, H. Decoration of gold nanoparticles with thiolated pH-responsive polymeric (PEG-b-p(2-dimethylamio ethyl methacrylate-co-itaconic acid) shell: A novel platform for targeting of anticancer agent. *Mater. Sci. Eng. C Mater. Biol. Appl.* **2017**, *81*, 561–570. [[CrossRef](#)] [[PubMed](#)]
191. Jabri, T.; Imran, M.; Shafiullah; Rao, K.; Ali, I.; Arfan, M.; Shah, M.R. Fabrication of lecithin-gum tragacanth muco-adhesive hybrid nano-carrier system for in-vivo performance of Amphotericin B. *Carbohydr. Polym.* **2018**, *194*, 89–96. [[CrossRef](#)] [[PubMed](#)]
192. Singh, P.; Pandit, S.; Garnæs, J.; Tunjic, S.; Mokkaapati, V.; Sultan, A.; Thygesen, A.; Mackevica, A.; Mateiu, R.V.; Daugaard, A.E.; et al. Green synthesis of gold and silver nanoparticles from Cannabis sativa (industrial hemp) and their capacity for biofilm inhibition. *Int. J. Nanomed.* **2018**, *13*, 3571–3591. [[CrossRef](#)]
193. Mukherjee, S.; Sushma, V.; Patra, S.; Barui, A.K.; Bhadra, M.P.; Sreedhar, B.; Patra, C.R. Green chemistry approach for the synthesis and stabilization of biocompatible gold nanoparticles and their potential applications in cancer therapy. *Nanotechnology* **2012**, *23*, 455103. [[CrossRef](#)]
194. Wang, Z.; Sun, J.; Qiu, Y.; Li, W.; Guo, X.; Li, Q.; Zhang, H.; Zhou, J.; Du, Y.; Yuan, H.; et al. Specific photothermal therapy to the tumors with high EphB4 receptor expression. *Biomaterials* **2015**, *68*, 32–41. [[CrossRef](#)]
195. Chen, R.; Wang, X.; Yao, X.; Zheng, X.; Wang, J.; Jiang, X. Near-IR-triggered photothermal/photodynamic dual-modality therapy system via chitosan hybrid nanospheres. *Biomaterials* **2013**, *34*, 8314–8322. [[CrossRef](#)]
196. Liu, J.; Liang, H.; Li, M.; Luo, Z.; Zhang, J.; Guo, X.; Cai, K. Tumor acidity activating multifunctional nanoplatfor for NIR-mediated multiple enhanced photodynamic and photothermal tumor therapy. *Biomaterials* **2018**, *157*, 107–124. [[CrossRef](#)]
197. Gamal-Eldeen, A.M.; Moustafa, D.; El-Daly, S.M.; Abo-Zeid, M.A.M.; Saleh, S.; Khoobchandani, M.; Katti, K.; Shukla, R.; Katti, K.V. Gum Arabic-encapsulated gold nanoparticles for a non-invasive photothermal ablation of lung tumor in mice. *Biomed. Pharmacother.* **2017**, *89*, 1045–1054. [[CrossRef](#)]
198. Gamal-Eldeen, A.M.; Moustafa, D.; El-Daly, S.M.; El-Hussieny, E.A.; Saleh, S.; Khoobchandani, M.; Bacon, K.L.; Gupta, S.; Katti, K.; Shukla, R.; et al. Photothermal therapy mediated by gum Arabic-conjugated gold nanoparticles suppresses liver preneoplastic lesions in mice. *J. Photochem. Photobiol. B* **2016**, *163*, 47–56. [[CrossRef](#)] [[PubMed](#)]
199. Silva, C.O.; Rijo, P.; Molpeceres, J.; Ascensão, L.; Roberto, A.; Fernandes, A.S.; Gomes, R.; Pinto Coelho, J.M.; Gabriel, A.; Vieira, P.; et al. Bioproduction of gold nanoparticles for photothermal therapy. *Ther. Deliv.* **2016**, *7*, 287–304. [[CrossRef](#)] [[PubMed](#)]
200. Kim, T.H.; Lee, S.; Chen, X. Nanotheranostics for personalized medicine. *Expert Rev. Mol. Diagn.* **2013**, *13*, 257–269. [[CrossRef](#)] [[PubMed](#)]

201. Shanavas, A.; Rengan, A.K.; Chauhan, D.; George, L.; Vats, M.; Kaur, N.; Yadav, P.; Mathur, P.; Chakraborty, S.; Tejaswini, A.; et al. Glycol chitosan assisted in situ reduction of gold on polymeric template for anti-cancer theranostics. *Int. J. Biol. Macromol.* **2018**, *110*, 392–398. [[CrossRef](#)] [[PubMed](#)]
202. Wang, L.; Li, D.; Hao, Y.; Niu, M.; Hu, Y.; Zhao, H.; Chang, J.; Zhang, Z.; Zhang, Y. Gold nanorod-based poly(lactic-co-glycolic acid) with manganese dioxide core-shell structured multifunctional nanoplatform for cancer theranostic applications. *Int. J. Nanomed.* **2017**, *12*, 3059–3075. [[CrossRef](#)]
203. Deng, X.; Li, K.; Cai, X.; Liu, B.; Wei, Y.; Deng, K.; Xie, Z.; Wu, Z.; Ma, P.; Hou, Z.; et al. A Hollow-Structured CuS@Cu<sub>2</sub>S@Au Nanohybrid: Synergistically Enhanced Photothermal Efficiency and Photoswitchable Targeting Effect for Cancer Theranostics. *Adv. Mater.* **2017**, *29*, 1701266. [[CrossRef](#)]
204. Simon, T.; Potara, M.; Gabudean, A.M.; Licarete, E.; Banciu, M.; Astilean, S. Designing Theranostic Agents Based on Pluronic Stabilized Gold Nanoaggregates Loaded with Methylene Blue for Multimodal Cell Imaging and Enhanced Photodynamic Therapy. *ACS Appl. Mater. Interfaces* **2015**, *7*, 16191–16201. [[CrossRef](#)]
205. Xiong, D.; Zhang, X.; Peng, S.; Gu, H.; Zhang, L. Smart pH-sensitive micelles based on redox degradable polymers as DOX/GNPs carriers for controlled drug release and CT imaging. *Colloids Surf B Biointerfaces* **2018**, *163*, 29–40. [[CrossRef](#)]
206. Zeng, Y.; Zhang, D.; Wu, M.; Liu, Y.; Zhang, X.; Li, L.; Li, Z.; Han, X.; Wei, X.; Liu, X. Lipid-AuNPs@PDA nanohybrid for MRI/CT imaging and photothermal therapy of hepatocellular carcinoma. *ACS Appl. Mater. Interfaces* **2014**, *6*, 14266–14277. [[CrossRef](#)]
207. Zhao, L.; Kim, T.H.; Kim, H.W.; Ahn, J.C.; Kim, S.Y. Enhanced cellular uptake and phototoxicity of Verteporfin-conjugated gold nanoparticles as theranostic nanocarriers for targeted photodynamic therapy and imaging of cancers. *Mater. Sci. Eng. C Mater. Biol. Appl.* **2016**, *67*, 611–622. [[CrossRef](#)]
208. Zhou, G.; Xiao, H.; Li, X.; Huang, Y.; Song, W.; Song, L.; Chen, M.; Cheng, D.; Shuai, X. Gold nanocage decorated pH-sensitive micelle for highly effective photothermo-chemotherapy and photoacoustic imaging. *Acta Biomater.* **2017**, *64*, 223–236. [[CrossRef](#)] [[PubMed](#)]
209. Fazal, S.; Jayasree, A.; Sasidharan, S.; Koyakutty, M.; Nair, S.V.; Menon, D. Green Synthesis of Anisotropic Gold Nanoparticles for Photothermal Therapy of Cancer. *ACS Appl. Mater. Interfaces* **2014**, *6*, 8080–8089. [[CrossRef](#)] [[PubMed](#)]
210. Lee, K.-C.; Chen, W.-J.; Chen, Y.-C. Using Dextran-encapsulated gold nanoparticles as insulin carriers to prolong insulin activity. *Nanomedicine* **2017**, *12*, 1823–1834. [[CrossRef](#)] [[PubMed](#)]
211. Bhumkar, D.R.; Joshi, H.M.; Sastry, M.; Pokharkar, V.B. Chitosan Reduced Gold Nanoparticles as Novel Carriers for Transmucosal Delivery of Insulin. *Pharm. Res.* **2007**, *24*, 1415–1426. [[CrossRef](#)]
212. Qu, L.; Biant, C.; Sun, J.; Ren, Z.; Han, J.; Xia, S. Electrochemical synthesis of gold nanoparticles in polypyrrole for antibody immobilization. In Proceedings of the 4th IEEE International Conference on Nano/Micro Engineered and Molecular Systems, NEMS 2009, Shenzhen, China, 5–8 January 2009.
213. Qu, L.; Xia, S.; Bian, C.; Sun, J.; Han, J. A micro-potentiometric hemoglobin immunosensor based on electropolymerized polypyrrole–gold nanoparticles composite. *Biosens. Bioelectron.* **2009**, *24*, 3419–3424. [[CrossRef](#)]
214. Shamaeli, E.; Alizadeh, N. Functionalized gold nanoparticle-polypyrrole nanobiocomposite with high effective surface area for electrochemical/pH dual stimuli-responsive smart release of insulin. *Colloids Surfaces B Biointerfaces* **2015**, *126*, 502–509. [[CrossRef](#)]
215. Chan, C.K.W.; Zhang, L.; Cheng, C.K.; Yang, H.; Huang, Y.; Tian, X.Y.; Choi, C.H.J. Recent Advances in Managing Atherosclerosis via Nanomedicine. *Small* **2018**, *14*, 1702793. [[CrossRef](#)]
216. de Oliveira Gonçalves, K.; da Silva, M.N.; Sicchieri, L.B.; de Oliveira Silva, F.R.; de Matos, R.A.; Courrol, L.C. Aminolevulinic acid with gold nanoparticles: A novel theranostic agent for atherosclerosis. *Analyt* **2015**, *140*, 1974–1980. [[CrossRef](#)]
217. Nascimento da Silva, M.; Sicchieri, L.B.; Rodrigues de Oliveira Silva, F.; Andrade, M.F.; Courrol, L.C. Liquid biopsy of atherosclerosis using protoporphyrin IX as a biomarker. *Analyt* **2014**, *139*, 1383. [[CrossRef](#)]
218. Peng, C.; Li, Y.; Liang, H.; Cheng, J.; Li, Q.; Sun, X.; Li, Z.; Wang, F.; Guo, Y.; Tian, Z.; et al. Detection and photodynamic therapy of inflamed atherosclerotic plaques in the carotid artery of rabbits. *J. Photochem. Photobiol. B Biol.* **2011**, *102*, 26–31. [[CrossRef](#)]
219. Qin, J.; Peng, C.; Zhao, B.; Ye, K.; Yuan, F.; Peng, Z.; Yang, X.; Huang, L.; Jiang, M.; Tang, G.; et al. Noninvasive detection of macrophages in atherosclerotic lesions by computed tomography enhanced with PEGylated gold nanoparticles. *Int. J. Nanomed.* **2014**, 5575–5590.

220. De Oliveira Gonçalves, K.; Vieira, D.P.; Courrol, L.C. Synthesis and characterization of aminolevulinic acid gold nanoparticles: Photo and sonosensitizer agent for atherosclerosis. *J. Lumin.* **2018**, *197*, 317–323. [[CrossRef](#)]
221. Tammam, S.N.; Khalil, M.A.F.; Abdul Gawad, E.; Althani, A.; Zaghoul, H.; Azzazy, H.M.E. Chitosan gold nanoparticles for detection of amplified nucleic acids isolated from sputum. *Carbohydr. Polym.* **2017**, *164*, 57–63. [[CrossRef](#)] [[PubMed](#)]
222. Han, S.; Kim, Y. Polypyrrole-coated hollow gold nanoshell exerts anti-obesity effects via photothermal lipolysis. *Colloids Surfaces A Physicochem. Eng. Asp.* **2019**, *570*, 414–419. [[CrossRef](#)]
223. Kandimalla, R.; Dash, S.; Bhowal, A.C.; Kalita, S.; Talukdar, N.C.; Kundu, S.; Kotoky, J. Glycogen-gold nanohybrid escalates the potency of silymarin. *Int. J. Nanomed.* **2017**, *12*, 7025–7038. [[CrossRef](#)]
224. Vinodhini, A.; Govindaraju, K.; Singaravelu, G.; Sadiq, A.M.; Kumar, V.G. Cardioprotective potential of biobased gold nanoparticles. *Colloids Surf B Biointerfaces* **2014**, *117*, 480–486. [[CrossRef](#)]
225. Matsui, J.; Akamatsu, K.; Hara, N.; Miyoshi, D.; Nawafune, H.; Tamaki, K.; Sugimoto, N. SPR Sensor Chip for Detection of Small Molecules Using Molecularly Imprinted Polymer with Embedded Gold Nanoparticles. *Anal. Chem.* **2005**, *77*, 4282–4285. [[CrossRef](#)]
226. Tian, K.; Siegel, G.; Tiwari, A. A simple and selective colorimetric mercury (II) sensing system based on chitosan stabilized gold nanoparticles and 2,6-pyridinedicarboxylic acid. *Mater. Sci. Eng. C* **2017**, *71*, 195–199. [[CrossRef](#)]
227. Xue, L.; Xie, W.; Driessen, L.; Domke, K.F.; Wang, Y.; Schlücker, S.; Gorb, S.N.; Steinhart, M. Advanced SERS Sensor Based on Capillarity-Assisted Preconcentration through Gold Nanoparticle-Decorated Porous Nanorods. *Small* **2017**, *13*, 1603947. [[CrossRef](#)]
228. Qiu, Z.; Tang, D.; Shu, J.; Chen, G.; Tang, D. Enzyme-triggered formation of enzyme-tyramine concatamers on nanogold-functionalized dendrimer for impedimetric detection of Hg(II) with sensitivity enhancement. *Biosens. Bioelectron.* **2016**, *75*, 108–115. [[CrossRef](#)]
229. Lee, W.; Lee, S.Y.; Zhang, X.; Rabin, O.; Briber, R.M. Hexagonally ordered nanoparticles templated using a block copolymer film through Coulombic interactions. *Nanotechnology* **2013**, *24*, 45305. [[CrossRef](#)] [[PubMed](#)]
230. Adams, S.M.; Campione, S.; Caldwell, J.D.; Bezares, F.J.; Culbertson, J.C.; Capolino, F.; Ragan, R. Non-lithographic SERS substrates: Tailoring surface chemistry for Au nanoparticle cluster assembly. *Small* **2012**, *8*, 2239–2249. [[CrossRef](#)] [[PubMed](#)]
231. Hammock, M.L.; Sokolov, A.N.; Stoltenberg, R.M.; Naab, B.D.; Bao, Z. Organic transistors with ordered nanoparticle arrays as a tailorable platform for selective, in situ detection. *ACS Nano* **2012**, *6*, 3100–3108. [[CrossRef](#)] [[PubMed](#)]
232. Lu, M.; Zhu, H.; Bazuin, C.G.; Peng, W.; Masson, J.F. Polymer-Templated Gold Nanoparticles on Optical Fibers for Enhanced-Sensitivity Localized Surface Plasmon Resonance Biosensors. *ACS Sens.* **2019**, *4*, 613–622. [[CrossRef](#)] [[PubMed](#)]



© 2019 by the authors. Licensee MDPI, Basel, Switzerland. This article is an open access article distributed under the terms and conditions of the Creative Commons Attribution (CC BY) license (<http://creativecommons.org/licenses/by/4.0/>).